United States
Environmental Protection
Agency

Office of
Radiation Programs
Washington DC 20460

EPA 520/1-82-002
June 1982

Radiation

EPA

Analysis of Current Meter Records at the Northwest Atlantic 2800 Metre Radioactive Waste Dumpsite

EPA 520/1-82-002

ANALYSIS OF CURRENT METER RECORDS AT THE NORTHWEST ATLANTIC 2800 METRE RADIOACTIVE WASTE DUMPSITE

by

Peter Hamilton

June 17, 1982

Contract No. 68-01-6235

Submitted to: U.S. Environmental Protection Agency
Office of Radiation Programs
Washington, D. C. 20460

Project Officer: Robert S. Dyer

ABSTRACT

In August 1976, four current meter moorings were deployed for a period of three months at the Atlantic 2800 m radioactive waste disposal site as part of a series of scientific surveys conducted by the Environmental Protection Agency for the purpose of assessing conditions at dumpsites which had been active in the past. The Atlantic 2800 m site covers an area of approximately 350 square kilometres on the Continental Rise of the Mid-Atlantic Bight and is centered at 38°30'N and 72°06'W. The four moorings were placed in a rectangular array, each with a current meter 5.1 m off the bottom. The southwest mooring also had an additional meter at 96 m from the bottom.

The current and temperature data from the meters were analyzed in terms of the dynamic processes occurring on the Continental Rise and the implications of these measurements for transport of radionuclides in the water and attached to sediments discussed.

The principle findings are that substantial, 3-4 cm/s, southwesterly mean currents were observed near the bottom and that the low frequency part of the spectrum is dominated by fluctuations with about a 16-day period which could be explained as bottom trapped topographic Rossby waves with horizontal wavelengths of about 200 km. Bottom boundary layer effects on the low frequency wave motions, measured by the lower current meters, have only minor influences on the agreement of the observations with basic Rossby wave theory. The implications are that long-term water mass transport is dominated by the mean flow along the isobaths with excursions of about 300-400 km over three months. The Rossby waves disperse dissolved radionuclides with an effective horizontal diffusion coefficient of about 7×10^6 cm^2/s.

The high frequency motions superimposed on the low frequency currents are dominated by inertial oscillations (period 19.3 hours) which are intermittent and vary in amplitude. Maximum amplitude is about 10 cm/s. The passage of Hurricane Belle close to the site on August 10, 1976 gave rise to large amplitude inertial oscillations about 24 days later. Such inertial events provide about as much mixing energy to the bottom boundary layer as do the maximum low frequency currents ($\sim$ 20 cm/s). Based on the maximum speeds

observed, the propensity for sediment transport during the measurement period was judged to be very small. Measured internal wave motions were dominated by the semi-diurnal internal tide, amplitudes 0.5-1.5 cm/s, which is generated from the astronomical or barotropic tide in the region of the shelf break and slope to the northwest of the site.

TABLE OF CONTENTS

Section		Page
	ABSTRACT	i
	TABLE OF CONTENTS	iii
I	INTRODUCTION	1
II	LITERATURE REVIEW	5
	2.1 Introduction	5
	2.2 Deep Current Measurements in the Mid-Atlantic Bight	7
	2.3 Topographic Rossby Waves	11
	2.4 Surface Currents over the Continental Rise	12
	2.5 Hurricane Belle	15
III	DATA COLLECTED	17
IV	LOW-FREQUENCY CURRENTS	20
	4.1 Zero Order Statistics	20
	4.2 Time Dependent Motions	22
	4.3 Spectra	29
	4.4 Spatial Structure	38
	4.5 Dispersion by Low-Frequency Currents	44
V	INERTIAL CURRENTS	63
VI	TIDAL CURRENTS	77
VII	HIGH-FREQUENCY INTERNAL WAVES	83
VIII	THE NORTHWEST ATLANTIC 3800 m RADIOACTIVE WASTE DUMPSITE	84
IX	SUMMARY	86
X	RECOMMENDATIONS	89
	ACKNOWLEDGEMENTS	91
	REFERENCES	92

I. INTRODUCTION

Ocean dumping of low level radioactive wastes by the Unites States mostly occurred between 1946 and 1962. On the Atlantic coast two deep water sites received the majority of these wastes (Dyer, 1976; Luedecke, 1959). This report is concerned with the 2800 m dumpsite centered at 38°30'N, 72°06'W on the upper Continental Rise of the Mid-Atlantic Bight. The 2800 m dumpsite covers an area of approximately 350 square kilometres. Figure 1.1 shows a chart of the region with the dumpsite position marked. The Continental Rise slopes gently away from the junction of the steep Continental Slope with the Rise, at approximately 2000 m depth, towards the deep Sargasso Sea Abyssal Plain with depths greater than 4000 m. The Continental Rise and Slope are frequently dissected by steep-sided canyons. The reader is referred to the bathymetric chart of the Wilmington Canyon (NOS NJ 18-6) and Figure 4.1 for detailed topography of the dumpsite region. The Wilmington Canyon chart's eastern boundary is 72°W, thus detailed topography to the east of the dumpsite is lacking.

Other dumpsites in the region which have been the subject of scientific studies are the 3800 m radioactive waste dumpsite situated at 37°50'N, 70°35'W (Dyer, 1976) in the lower reaches of the Hudson Canyon, and the 106 mile Ocean Waste Disposal Site, a 1500 square kilometre area just off the Continental Shelf centered approximately at 38°45'N, 72°15'W, about 30 km NNE from the 2800 m dumpsite.

The 106 mile site has been studied as part of the NOAA dumpsite evaluation program (Ingham et al, 1977; Devine et al, 1981). These studies, however, are not particularly relevant to the radioactive waste dumpsites, as the primary focus was to examine the dispersion of industrial and chemical wastes within the surface layers as they are discharged from a barge. The physical oceanography of the surface waters of the 106 mile site region was also studied as part of this program.

The fate of radioactive waste packages dumped at U.S. dumpsites needs to be assessed before there is consideration of further ocean disposal of low

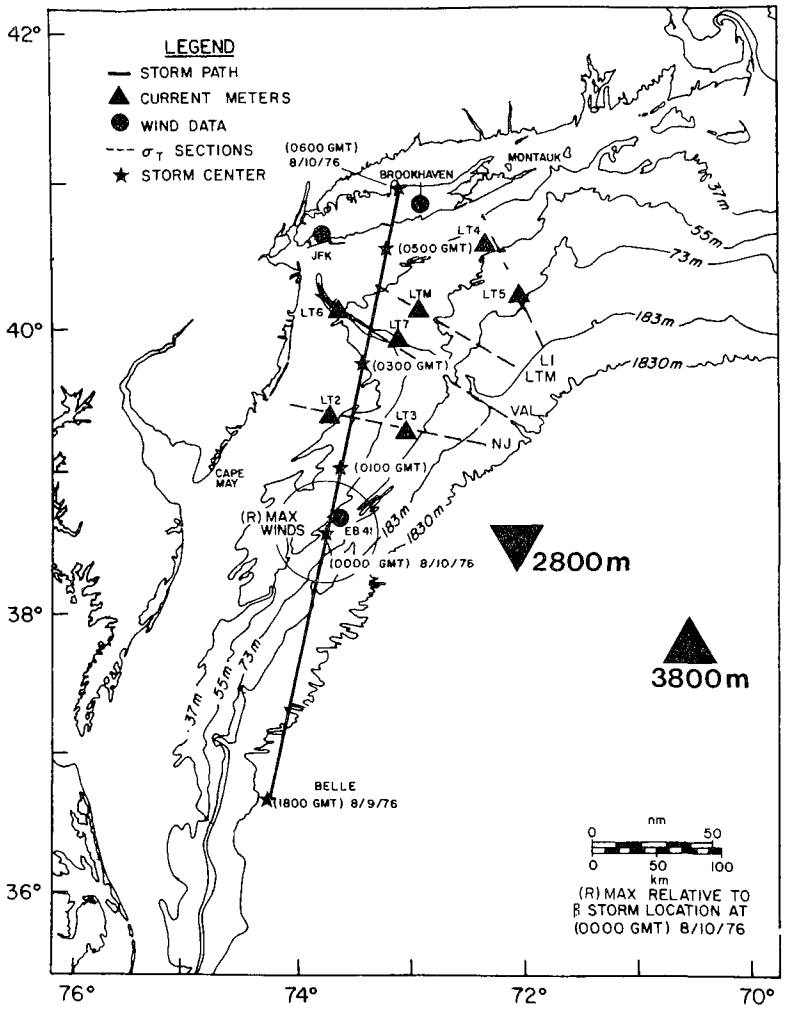

Figure 1.1. Chart showing storm track of Belle and stations from which all data were obtained (from Mayer et al. 1981). Positions of the two deepwater radioactive waste dumpsites (2800 m and 3800 m) are marked by large triangles.

level radioactive wastes. As part of a survey program of U.S. dumpsites, the EPA made near bottom current measurements at the 2800 m dumpsite for a period of three months in 1976. The measurements were made in order to evaluate the current regime at the site and its effects on the dispersion of radioactive nuclides. The current speeds measured would also indicate whether transport of sediment could occur. As part of the evaluation of physical mechanisms of dispersion, it is necessary to analyze the currents in terms of the physical processes occurring at the site. Physical dynamics of deep ocean currents often have a large range of characteristic length and time scales. Thus, the purpose of this report is to analyze the EPA current measurements in terms of physical processes occurring at the most energetic parts of the spectrum from very low frequencies (periods $\sim$ 1-week to 1-month), through inertial ($\sim$ 19 hours) and tidal ($\sim$ 12.5 hours) to high frequencies ($\sim$ 1 hour). The characteristic motions at different frequencies are placed in the context of western North Atlantic circulation and dynamics and the physical processes evaluated, as far as is able with limited data, in terms of dispersion and transport of radionuclides.

The surface waters of the Continental Rise in the mid-Atlantic Bight are dominated by the north (cold) wall of the Gulf Stream, which meanders over the region offshore of the shelf break. It is also thought that the Gulf Stream is a source of the energetic low frequency motions observed below 1000 m. The surface waters are often dominated by anticyclonic eddies, which are pinched off meanders from the Gulf Stream, which propagate west and southwest along the Shelf Slope before dissipating or being reabsorbed into the Gulf Stream. There is no direct evidence that these eddies affect the circulation below 1000 m on the Continental Rise.

The present report is divided into the following sections: Section II presents a review of the literature and physical oceanography of the region as it is relevant to EPA's current measurements. This section also includes a brief review of relevant theories. Sections III-VII give a detailed analysis of the data. These sections assume some knowledge of physical oceanography, modern time series analysis techniques and wave kinematics and is written primarily for the scientific reader. However, the conclusions which follow (Sections IX and X), summarize the important findings of the analysis

and recommendations are made for future studies. Where possible the relevance of the 2800 m dumpsite current meter data as well as data in the literature related to the 3800 m radioactive waste dumpsite will be discussed. No current meter measurements have been made at this latter dumpsite.

II. LITERATURE REVIEW

2.1 Introduction

The dispersion of radionuclides by bottom currents occurs over long time periods by transport by the mean currents and by eddy diffusion by the fluctuating or time varying components of the current and pollutant fields (Csanady, 1973). In most ocean environments the fluctuating components are greater than the mean, and energy of the fluctuating components varies with frequency. The physical processes which result in fluctuating currents include planetary wave motions (Rossby waves), eddies, inertial motions, and internal tide and high frequency internal waves. All these time varying motions can be regarded as turbulence which disperses natural (such as temperature and salinity) and man-derived constituents (such as radionuclides).

An idea of the distance parcels of water, on the lower Continental Rise below 1000 m, may travel in the course of a year and also an estimate of the scales of the eddy motions in the northwestern Atlantic is shown by the tracks of isobaric Lagrangian deep ocean floats. These floats are tracked by shore based acoustic listening stations (Figure 2.1, from Schmitz et al, 1981). Float LR1 was launched on 9 October 1977 (modified Julian day number 3425) with a nominal depth of 1300 m and was tracked for 476 days. Float LR2 was launched on 29 July 1978 (modified Julian day number 3718) with a nominal depth of 1300 m and was tracked for 281 days. The floats are approximately isobaric; i.e., remain on a pressure surface and so remain at approximately the same depth as they move, and therefore do not track an exact water particle path, since a water particle may change depth by advection along density surfaces. Float LR1 passed close to the 2800 m dumpsite on day 3725, traveled eastwards undergoing some large cyclonic circulations, passed under the Gulf Stream and ending up 175 days later in the Sargasso Sea more than 8 degrees of longitude east of the dumpsite. Thus the Gulf Stream appears to have little effect on these deep float motions though some of the intermediate mesoscale cyclonic fluctuations are visually coherent with surface Gulf Stream meanders (Schmitz et al, 1981).

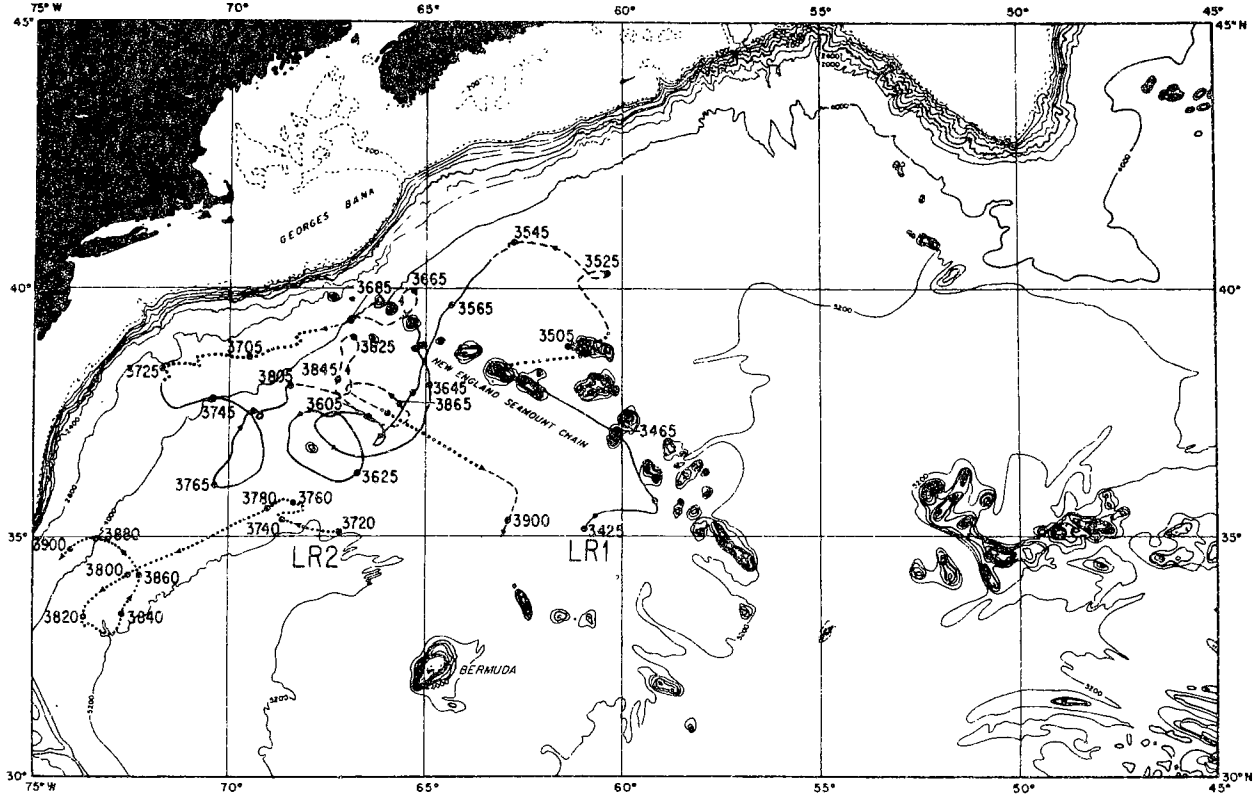

Figure 2.1. Trajectories for floats LR1 and LR2, as indicated (nominal depth 1300 M). Numbers next to the tracks denote time as a modified Julian day number. The quality of the position fixes for LR1 varied considerably: solid lines indicate good quality; solid squares, intermediate quality; dashes, poor quality (from Schmitz et al. 1981).

The long time periods and large scales of the fluctuating motions illustrated by the float tracks are appropriate for the dispersion of the radionuclides from a source on the bottom because of the time scales associated with the radioactive decay of some of the waste constituents (100-1000 years). Both slow leaks from the waste packaging and catastrophic instantaneous release of radionuclides in deep water would be dispersed by the same physical processes.

2.2 Deep Current Measurements in the Mid-Atlantic Bight

Apart from the recent employment of deep lagrangian floats to study the deep northwestern Atlantic circulation, most of the circulation studies on the Continental Shelf, Slope, and Rise of the Mid-Atlantic Bight (Figure 1.1) have used moored current meters. The analysis of these measurements reported in the literature have concentrated on the low frequency motions with periods ranging from a few days to several months, because the large scale circulations have most of their energy at these periods. There have been a few studies on internal tide and internal wave motions associated with the Continental Slope, but discussion of these phenomena is deferred to the appropriate analysis sections since they play a much smaller role than the low frequency currents in the long term dispersal of radioactive waste.

Some early deep water current measurements were made in this region, including the studies of Volkmann (1962) and Zimmerman (1971), but they are generally far too short a time period to resolve the important low frequency motions. The first long-term comprehensive set of measurements were associated with the Woods Hole Oceanographic Institution (WHOI) Site D projects (Thompson, 1971; 1977; Schmitz, 1974). Site D is situated on the New England Continental Rise at longitude 70°W in a similar depth of water (2650 m) to the radioactive waste dumpsite. The topography at Site D has a general east-west trend. Moorings with subsurface flotation were deployed between 1971 and 1974. Earlier moorings at Site D used surface flotation and current measurement were contaminated by motions of the surface float. Additionally, in 1974 an array of 15 moorings with 32 current meters were deployed along 70°W and ∿ 69°30'W across the Continental Rise from the slope region to the Gulf Stream. This was known as the Rise Array (Luyten, 1977; Thompson, 1977)

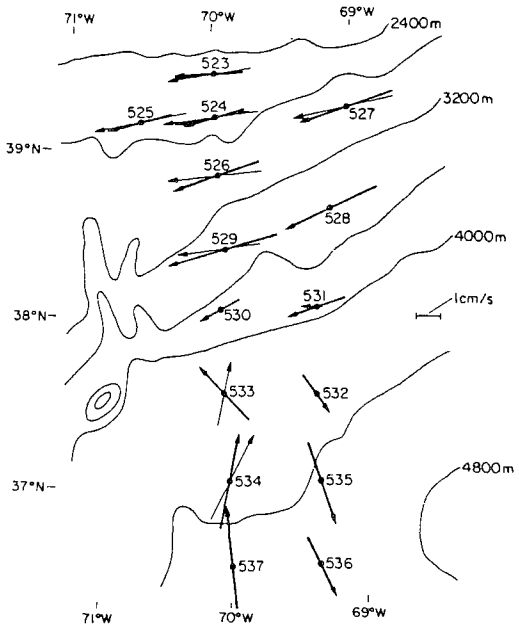

Figure 2.2. Rise Array Mooring Locations

Locations and numbers of moorings in large array. The isobaths are taken from Uchupi. The arrows show the mean flow over 8 months. The thick arrows are mostly 200 m above the bottom, and the thinner 1000 m.

(from Thompson, 1977)

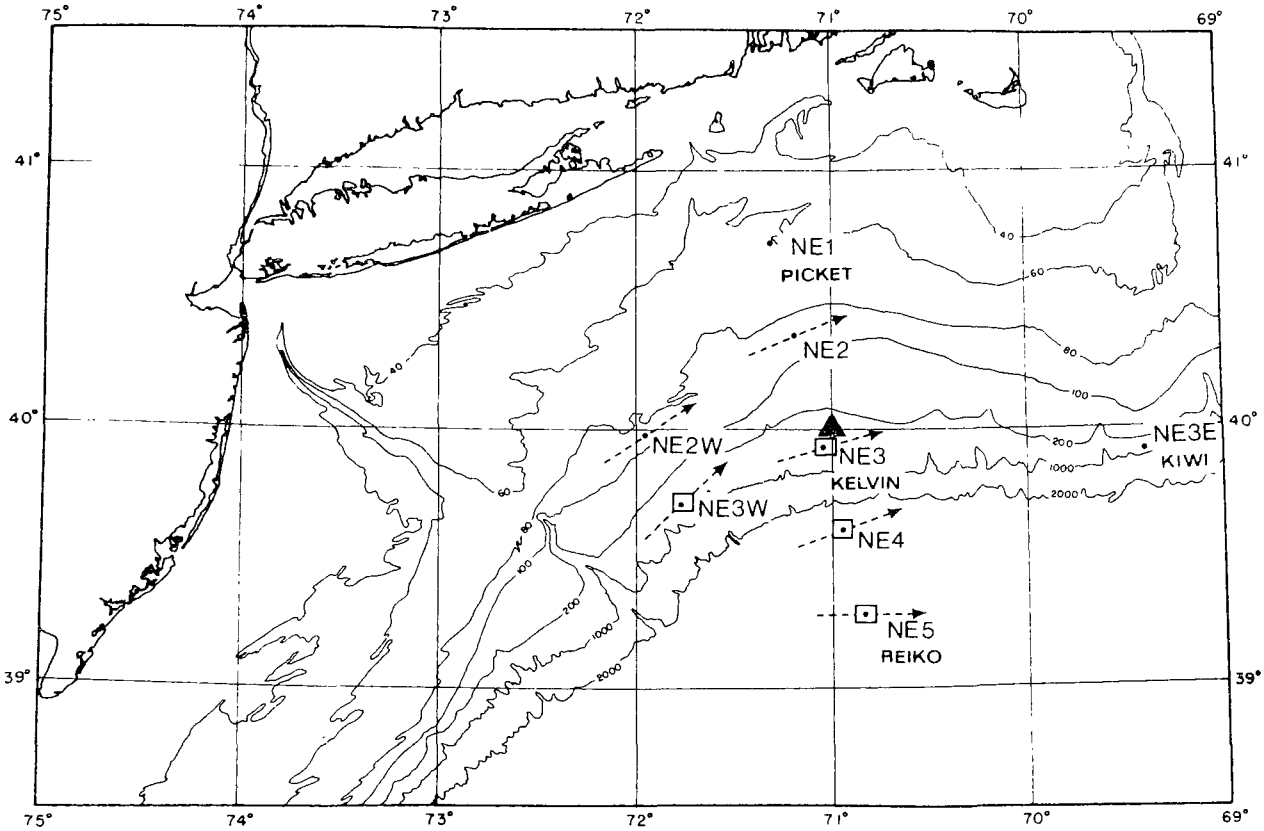

Figure 2.3. NESS Array

Bathymetric map of the Middle Atlantic Bight showing the location of the moored array. The rectangles represent areas where detailed bathymetric surveys were made during the experiment and the dashed arrows represent the estimated trend of the local topography at the mooring site. A time series of surface wind data has been obtained for the location shown by the triangle.

(from Ou and Beardsley, 1980)

which was in place for a period of about eight months, and, generally, each mooring had current meters placed at 1000 m and 200 m off the bottom. Figure 2.2 (from Thompson, 1977) shows the moorings of the Rise Array. Very few deep water current measurements have been made in this region since the discontinuation of the Site D moorings. However, more recently measurements have been made across the Continental Shelf and Slope region. (Ou and Beardsley, 1980; Ou et al, 1980) from February to August 1976. Figure 2.3 gives the positions of the moorings. One of the purposes of this experiment was to study the propagation of long period wave motions across the continental margin. Only the two deep moorings, NE4 and NE5 had meters at a depth of 2000 m, all the remaining moorings had instruments at depths shallower than 300 m (Ou and Beardsley, 1980).

The major result from the site D and Rise Array studies is that the low frequency currents are dominated by topographic Rossby waves (Thompson, 1977). Topographic Rossby waves are low frequency fluctuations with periods usually greater than a week, which exist on sloping topography. Their principal characteristics are that the fluctuations are coherent with depth and bottom intensified with maximum speeds occurring near the bottom. The waves propagate westwards at Site D. The original theories of topographic Rossby waves were given by Rhines (1970) and with respect to site D, Thompson (1971) and are summarized in the next section. A reanalysis of the Rise Array data (Hogg, 1981) indicates that long period barotropic Rossby waves (amplitude of the fluctuations is independent of depth) dominate in water of 4000 m under the Gulf Stream and as these propagate in a general northward direction towards the slope, the waves become modified into shorter wavelength bottom trapped topographic Rossby waves. There is also some indication from Ou and Beardsley (1980) that these Continental Rise Rossby waves are partially reflected by the slope and shelf regions with the effect that energy is intensified close to the Rise-Slope junction.

The current measurements at the 2800 m dumpsite will be compared with the predictions of the theory of topographic Rossby waves and also the Rise array measurements. The reader is referred to Thompson (1977), Hogg (1981) and also Schmitz (1980) for more details on the interpretation of deep ocean current meter observations in terms of Rossby waves.

2.3 Topographic Rossby Waves

The theory is basically the conservation of potential vorticity assuming a uniform sloping bottom and a uniformly stratified ocean. The dynamics are linear so that non-linear advective terms are neglected. Wave solutions are assumed so that all variables have the form:

$$P(x,y,z,t) = P(z)\ e^{i(kx + \ell y - \omega t)} \qquad (2.1)$$

where (x,y,z) is the right-handed coordinate set with x and y directed parallel and normal to the direction of the isobaths, respectively and z is directed vertically upwards, P is the pressure, ω the frequency of the wave, and k, ℓ, the horizontal wave numbers in the x and y directions, respectively. The vertical distribution, P(z), is the solution of an eigenvalue equation. This eigenvalue equation has simple solutions if the stratification is uniform, namely

$$P(z) = P_o \cosh\ (NKz/f) \qquad (2.2)$$

$$\omega = -k\ \alpha N/K^2 \cosh\ (NHK/f) \qquad (2.3)$$

where $K^2 = k^2 + \ell^2$; α is the bottom slope defined by $h = H_o + \alpha y$, where h is the depth; f is the Coriolis paramenter; and N is the Brunt-Väisälä frequency defined by

$N^2 = -g(\partial\rho/\partial z)\ /\rho$; where g is the acceleration due to gravity and ρ is the density.

Important features of this solution are:

1) The wave motion is bottom intensified. Thus, the current amplitudes increase in magnitude towards the bottom.

2) There is no phase difference between currents at different depths, therefore, at any particular wave frequency the motion is columnar.

3) The maximum frequency or cut-off frequency for topographic Rossby waves is $N\alpha$. Wave motions above this frequency are not supported by these dynamics.

4) From the dispersion relation (2.3), the phase velocity or equivalently the direction of K is in the fourth quadrant when the axes are aligned with the bathymetry, i.e. k and ℓ are always negative. The wave frequency, ω, is proportional to the bottom slope and the cosine of the angle the wave-number vector makes with the isobaths. At the highest allowed frequency, the phase velocity is parallel to the isobaths such that shallow water is on the right of the direction of wave propagation.

5) The phase relationship between U and V, the x and y components of the current vector respectively, is either in or out of phase (0° or 180°). The phase relations between the velocity components and temperature fluctuations are such that they are in quadrature.

6) The flux of momentum is in the downslope direction, but the flux of energy is given by the group velocity which is in a generally upslope direction.

These predictions are modified in the presence of changing slopes and bottom roughness with scales similar to the wavelengths of the wave motions as described by Hogg and Schmitz (1980) and Hogg (1981).

The implications of Thompson's (1977) and Hogg's (1981) studies are that the source of energy for the Rossby waves in this part of the Mid-Atlantic Bight are fluctuations related to the deep Gulf Stream.

2.4 Surface Currents over the Continental Rise

The surface waters above the thermocline between the Gulf Stream and the shelf break are extremely complex. The majority of the information on these surface waters comes from the studies of the 106 mile site (Warsh, 1975; Ingham et al., 1977; Mizenko and Chamberlin, 1981; Bisagni, 1981). The

physical oceanographic studies emphasize the frequent passage of anticyclonic eddies westwards and southwestwards along the Continental Slope. The eddies are formed from the pinching off of Gulf Stream meanders. The eddies often dissipate in the Slope region, but sometimes maintain their integrity for 100-200 days, eventually being reabsorbed into the Gulf Stream between Cape May and Cape Hatteras. Mizenko and Chamberlin (1981) discuss the tracks of twelve eddies, which occurred in 1977, using satellite observations of sea surface temperature. There appears to be a great deal of variability in the number of eddies formed each year and the length of time an eddy persists. Between 1975 and 1977 approximately eight eddies a year were observed and the 106 mile site was partially or completely occupied by eddies about 20 percent of the year in 1975 and 1976, and 69 percent of the year in 1977 (Mizenko and Chamberlin, 1981). The mixing of surface Slope water and shallow Continental Shelf water in the Mid-Atlantic Bight is extremely complex. It is not very well understood and involves the interaction of Gulf Stream anticyclonic eddies with primarily wind forced shelf waters. Very complex fronts over the Shelf break and slope region are observed to result from these interactions (Bisagni, 1981).

Gulf Stream meanders do not penetrate below about 1000 m from the surface and there is no evidence from existing observations on the Continental Rise that the eddies have any direct effect on deep circulations in this region. This is confirmed by the analysis below of EPA's current meter observations.

However, if radionuclides reach the surface layer by physical and/or biological pathways, then the eddy circulations and mixing across the shelf slope front would be important processes in the transport of radionuclides into productive shallow shelf waters. Also, if radionuclides become trapped in a surface layer anticyclonic eddy there is a possibility that the radioactive waste will enter the Gulf Stream system and thus be transported across the North Atlantic.

An idea the variability of the surface layer and the large scales involved in the dispersion of waste by surface currents is given by the results of experiments using satellite-tracked surface buoys equipped with near surface drogues (Richardson, 1981; Schmitz et al, 1981; Bisagni, 1980).

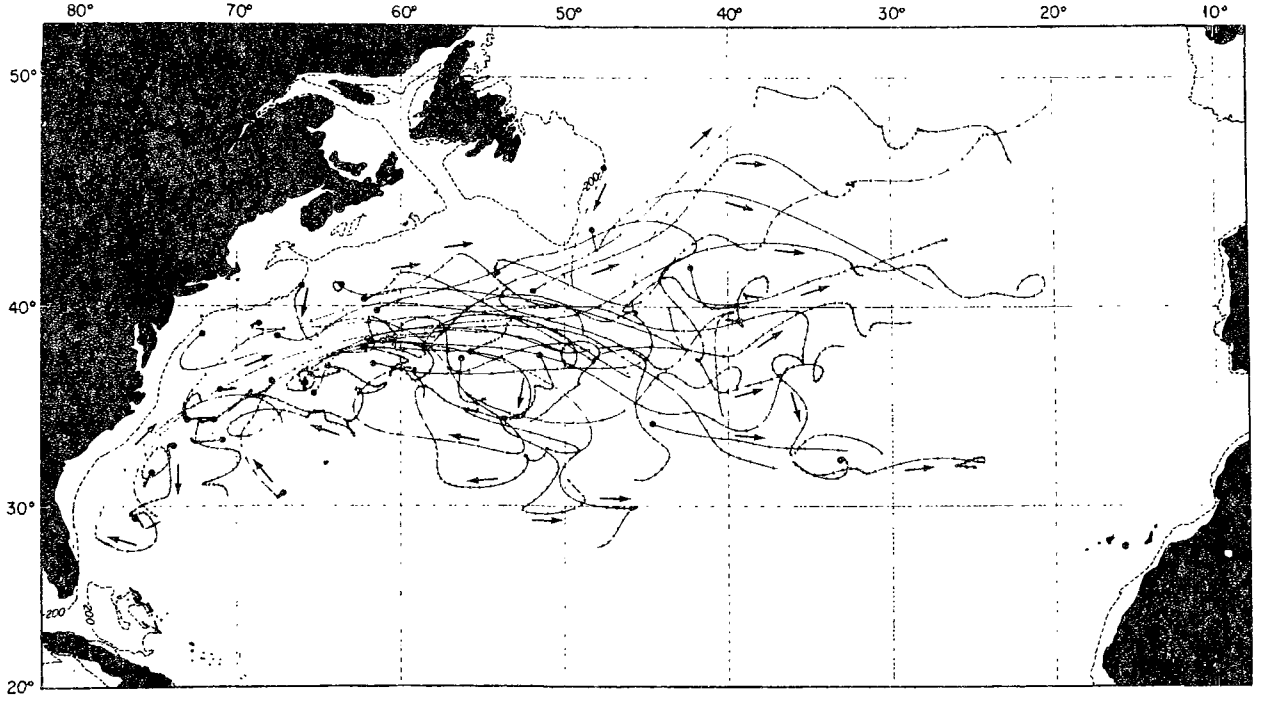

Figure 2.4. Surface buoy trajectories (tracked by satellite) smoothed with a 40-day Gaussian filter to show large-scale motion. Large dots mark the beginning of trajectories, smaller dots are evenly spaced at 5-day intervals (from Richardson, 1981).

Figure 2.4 shows smoothed trajectories of 35 buoys released in the Gulf Stream rings and nearby areas including the Continental Rise of the Mid-Atlantic Bight. The buoys do not follow water particles exactly because of slippage by the drogues and drift due to wind drag on the exposed part of the surface buoys. However, similar to the deep water floats (Figure 2.1), these observations give a good idea of the dispersion due to surface currents in the western North-Atlantic over approximately year long periods.

Two satellite-tracked surface buoys were also released at the 106 mile site in the fall of 1980 (Bisagni, 1980). The drogues moved southwards along the shelf slope towards Cape Hatteras. The drogues were then entrained into the Gulf Stream system, traversed the Stream and spun off into the Sargasso Sea. Eventually, two months after release, one of the buoys was positioned 20 km north of Bermuda. These trajectories from the 106 mile site are of course only approximate realizations of the true path of surface water parcels and at releases at different times, completely different tragectories may result, as Figure 2.4 illustrates.

2.5 Hurricane Belle

Approximately 10 days after the EPA moorings were deployed (see Section 3), on August 10, 1976, Hurricane Belle, a rapidly moving storm, passed over the Mid-Atlantic Bight and made landfall east of John F. Kennedy International (JFK) Airport. The storm path is shown in Figure 1.1 (Mayer et al, 1981). The center of the storm passed closest to the radioactive waste dumpsite at about 0000 hours GMT on August 10, a distance of about 75 km. Maximum wind speeds at this time were about 37 m/s (72 knots). Maximum wind speeds over the dumpsite, based on models of hurricane wind fields, would be expected to be about 18-20 m/s. The storm had profound effects in the observed circulation of the Continental Shelf where direct wind forcing is the major forcing mechanism for the circulation (Mayer et al, 1981). It is not expected that the effects of the hurricane would be observable in the low frequency currents at 2800 m. However, it may be expected that energy from the storm was transmitted to the sea floor primarily by increasing the amplitude of the inertial oscillations. This supposition is supported by the 2800 m

radioactive waste dumpsite current measurements and is discussed in some detail in Section V.

III. DATA COLLECTED

Five Vector Averaging Current Meters (VACM's) were placed on four moorings laid at the four corners of the dumpsite. Each meter measured water temperature and east (U) and north (V) components of velocity. Each mooring had one meter 5.1 m off the bottom and the southwest mooring had an additional meter at 96 m from the bottom. Table 3.1 gives the meter numbers, mooring positions, water depths taken from the bathymetric chart, and start and stop times. The mooring number is the first three digits of the meter number. The last two digits of the meter number give the position of the meter on the mooring numbering down from the meter closest to the surface.

The experiment was designed to look at the variability in space and time of bottom currents over the region of the 2800 m dumpsite. Meters 5.1 m off the bottom would be expected to be in the bottom boundary layer. Therefore, in order to measure currents outside the boundary layer, a meter 96 m from the bottom was placed on the southwest mooring. The flow field outside the boundary layer is the forcing for boundary layer models (e.g., Weatherly and Martin, 1978).

The data is of good quality with short gaps (usually about one hour) in records from meters 06601 and 06901. These were filled by linear interpolation to produce continuous records. Current meter 06701 had a failure in the north counter about 20 days from the end of the record, however, the north component can be reconstructed from the rotor count and the vane direction. The turbulence levels are so low that the vector components computed by resolving speed (rotor count) and direction into east and north components are identical with the vector averaged components for all records.

Similarly, the temperature records were checked for values obviously out of range, and the few erroneous values found were removed and the gap filled by linear interpolation.

VACMs record data at 15-minute intervals. The data records were preliminarily filtered by a three hour Lanzcos low pass filter and sampled at hourly intervals. This filter removes 8 hours of data at each end of the

EPA CURRENT METER DATA

Meter No.	Latitude	Longitude	Water Depth m	Height of Meter off bottom (m)	Location relative to dumpsite center	Start Time (GMT) (M/D/Y:HHMM)	Stop Time (GMT) (M/D/Y:HHMM)
06601	38°26'N	72°00'W	2845	5.1	SE	8/01/76:2300	11/10/76:1400
06701	38°36'N	72°00'W	2760	5.1	NE	8/02/76:0115	11/09/76:2045
06801	38°36'N	72°12'W	2720	5.1	NW	8/02/76:0315	11/11/76:0430
06901	38°25'N	72°12'W	2840	96.	SW	8/02/76:0615	11/11/76:0700
06902				5.1	SW	8/02/76:0615	11/11/76:0700

Table 3.1. Mooring Locations.

record. All records were adjusted to a common start time of 8/03/76:000 hours GMT (all times are in GMT). This procedure removes high frequency noise and results in records of manageable length.

The current meter data is analyzed and discussed in two frames of reference according to the processes being studied. If not explicitly stated, the U and V components used are in the east and north directions, respectively. If a rotated frame is specified, then the U and V components have been rotated clockwise through 45° so that the V component is parallel to the Continental Slope, and the U component is directed towards the deeper water perpendicular to the Continental Slope. The isobaths generally trend in a northeasterly direction. The rotated or isobath frame of reference is the natural coordinate system for some parts of the analysis. On the figures 'R45' after the meter number denotes a rotated frame of reference (e.g. Figure 4.2).

IV. LOW-FREQUENCY CURRENTS

4.1 Zero Order Statistics

The dumpsite topography and the mean flows for the five current meters are shown in Figure 4.1. The topography is fairly smooth for the northern part of the array, but the SW mooring 069 is on the northern edge of a canyon (the deep part of the North Toms Canyon) which disappears at 2700 m but reappears on the slope. The mean velocities are evidently influenced by the topography and follow the trend of the local isobaths. The mean flows are probably not very stable estimates given the long periods (10-20 days) of the fluctuations and the relatively short 3-month time series. However, the mean flow is substantial (3-4 cm/s) and shows the westward direction seen at site D and the Rise Array. As Thompson (1977) noted, this is one of the more substantial mean currents in the deep ocean.

To investigate the low frequencies, the three hour low passed time series data is filtered with a low pass 40-hour cosine filter to remove inertial and tidal fluctuations and then resampled at six hour intervals. Two and one-half days are lost from the ends of the series. Figure 4.1 also shows the amplitudes of the low frequency fluctuations along the principal axis of the motion. Principal axes are defined as the orthogonal directions for which the demeaned components of the current vector are uncorrelated and thus define the preferred direction of the fluctuations.

The amplitudes of the fluctuations exceed the mean currents. The amplitudes are also approximately equal along the principal axes for the two eastern moorings (066 and 067), but the motion is more polarized for the two western moorings. The fluctuations are weaker in the general direction which is perpendicular to the topography, also the near bottom current fluctuations at 069 are a little more polarized than at 96 m from the bottom. This may be an effect of the slightly steeper topography at the two western moorings, also the relative effect of the bottom slope on near bottom currents as against currents higher in the water column. The small counter clockwise rotation of mean flows and the principal axes of the fluctuating flows between 06901 and

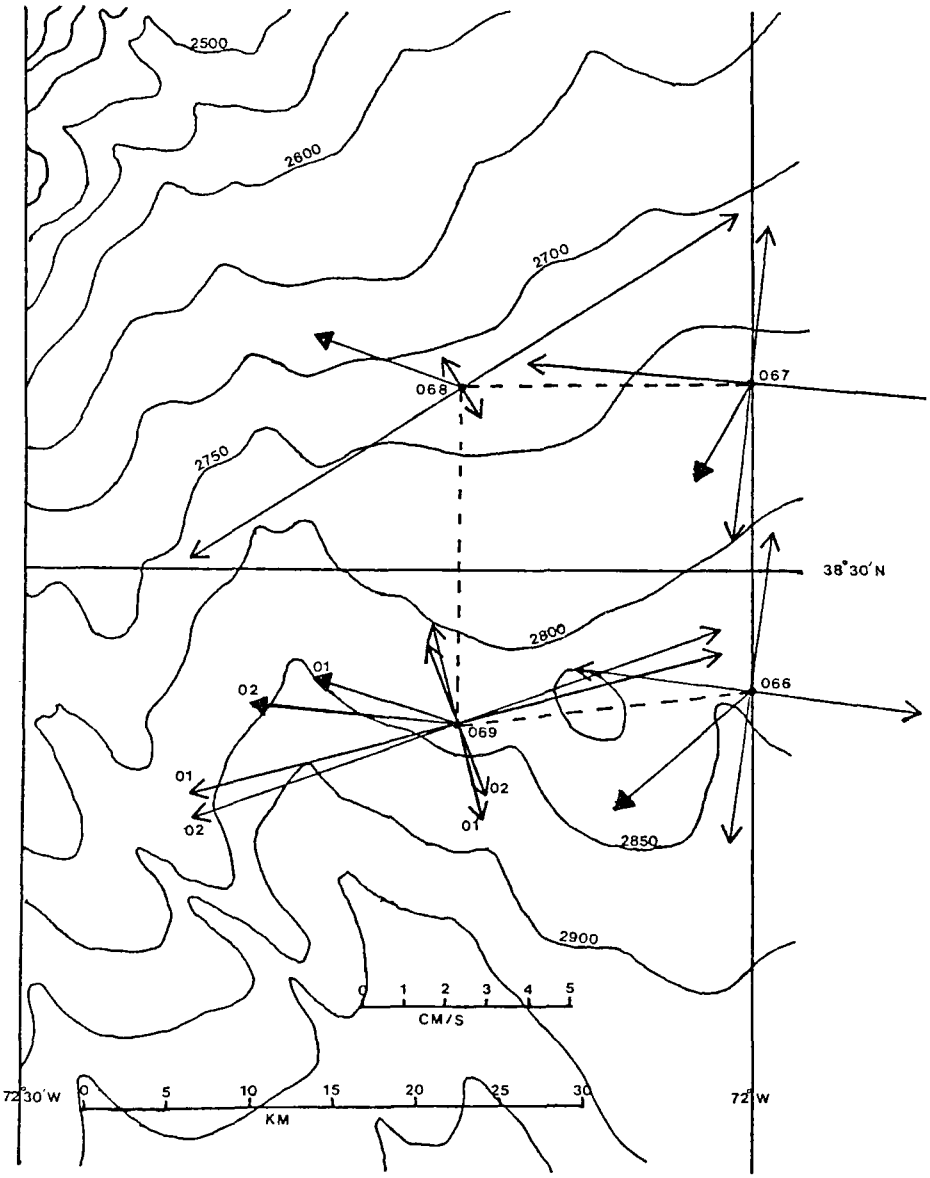

Figure 4.1. Bathymetric map of the 2800 m dumpsite showing the location of the moorings. The solid arrows show the mean flow for each meter and the open arrows are the principal axes with length proportional to the standard deviation of the filtered currents.

06902 is probably an effect of Ekman turning in the bottom boundary layer (Weatherly and Martin, 1978). There is also an increase in kinetic energy moving from the SE corner to the NW corner as shown by the increase in the sum of the amplitudes of the fluctuating components.

Table 4.1 shows the statistics in the rotated frame of reference with V component parallel to the slope. The angle brackets <> denote time averages and primes denote instantaneous deviations from the mean. The momentum flux $\langle U'V' \rangle$ is substantial and directed downslope for all the records as predicted by the theory. Negative momentum fluxes are also calculated for the Rise Array (Luyten, 1977; Thompson, 1978) for water depths less than 3000 m. There are theoretical reasons, reviewed by Hogg (1981), that the distribution of momentum flux across the upper rise may force the observed westward flowing mean current. The eddy heat fluxes $\langle U'T' \rangle$ are very small compared with the mean heat fluxes, as consequence of U' and T' being nearly in quadrature. The eddy heat fluxes are responsible for non-advective long-term diffusion of heat therefore, they can be regarded as an analogue to the dispersion by the fluctuating currents of any dissolved constituent or passive scaler quantity. The fact that eddy heat fluxes are small compared with the heat flux due to advection by the mean currents indicates that the dispersion by fluctuation components of velocity is relatively small compared with transport by the mean currents. The temperature variance $\langle T'^2 \rangle$ shows least energy at 066 and most energy at shallowest mooring 068 similar to the kinetic energy as remarked upon above. There is some decrease of $\langle T'^2 \rangle$ with depth of the records at 069, but the kinetic energy is almost identical at the two depths.

Comparison of these zero order statistics with the Rise Array and Site D measurements shows that the means and variances are very similar at comparable depths (Luyten, 1977: Table I).

4.2 Time Dependent Motions

The low passed filtered currents are shown in the vector plots (or stick plots) (Figure 4.2) for both East and North and rotated coordinate systems. The time series plots of the east and north components are shown separately in Figure 4.3, and both filtered and unfiltered temperature records are shown in

EPA CURRENT METER STATISTICS

Start date: August 3, 1976 Length = 98.5 days 45° Rotation

Meter	$\overline{U}$	$\overline{V}$	$\overline{T}$	$\langle u'^2 \rangle$	$\langle v'^2 \rangle$	$\langle u'v' \rangle$	$\langle \overline{U}\,\overline{T} \rangle$	$\langle \overline{V}\,\overline{T} \rangle$	$\langle T'^2 \rangle$	$\langle u'T' \rangle$	$\langle v'T' \rangle$
06601	-0.28	-4.19	2.46	16.74	15.09	5.95	- .69	-10.31	.00868	.0519	.0783
06701	0.78	-2.61	2.49	22.24	18.50	10.20	1.94	- 6.50	.01328	-.0701	-.0452
06801	-3.26	-1.58	2.50	13.16	45.15	7.62	-8.15	- 3.95	.01614	.0766	-.2282
06901	-2.97	-1.72	2.65	19.31	28.70	8.60	-7.85	- 4.56	.00938	.0101	-.2452
06902	-3.68	-2.91	2.46	17.80	31.58	8.92	-9.05	- 7.16	.00773	.0410	-.1511

Table 4.1.

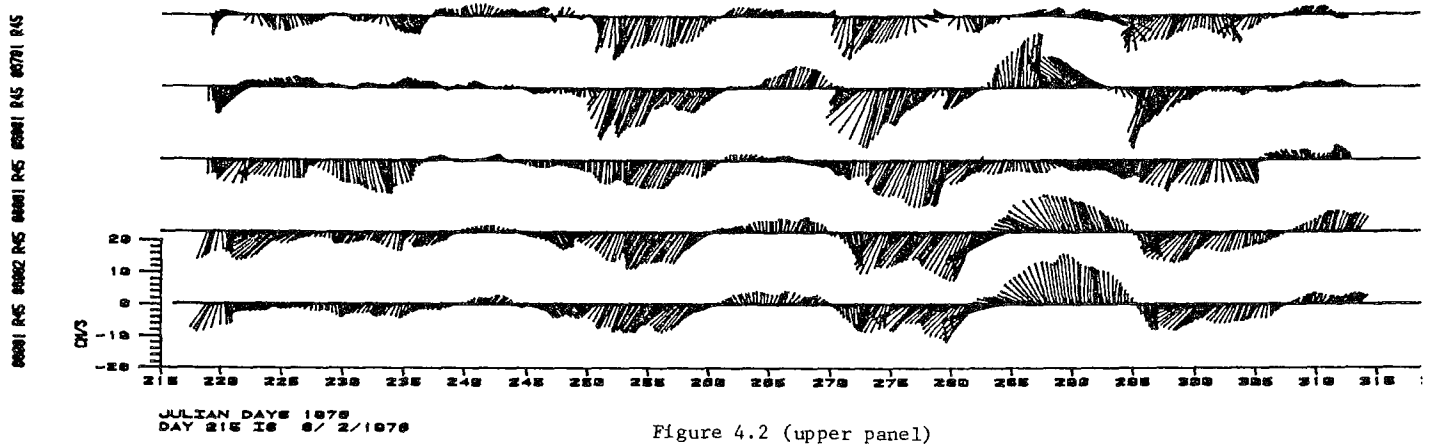

Figure 4.2 (upper panel)

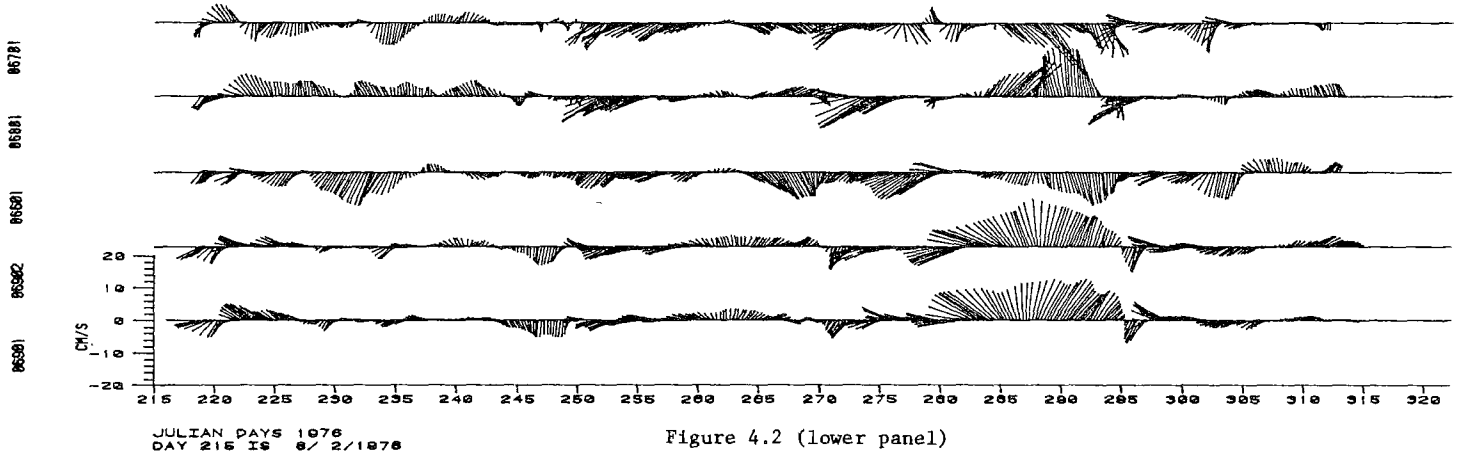

Figure 4.2 (lower panel)

Figure 4.2. Stick plots of the low passed filtered currents in the north and east frame of reference (lower panel) and in the rotated frame (upper panel).

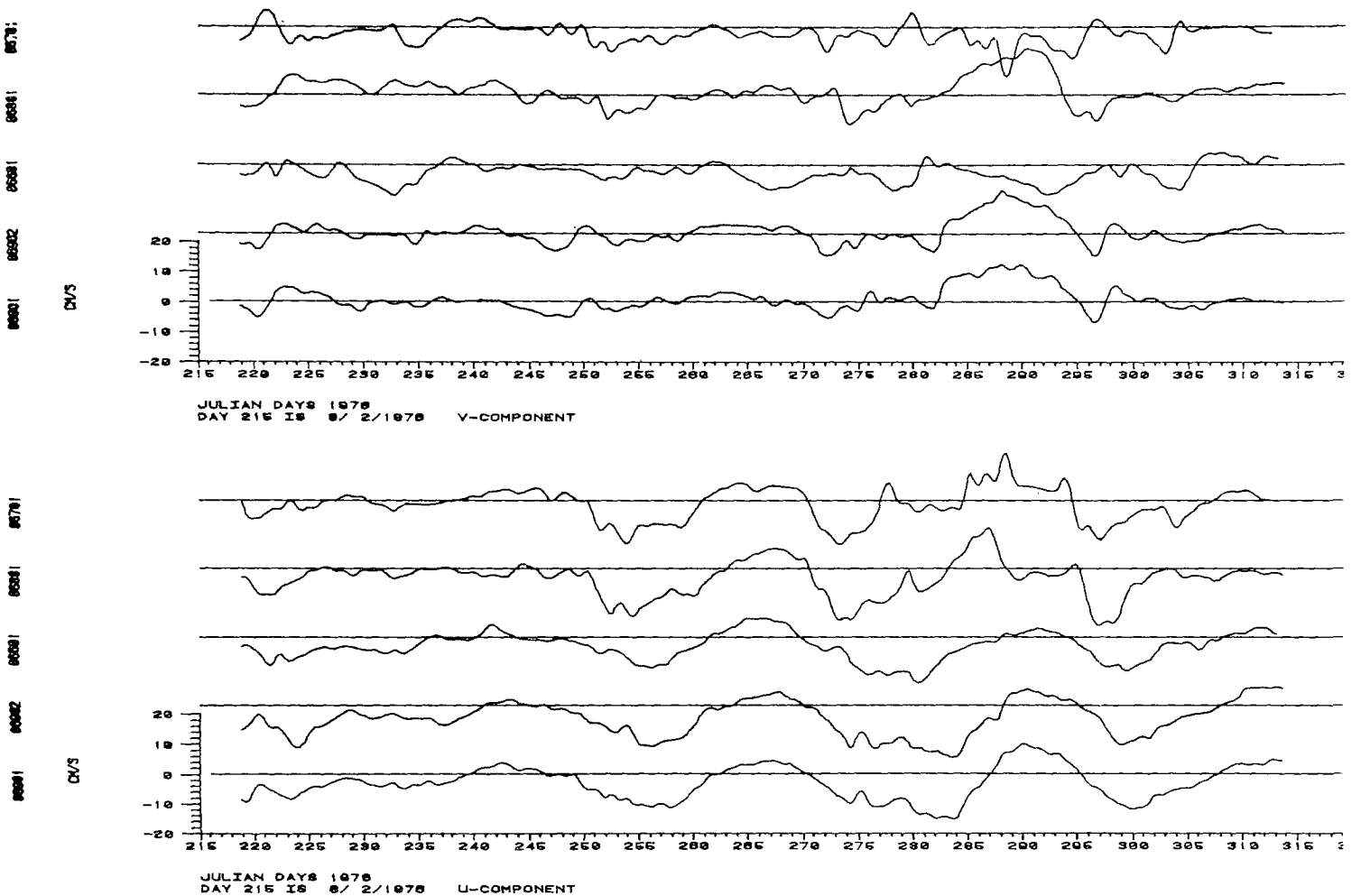

Figure 4.3. Time series plots of the low passed filtered U (East) and V (North) components for the five current meters.

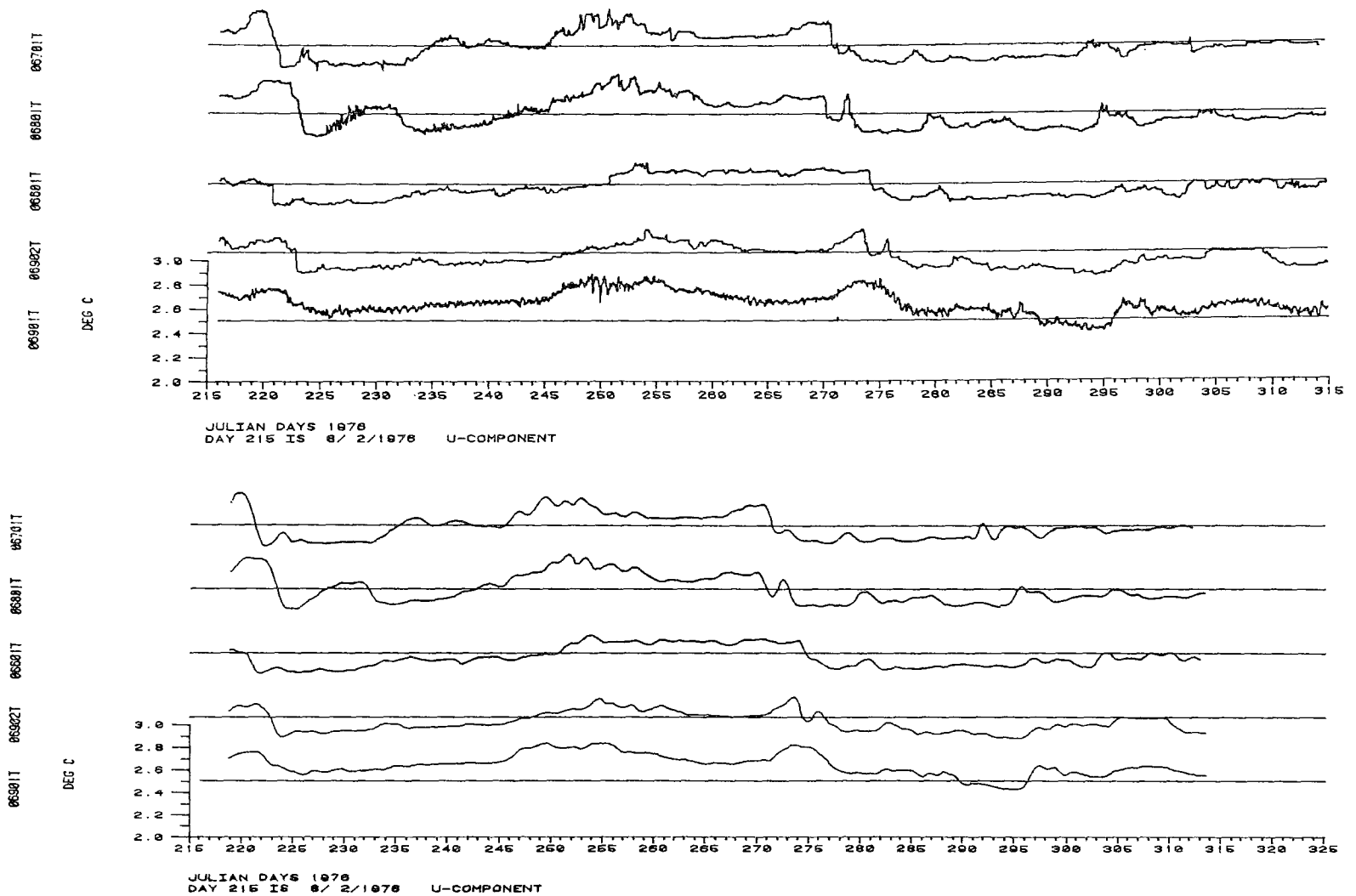

Figure 4.4. Unfiltered and low passed filtered temperature time series plots for the five meters.

Figure 4.4. Immediately apparent are low frequency fluctuations with periods of the order 15-20 days. Magnitudes vary from periods of low currents of less than 5 cm/s to large events where speeds can approach 20 cm/s. The longer period fluctuations are visually coherent over the array for some events (i.e. days 245-265, Figure 4.2), but show some striking differences in others. Thus, between days 260 and 295, the western moorings 068 and 069 show northeasterly to northerly currents while 067 and 066 show southerly or southeastern flow. This is rather remarkable considering that the moorings are only separated by distances on the order of 15-20 km. The moorings of the Rise Array, separated by distances on the order of 50 km, also show a similar type of spatial variability (Luyten, 1977). Also in evidence from these time series plots, particularly the temperature plot (Figure 4.4), is a propagation of disturbances from the northeast to the southwest. Particularly note the sharp temperature jump of about 0.2°C as it moves through the array between days 272 and 276. Comparing Figure 4.4 with 4.2 shows that it is associated with a current reversal and relatively strong flows towards the southeast.

The most energetic motions are apparently associated with motions with periods greater than a week. This is clearly illustrated by plotting the power spectra on an energy preserving plot. Figure 4.5 shows the kinetic energy spectra of 06901 and 06902 where equal areas under the curve represent equal amounts of energy. The peak in the spectrum is at about 0.06 cycles per day (cpd) ($\sim$ 16 day period) which is close to that reported at site D by Thompson (1977), where much longer time series were available for the spectral estimates. It is noted that the three month time series is just long enough to satisfactorily resolve this peak. The energy falls by an order of magnitude from this peak at 16-day period for periods shorter than about eight days. This is associated with the cut-off frequency for short topographic Rossby waves, $N\alpha$. Thus, the steeper the bottom slope the more wave energy can be supported at higher frequencies. The existence of this cut-off frequency explains why there is a gap in the energy spectra for periods between eight days and one day. For periods shorter than one day, tidal and inertial motions become dominant. An estimate for the bottom slope, α, is a little difficult to make, given the variable topography, but a reasonable value is about 0.0057, and a typical deep water value of N is $1.5 \times 10^{-3}\ s^{-1}$ gives a maximum frequency of about an 8.5 day period. If N is estimated from the mean

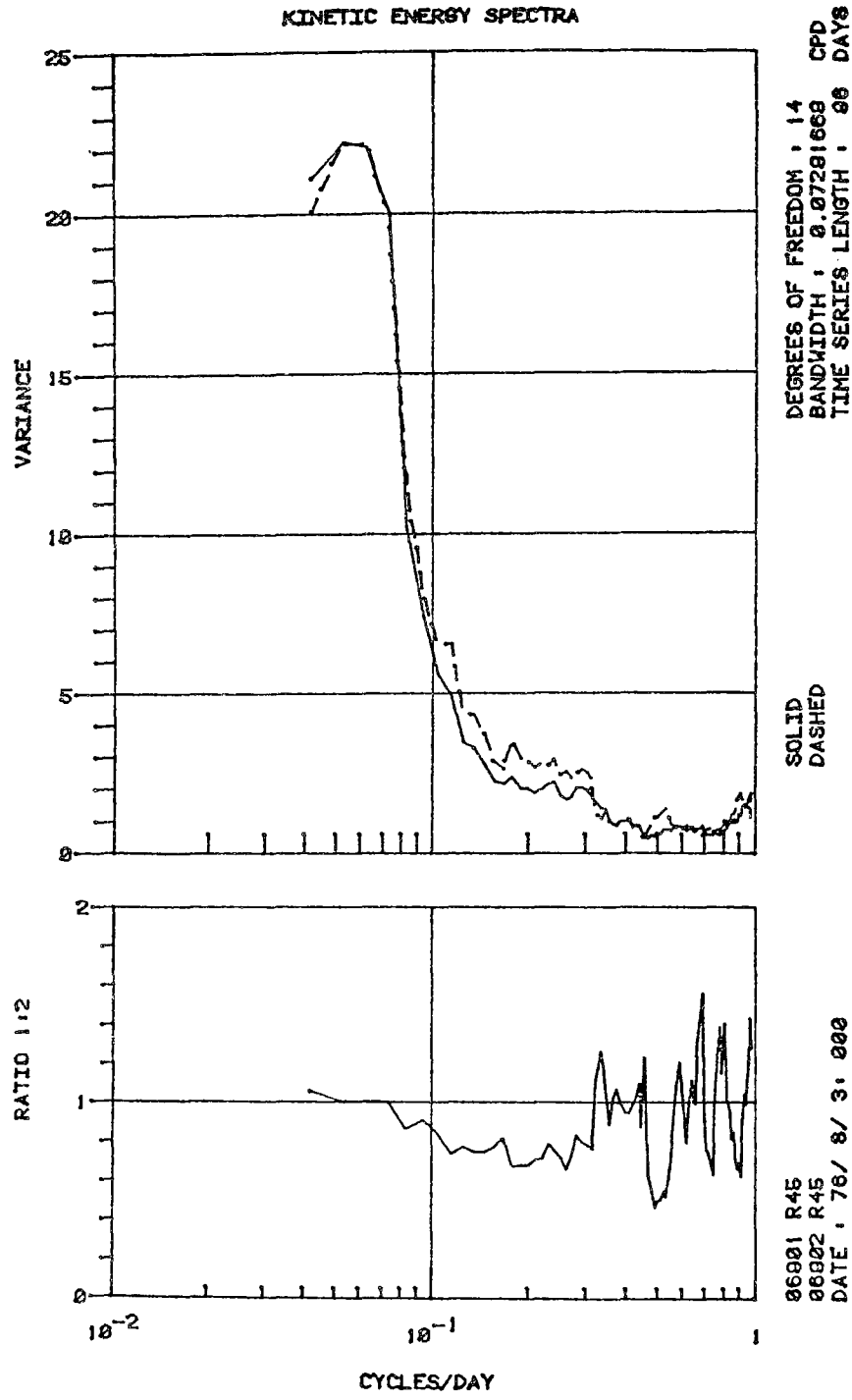

Figure 4.5. KE spectra for 06901 and 06902 plotted on an energy preserving plot. The lower panel gives the ratio of KE at 06901 to 06902 as a function of frequency.

temperatures (Table 4.1) assuming constant salinity, then $N \sim 1.33 \times 10^{-3} s^{-1}$ gives good agreement with the estimate of the cut off frequency given above and explains the low energy of the currents at frequencies between 0.1 and 0.6 cpd compared with the kinetic energy (K.E.) peak at 0.06 cpd (Figure 4.5).

The theory of topographic Rossby waves also predicts that the energy of the currents increases with depth. Therefore, the ratio of K.E. at 06901 to the K.E. at 06902 is predicted to be less than one at frequencies smaller than the cut off frequency. Thus K.E. ratio is shown in Figure 4.5 and is seen to be equal or slightly greater than one at the peak of the spectrum (0.06-0.07 cpd). However, this apparent discrepancy with theory may be explained by the fact that the bottom current meter 06902 is within the bottom boundary layer, where bottom friction would be expected to decrease the amplitudes of the current fluctuations from that of currents immediately above the boundary layer. The fact that the K.E. are equal at the 16-day period indicates that there is a maximum in wave K.E. between 96 m and 5 m off the bottom. If a bottom boundary layer depth (Ekman depth) of 10 m is assumed (Weatherly and Martin, 1978), then using the estimate for the horizontal wave length of 190 km (given in section 4.4 below) and $N = 1.33 \times 10^{-3} s^{-1}$, then equation (2.2) predicts a factor 1.076 increase in K.E. at 10 m from the bottom over the K.E. at 96 m from the bottom, if there is no frictional damping. This predicted increase is very small, so currents measured by 06901 are probably reasonably representative of currents outside the boundary layer region. The negligible difference in K.E. between 06901 and 06902, along with the near coincidence of principle axes for these measurements, indicates that bottom boundary layer frictional effects, including Ekman turning, have minor influences at 06902, when compared with low frequency fluctuations measured above the boundary layer.

4.3 Spectra

The power spectra are plotted in Figures 4.6-4.10 for velocity spectra, and 4.11-4.13 for temperature spectra. The former group was plotted using rotary components where the velocity vector is decomposed into clockwise (-) and anticlockwise (+) components rotating at constant angular velocity equal to the frequency. This form of presentation has the advantage that the rotary

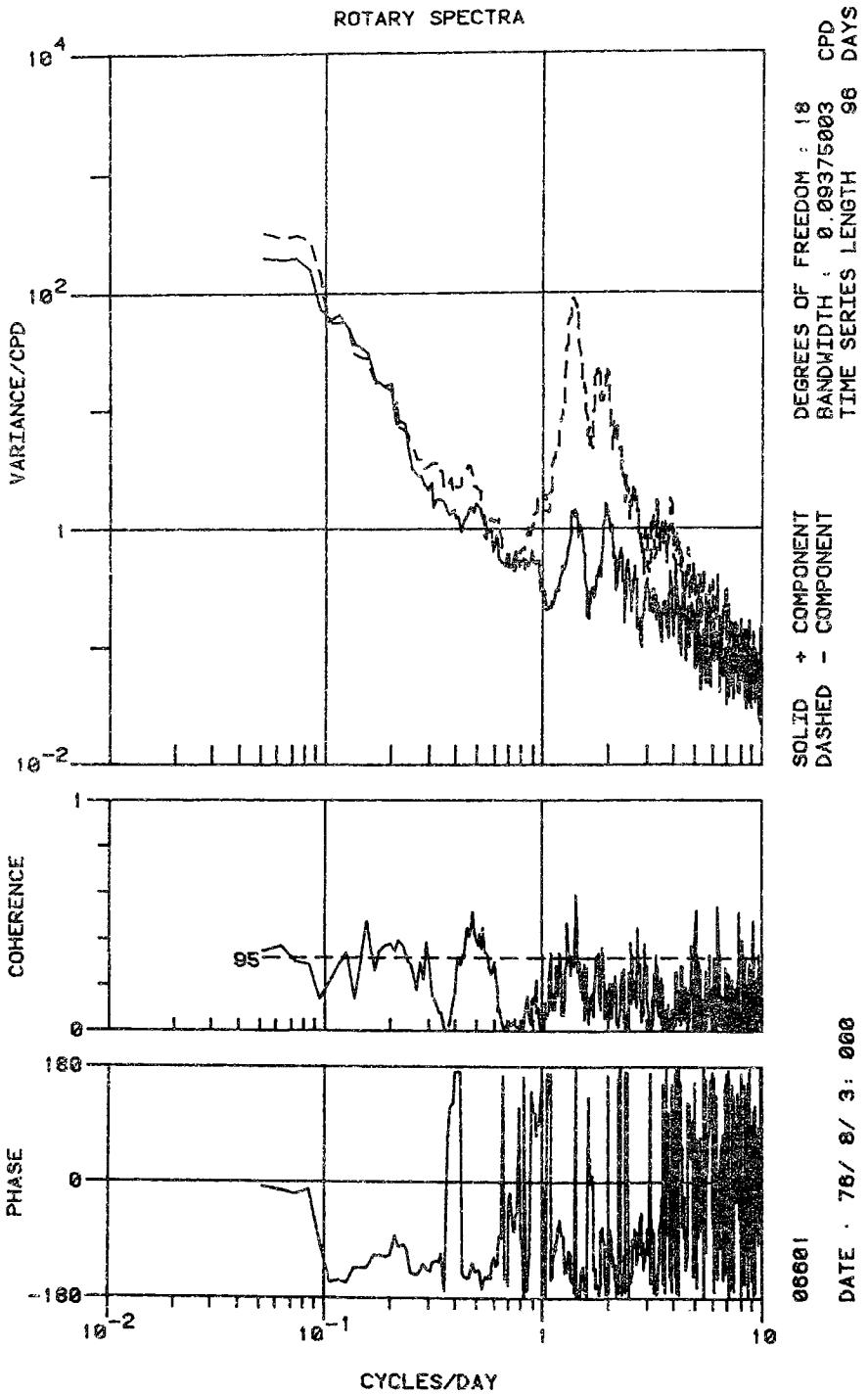

Figure 4.6. Rotary power spectra for meter 06601.

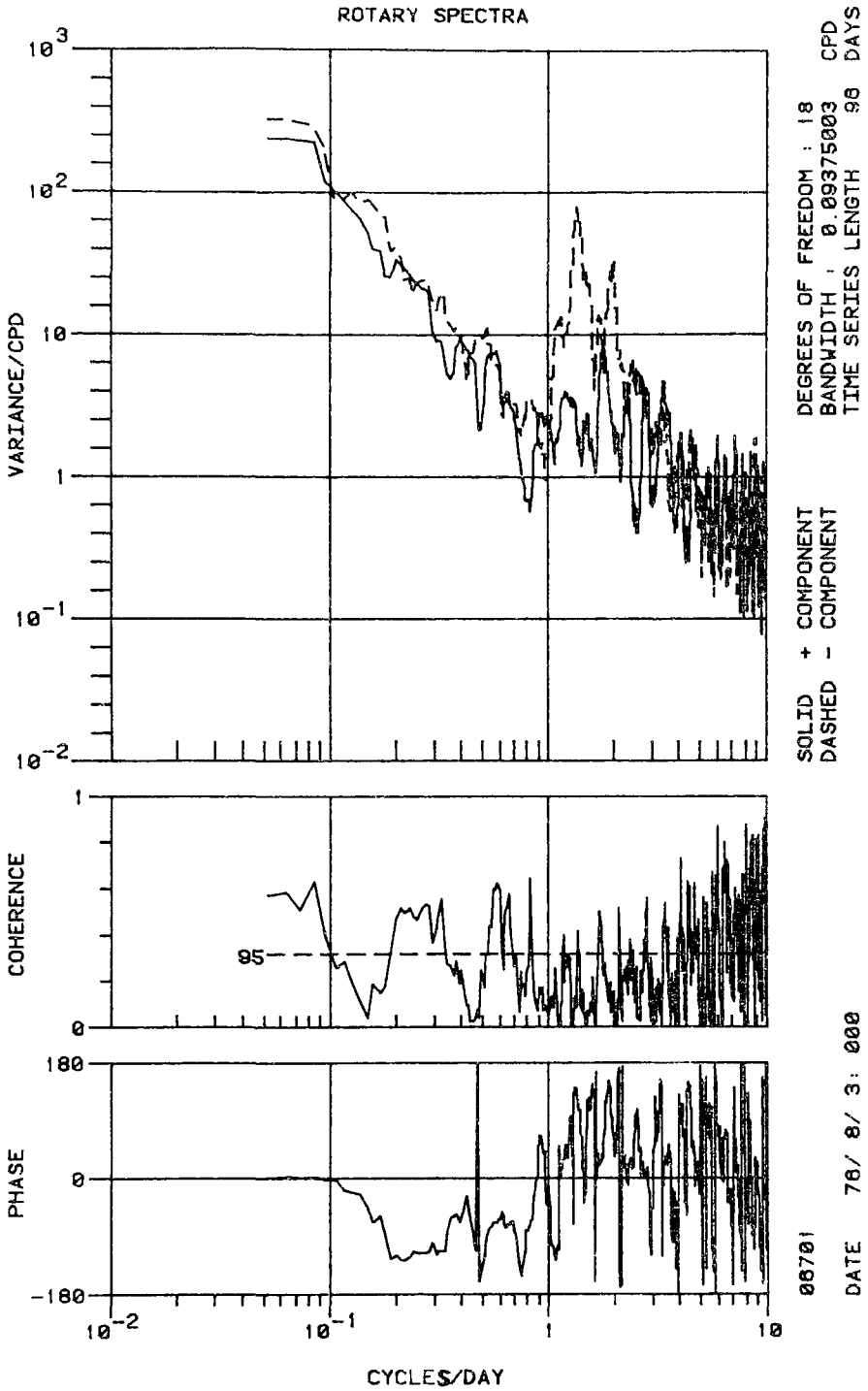

Figure 4.7. Rotary power spectra for meter 06701.

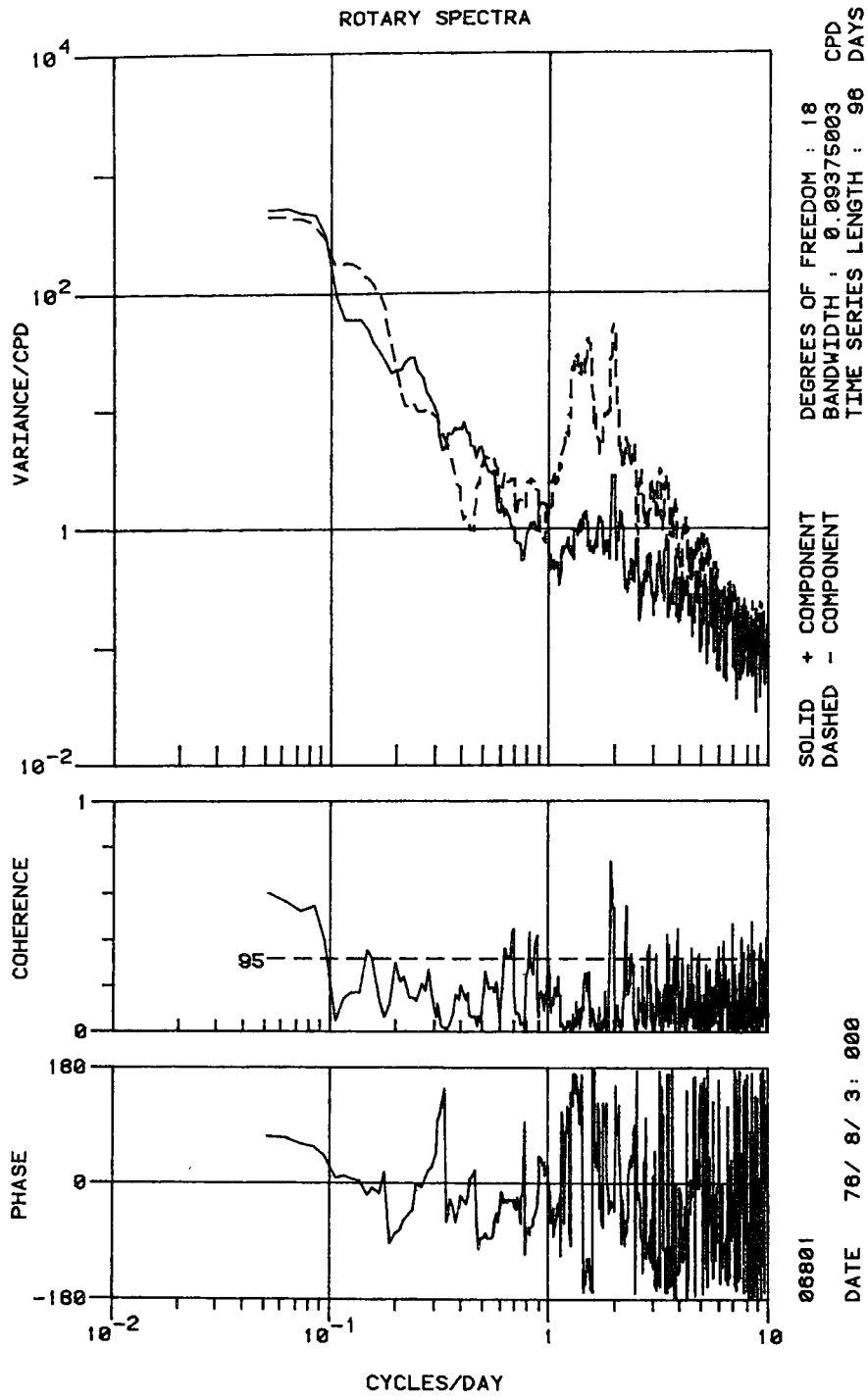

Figure 4.8. Rotary power spectra for meter 06801.

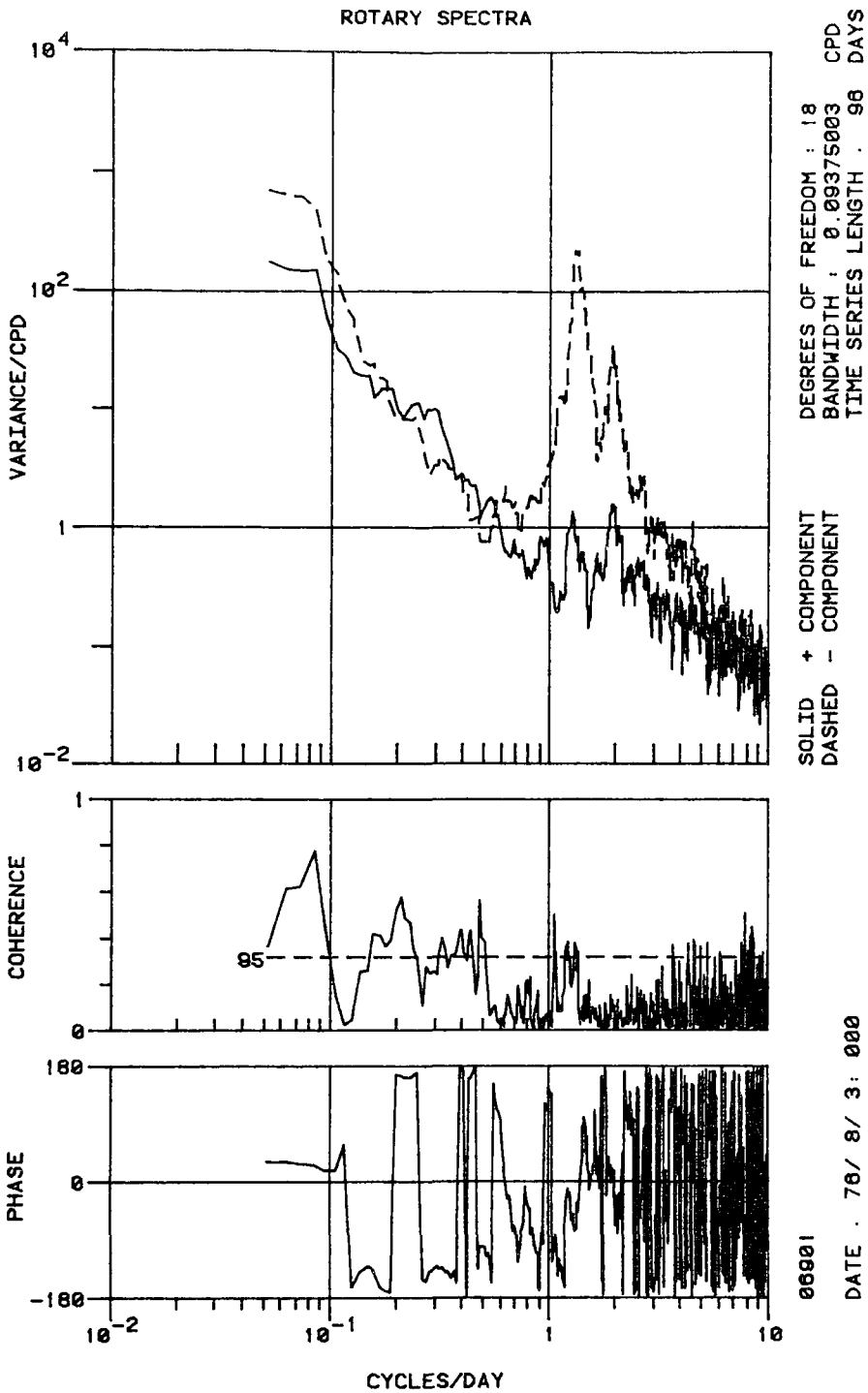

Figure 4.9. Rotary power spectra for meter 06901.

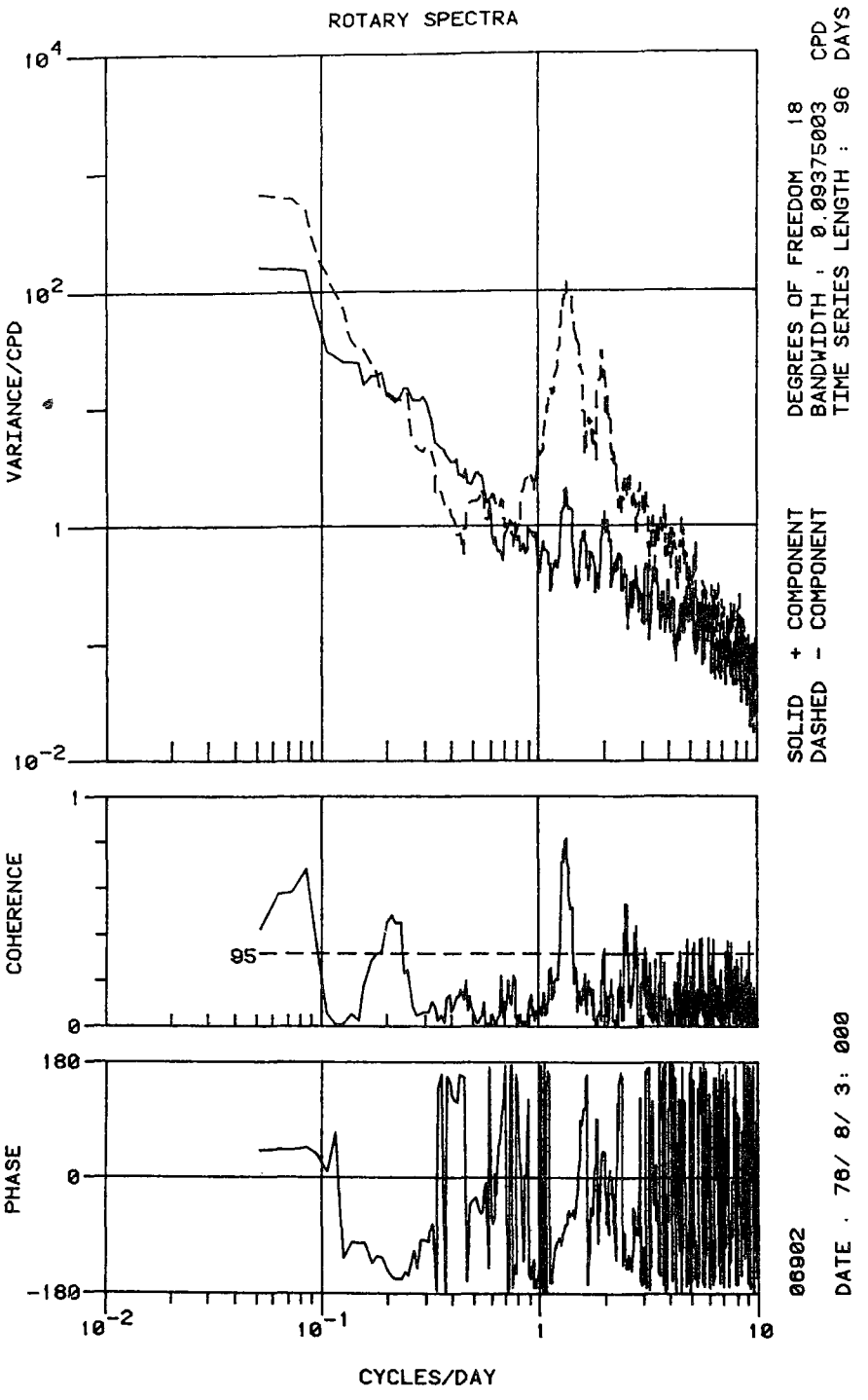

Figure 4.10. Rotary power spectra for meter 06902.

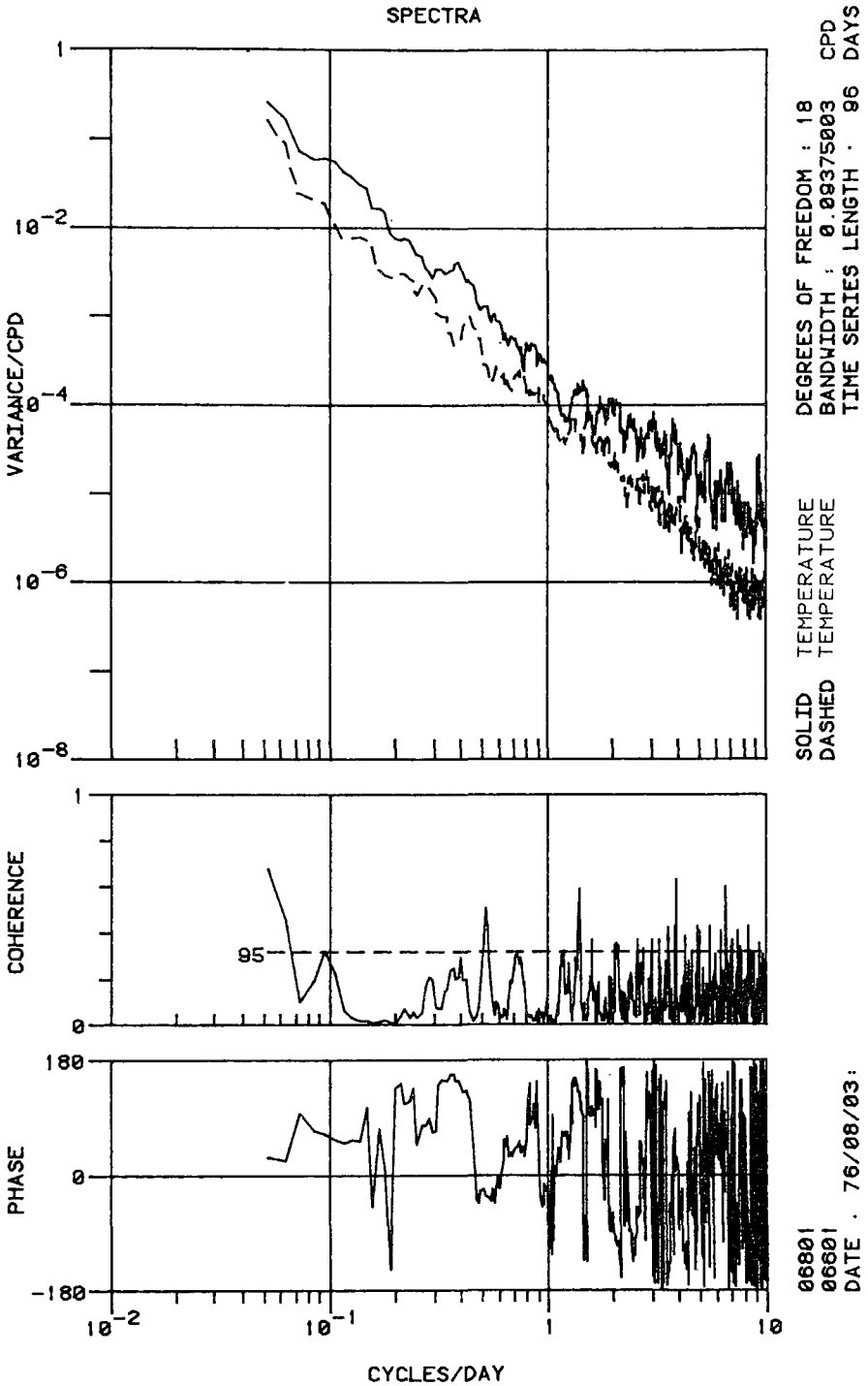

Figure 4.11. Temperature power spectra, coherence squared, and phase for 06801 and 06601.

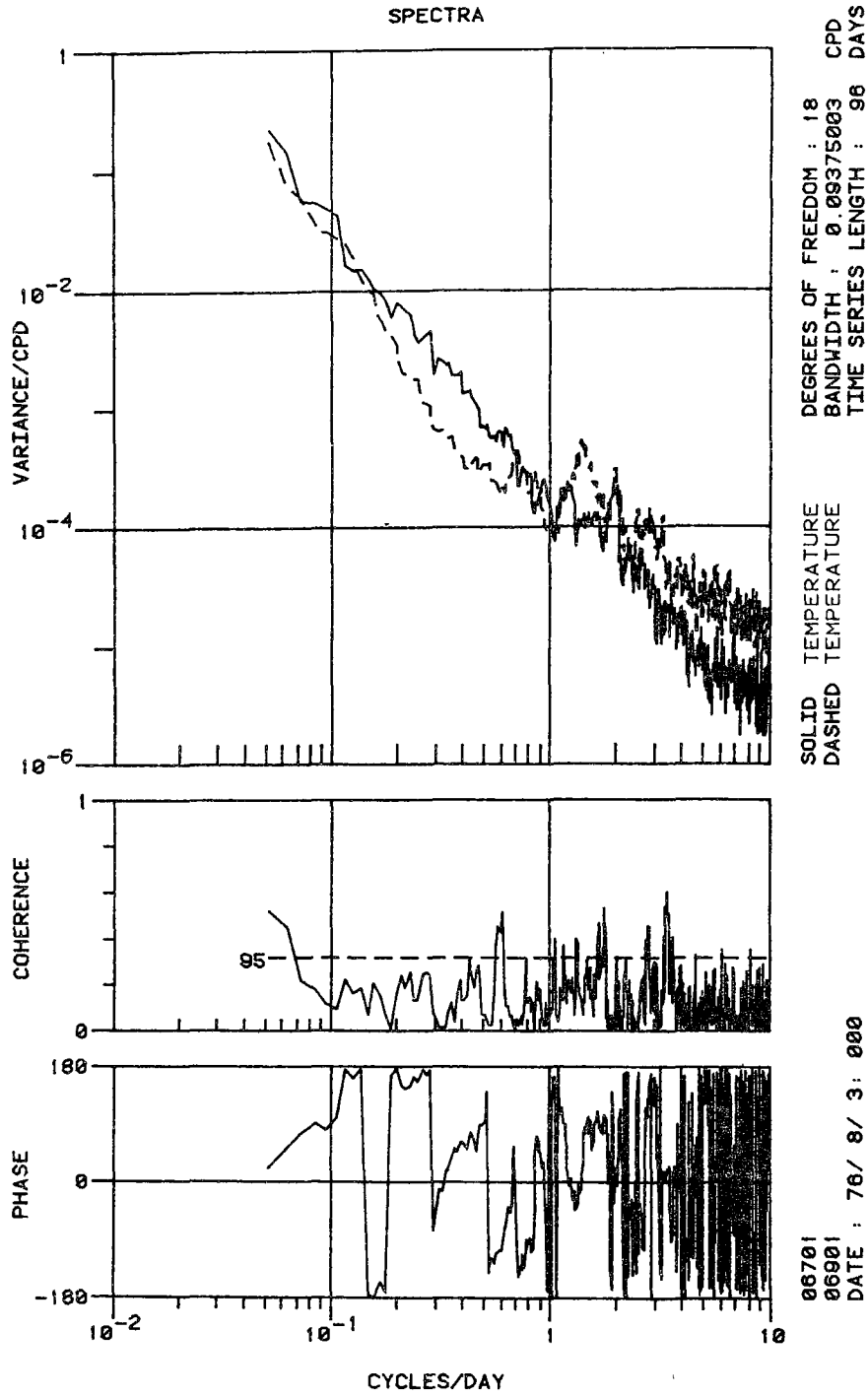

Figure 4.12. Temperature power spectra and coherence squared and phase for 06701 and 06901.

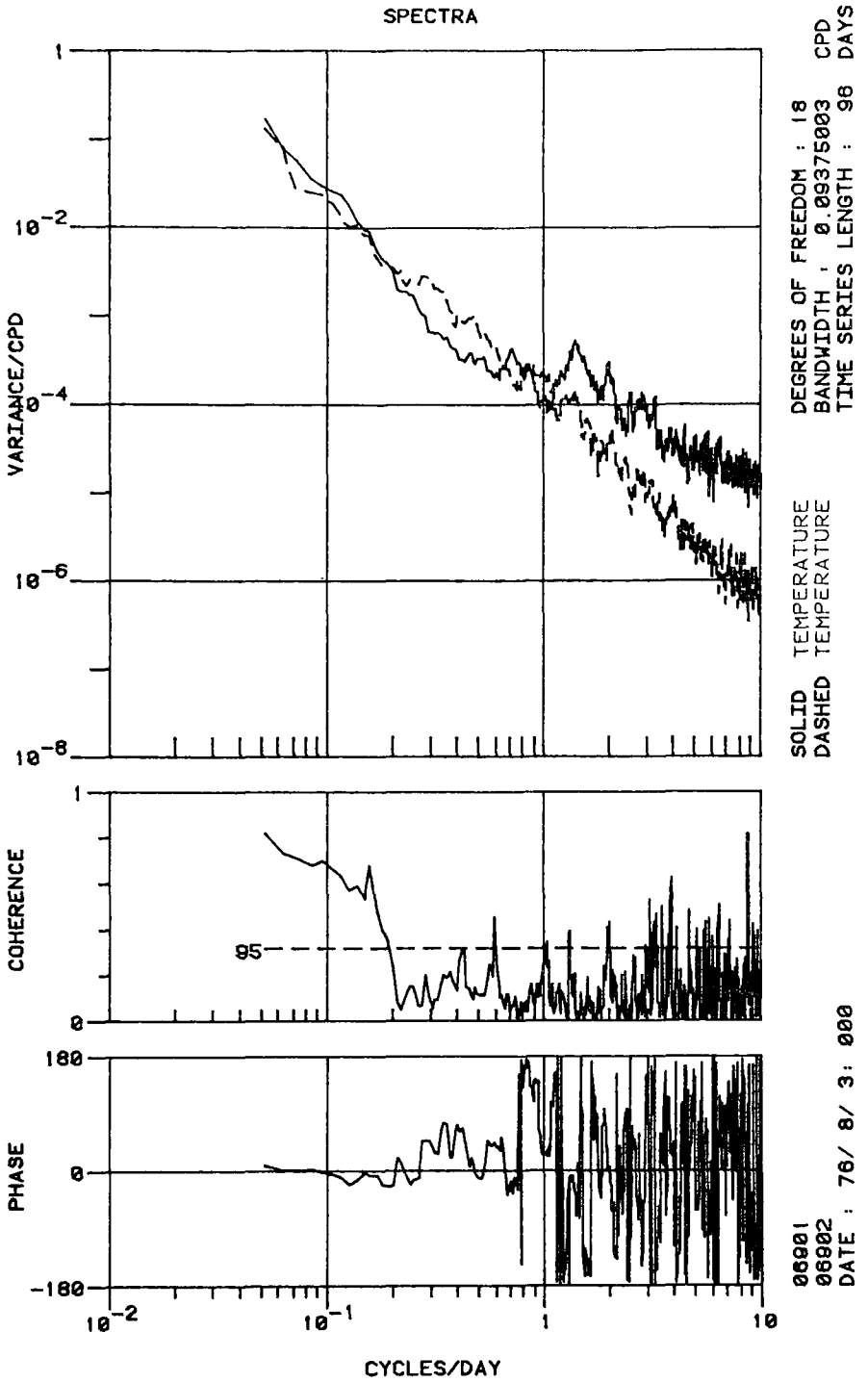

Figure 4.13. Temperature power spectra and coherence squared and phase for 06901 and 06902.

components are not dependent on the frame of reference. For example, the inertial and semidiurnal tidal peaks have an order of magnitude more energy in the clockwise rotating component were the V component leads the U component by 90°. Inertial and tidal motions will be discussed in later sections.

It is immediately apparent that only the currents from the meters on mooring 069 have one rotary component that dominates at frequencies less than 0.13 cpd. This is again the clockwise component (Figures 4.9 and 4.10). The other three records, the anticlockwise and clockwise motions have approximately equal energy and moderately high coherence (or stability in this context), indicating that the velocity fluctuations along the principal axes at low frequencies have phase lags of 0° or 180° approximately. The lowest panel of these plots, marked phase on Figures 4.6-4.10, is the angle of orientation from the x (or east) axis of the principal axes of the motion at frequencies where the coherence or stability is significant. (Purely rotary motion has no definable principal axes.) It can be seen that the orientation calculated for frequencies less than 0.1 cpd in Figures 4.6-4.10 is very similar to the orientation of the principal axes shown in Figure 4.1.

All the spectra are red and show lack of energy in the 1-day to 1-week band. Most of the minor peaks in this band are not significant at the 99% level.

4.4 Spatial Structure

The coherences at low frequencies in the topographic Rossby wave band, and thus the spatial structure of the current and temperature records, are investigated using Empirical Orthogonal Function (EOF) analysis in the frequency domain. This method has been described by Wallace and Dickinson (1972) and applied in a similar context to deep ocean currents by Hogg and Schmitz (1980) and Hogg (1981).

EOF analysis has a number of advantages over conventional coherence and phase analysis. The technique involves constructing the cross spectral matrix for a given frequency band, then using standard numerical methods to construct the eigenvalues and complex eigenvectors of the matrix. The eigenvectors are

called modes, and usually there are as many modes as sets of spectra used to construct the cross-spectral matrix. Each eigenvector mode is orthogonal to all the other modes (i.e. there is no coherence between modes) and represents the spatial structure of the records. The associated eigenvalue gives the variance of the mode, and since the eigenvalues are ordered by variance, only a few low numbered modes account for a large fraction of the total variance of all the records for the given frequency band. It is noted that EOF analysis is a statistical technique, and shape of the eigenvectors or modes is purely a reflection of the statistics of the data and may not necessarily have any physical significance. However, physical significance can usually be attached to a mode if it explains a large percentage of the total variance (50-70% for the first mode for this data), and the coherence squared of each data record with the mode is significant for a large majority of the data records. The eigenvectors are complex, so that they give the spatial structure in the form of amplitude and phase differences. The significance levels and confidence limits on these amplitudes and phases are given by the number of degrees of freedom used to calculate the cross-spectral matrix.

The similarity of the low frequency motions at 5.1 and 96 m from the bottom at mooring 069 has been discussed above and indicates that bottom boundary layer frictional effects only have a minor influence on the near bottom flows compared with flows above the boundary layer. Therefore, the spatial structure of the wave motions can be investigated using measurements from the four bottom current meters assuming that frictional effects can be neglected and currents are almost identical to currents above 100 m from the bottom. This extrapolation to water movements above the boundary layer assumes that the depth and shear structure of the bottom boundary layer are similar at all four moorings. Boundary layer effects on the Rossby wave motions are discussed further below.

The normalized cross-spectral matrix was constructed for all the variables (U,V and T) of the four bottom current meters (i.e. excluding 06901) and the eigenvalues and eigenvectors calculated for the low frequency band, $\omega < 0.146$ cpd. This first mode accounts for 48.5% of total variance. Only this mode was considered to be important, since the second mode had generally low coherence with individual records and accounted for only 26.2% of the total

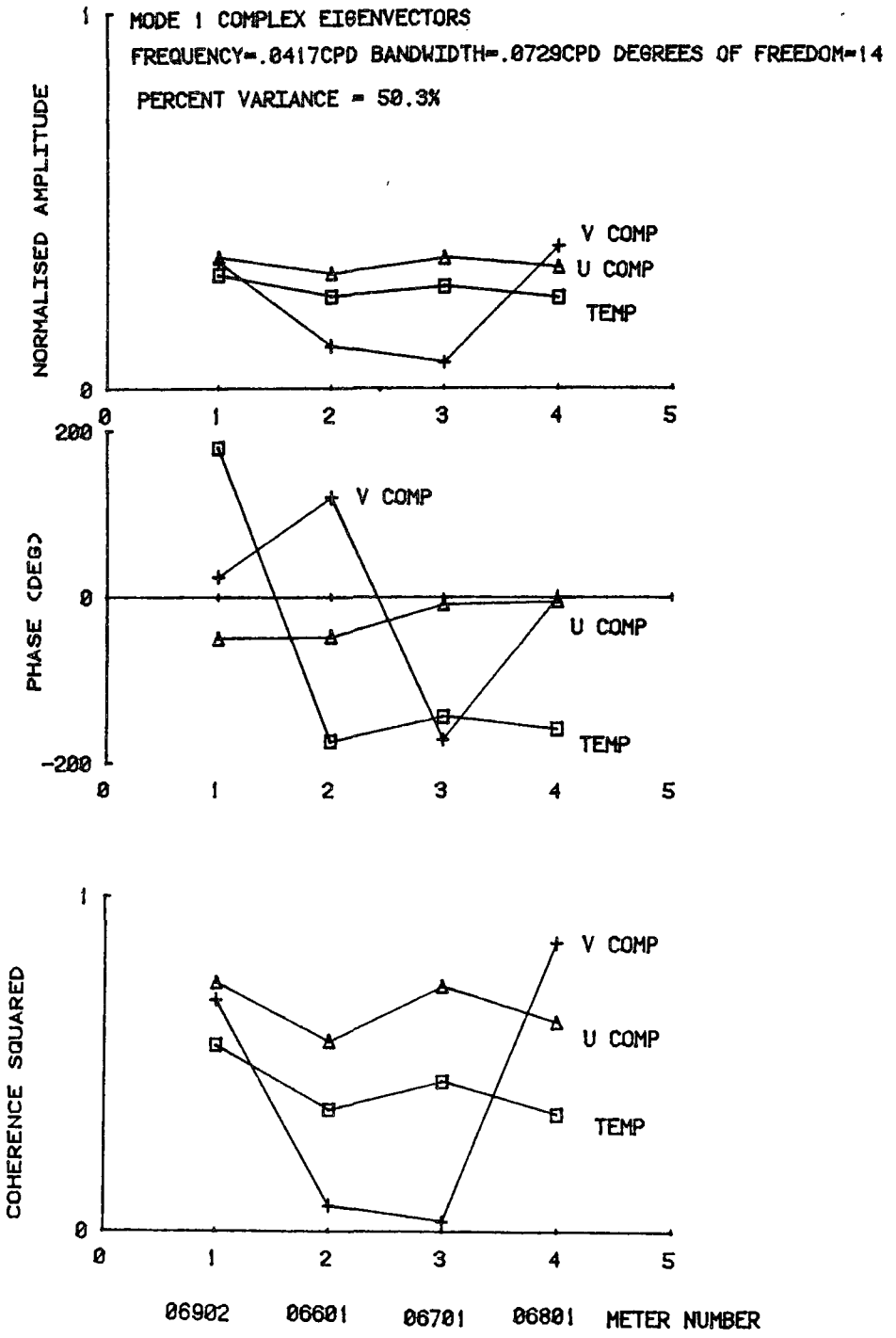

Figure 4.14. Amplitude, phase and coherence squared of the record with the mode for the first mode EOF of the low frequency band.

variance. There are 28 degrees of freedom, and the 95% significance level for coherence squared is 0.206. The analysis was also performed considering only the U and V components, also dividing the low frequency band into two, each with 14 degrees of freedom. The results for the lowest frequency band for U, V and T using 14 degrees of freedom are shown in Figure 4.14. Using U and V only, the first mode represents 73.4% of the total variance. However, the results from these latter calculations show only minor changes in structure when compared to Figure 4.14.

Examination of Figure 4.14 shows that U and T have similar spatial structure and reasonably consistent phase difference of $\sim 180°$. The V component magnitude and phases at moorings 066 and 067 have wide error margins due to the low coherence squared of the data with the mode, but even so, the phase differences are reasonably close to 180°. However, the V component leads the U component by about 90° for mooring 069, indicating predominantly clockwise rotary currents, whereas the U and V component are clearly in phase at 068. The theory of topographic Rossby waves outlined above requires phase differences between U and V of 0° or 180°; therefore, pure topographic wave motion is evidently being modified in the SW corner of the array. Phase differences between U and V, which differed from 0 or 180°, were also found by Thompson (1977) and Hogg (1981) for the Rise Array data.

The phases of U and T in Figure 4.14 indicate southward phase propagation. From these phase differences between the variables, the wave numbers can be calculated from

$$\Delta\phi_{ij} = k\,\Delta x_{ij} + \ell\Delta y_{ij} \qquad (4.1)$$

where $\Delta\phi_{ij}$ is the phase difference of a variable (U, V or T) between moorings, i and j, $(\Delta x_{ij}, \Delta y_{ij})$ is the spacing between the moorings in east and north coordinates, and (k, ℓ) are the horizontal wave numbers which are the reciprocals of the east and north components of the wave length. Estimates for k and ℓ were found by using the phase differences from the first mode for all four stations and using the variables separately and in combination and calculating the best fit by a least squares technique. The results are shown

EPA CURRENT METER DATA

Wave Number Estimates

(north and east coordinates)

Variables	Frequency (CPD)	Degrees of Freedom	Wave Number k (cycles/km)	l	$K = (k^2+\ell^2)^{\frac{1}{2}}$	Wave Length (km)	Angle (Degrees from North
U			.000196	-.005732	.005735	174	178°
V			-.022007	-.000943	.022027	45	268°
T	.0781	28	-.002148	-.004530	.005013	199	205°
U,V,T			-.007985	-.003735	.008815	113	245°
U,T			.000974	-.005131	.005223	191	191°
U,T	.0417	14	-.000552	-.004846	.004877	205	186°
U,T	.1146	14	-.005298	-.009326	.010711	93	210°

Table 4.2.

EPA CURRENT METER DATA

Vertical Phase Differences at Mooring 069

Frequency - 0.0781 cpd., Degrees of Freedom 28

Variable	Phase Difference 6901-6902	95% Sig. Level
U	12.7°	11°
V	14.7°	9°

Table 4.3.

in Table 4.2. Except for taking the phases from the first eigenmode, the estimates are made using essentially the same method as Thompson (1977).

Not unexpectedly, the most consistent results came from the least square solution using U and T together. The calculated wave vector points into the SW quadrant and the wavelength is approximately 200 km. Therefore, the topographic Rossby waves show a component of phase velocity directed towards the southwest or along the isobaths and there is good agreement with Thompson's similar calculations for Site D and the Rise Array (Thompson, 1977). If we divide the low frequency band into two, then the higher frequency has a shorter wavelength (93 km), and the wave vector is rotated towards the isobath direction when compared with the lower frequency. This is precisely the kind of behavior to be expected as the frequency increases towards the cut-off frequency, $N\alpha$.

The final comparisons with topographic Rossby wave theory to be made by using the dumpsite data are the vertical phase differences at mooring 069. Topographic Rossby waves should show essentially columnar motion with an increase in energy towards the bottom. The dumpsite data shows negligible increase in energy between 96 m and 5.1 m off the bottom, and it is therefore of interest to investigate whether the phase differences are significantly different from zero. Again, the EOF method is used to calculate the phase differences. The results are presented in Table 4.3 and show phase differences slightly greater that the 95% significance level for zero phase difference. Meter 06902 is within the bottom boundary layer; therefore, bottom frictional effects will affect the phase of the currents (Weatherly and Martin, 1978). The fluctuating currents within the boundary layer are predicted to lag the currents outside the boundary layer and this is confirmed in Table 4.3. The small phase lag, the small angle of Ekman veering seen in the mean and fluctuating low frequency currents (Figure 4.1), and the negligible reduction of kinetic energy at 06902 compared with 06901 indicates that current meter 06902 is close to the top of the boundary layer, thus the average boundary layer thickness may be similar to the 6-12 m indicated by Weatherly and Martin (1978) for their data in a stratified boundary layer above a sloping bottom, rather than the theoretical neutral boundary layer thickness of order 30 m.

4.5 Dispersion by Low Frequency Currents

The low frequency motions can be summarized as being dominated by topographic Rossby waves at frequencies lower than the cut-off frequency ($\sim$ 9-day period) which is determined by the stratification and the slope of the bottom. The peak in the low frequency spectrum falls at about the 16-day period. The wavelength of the topographic waves is on the order of 200 km and phase propagation is directed into the southwest quadrant with the propagation of energy being in the upslope direction. The motions seem to be bottom trapped with amplitudes of about 7 cm/s. The currents are evidently influenced by topography, particularly in the orientation of the principal axes and direction of the mean currents. The latter are substantial, averaging about 3-4 cm/s in a generally westward direction. As expected, there is very little energy in the 1-day to 1-week period of the spectrum. Figure 4.1 and Table 4.1 provide a good summary of the low frequency motions.

Dispersion by the low frequency motions is a stochastic problem for large space and time scales. An important measure of the time scales, or persistence of the currents are the auto correlations, $R_u(\tau)$, $R_v(\tau)$ and $R_T(\tau)$ for velocity and temperature,

where
$$R_u(\tau) = \frac{\langle U'(t)\ U'(t+\tau)\rangle}{\langle U'^2\rangle}, \text{ etc.}$$

The autocorrelations plotted against lag, τ, for the U and V components and temperature are shown in Figures 4.15-4.19. The velocity correlations fall to zero at lags of 3-7 days with the majority around 5-6 days and the temperature correlations at lags of 15-18 days. These times represent the memory of the velocity and temperature fields. Therefore, time scales on the order of 5-15 days are important for long time (order years) dispersion of radioactivity from the bottom. These correlation functions would play a fundamental role in any stochastic theory that may be developed to model long-term dispersion in the boundary layer (Csanady, 1973). (For an example of a stochastic model applied to climate variability, see Hasselmann, 1976).

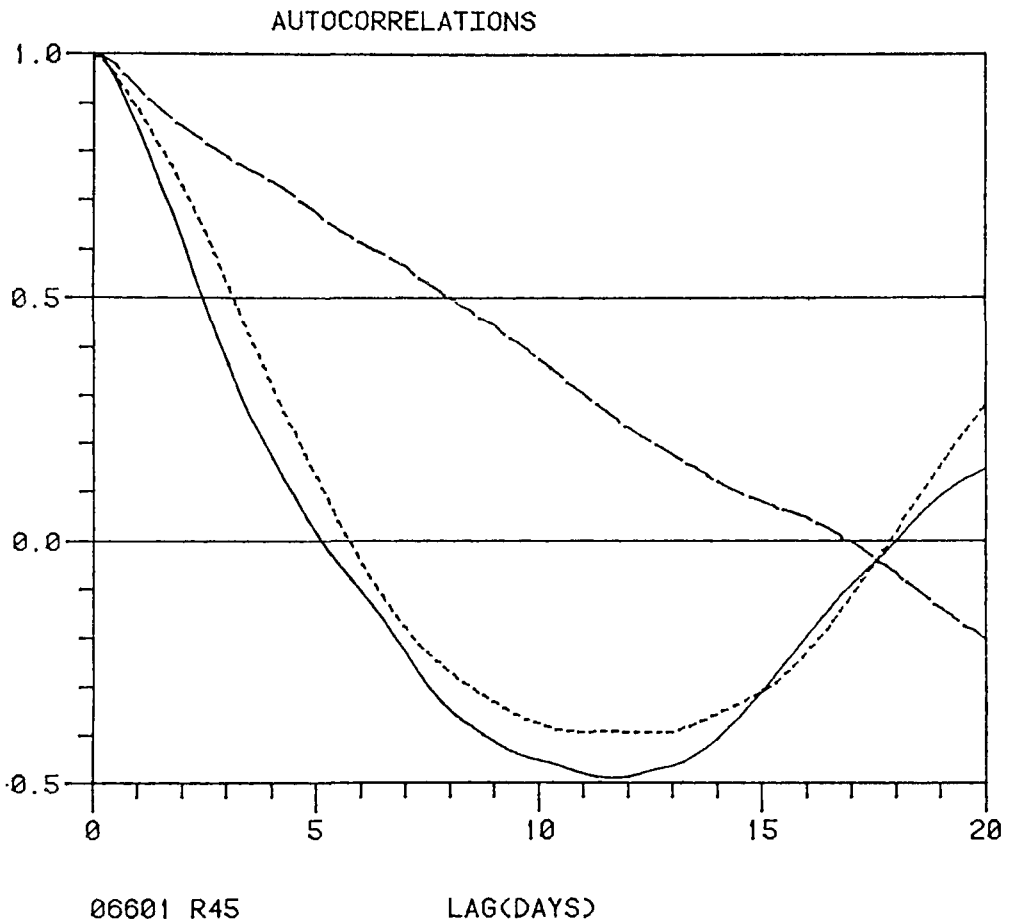

Figure 4.15. Autocorrelations as a function of lag, τ, for low passed data for meter 06601 (———) $R_u(\tau)$, (-----) $R_v(\tau)$, (— — —) $R_t(\tau)$

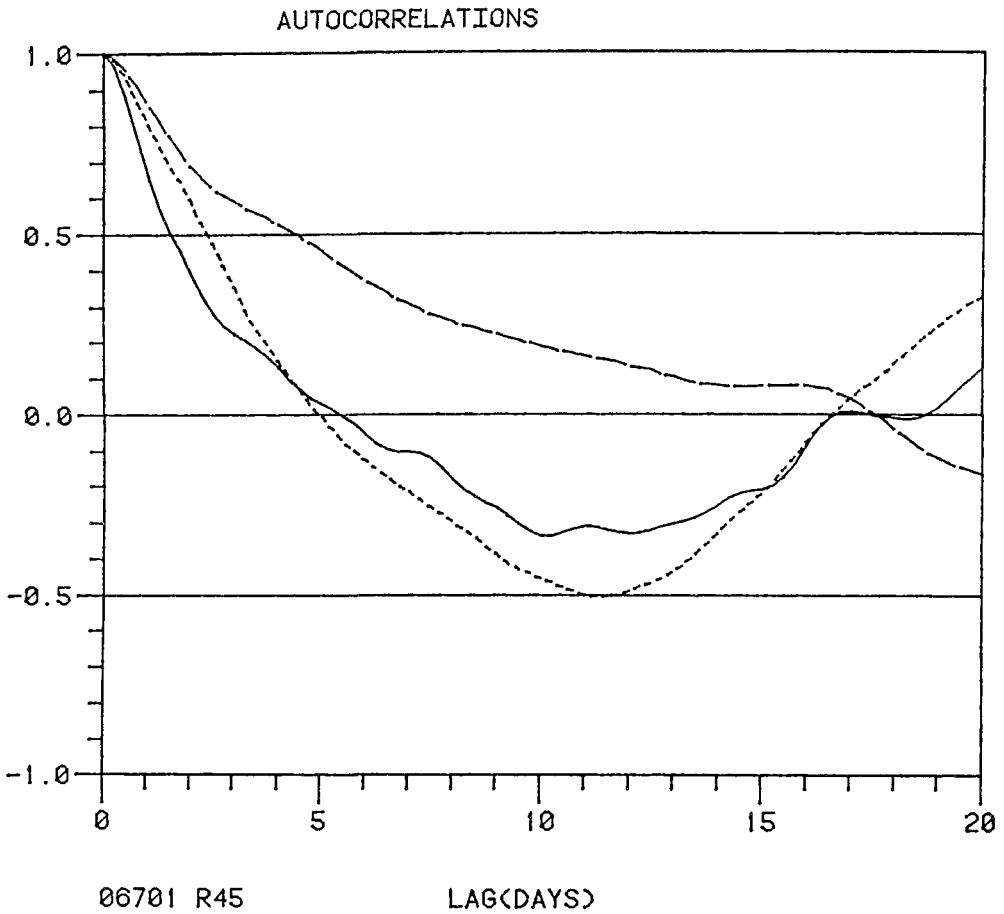

Figure 4.16. Autocorrelations as a function of lag, τ, fcr low passed data for meter 06701 (———)$R_u(\tau)$, (-----)$R_v(\tau)$, (— — —) $R_t(\tau)$

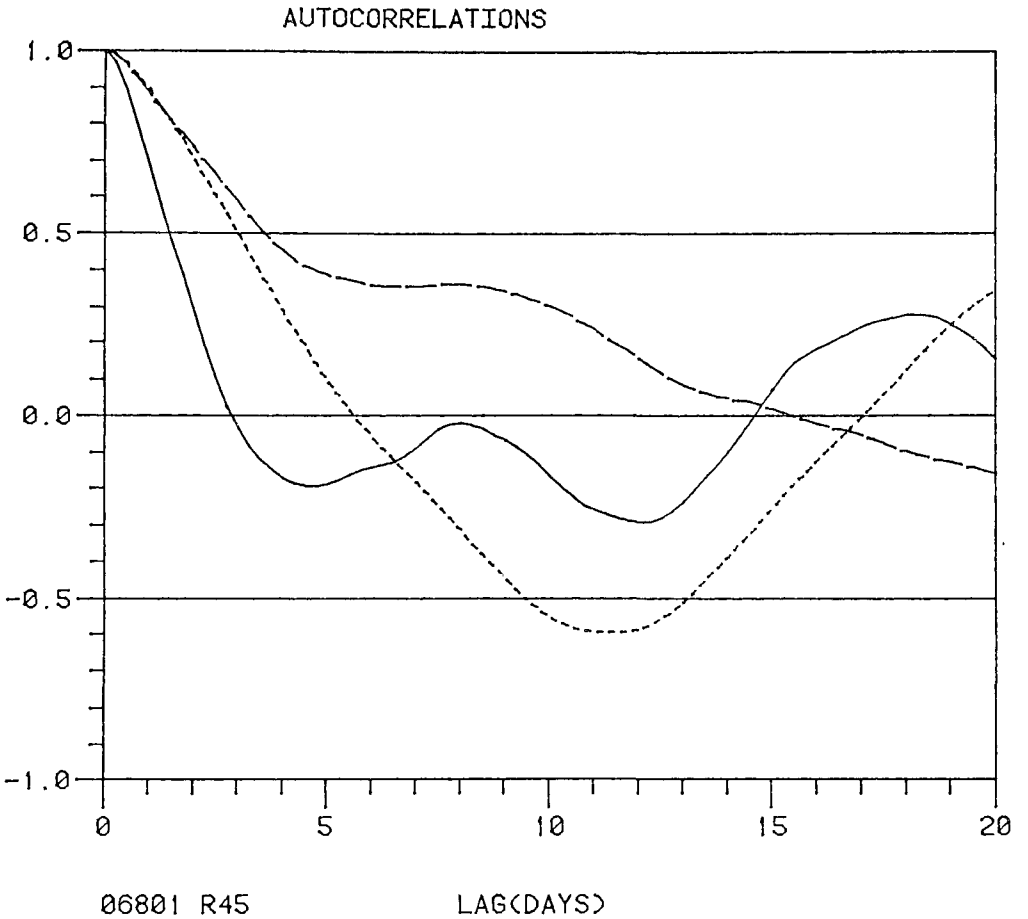

Figure 4.17. Autocorrelations as a function of lag, τ, for low passed data for meter 06801 (———)$R_u(\tau)$, (-----)$R_v(\tau)$, (— — —) $R_t(\tau)$

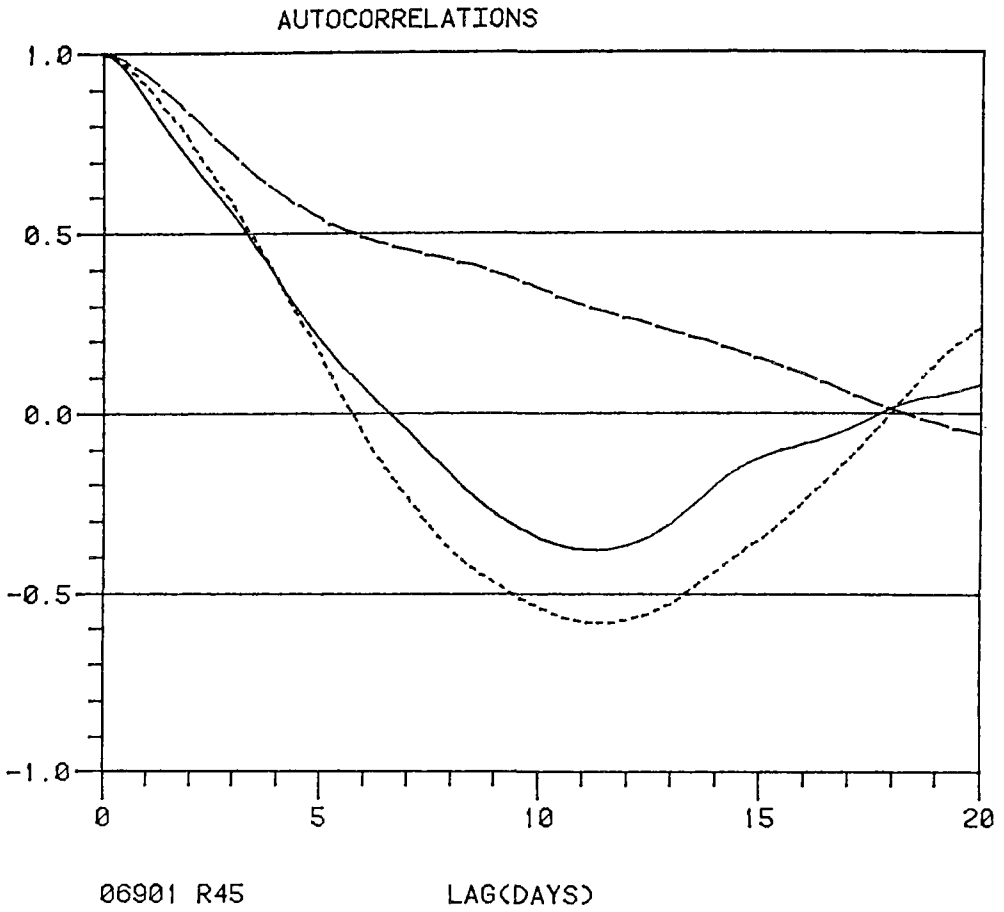

Figure 4.18. Autocorrelations as a function of lag, τ, for low passed data for meter 06901 (———)$R_u(\tau)$, (-----)$R_v(\tau)$, (— — —) $R_t(\tau)$

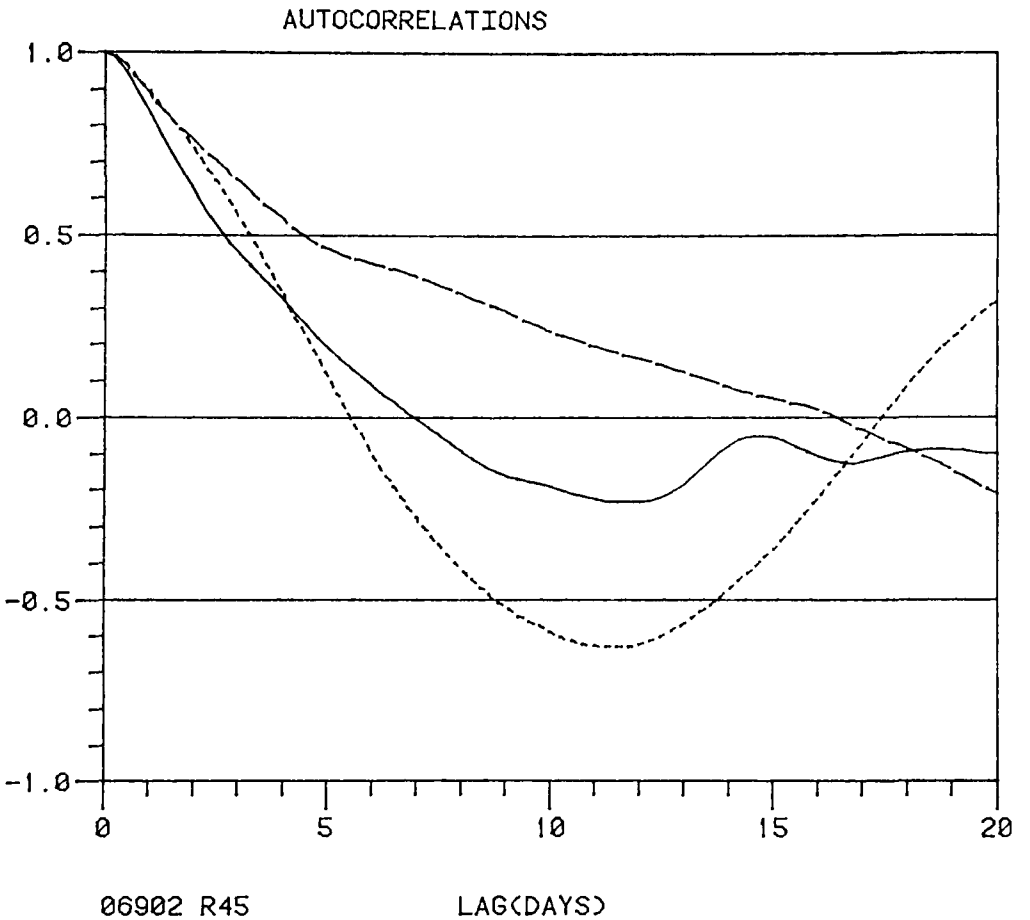

Figure 4.19. Autocorrelations as a function of lag, τ, for low passed data for meter 06902 (———)$R_u(\tau)$, (-----)$R_v(\tau)$, (— — —) $R_t(\tau)$

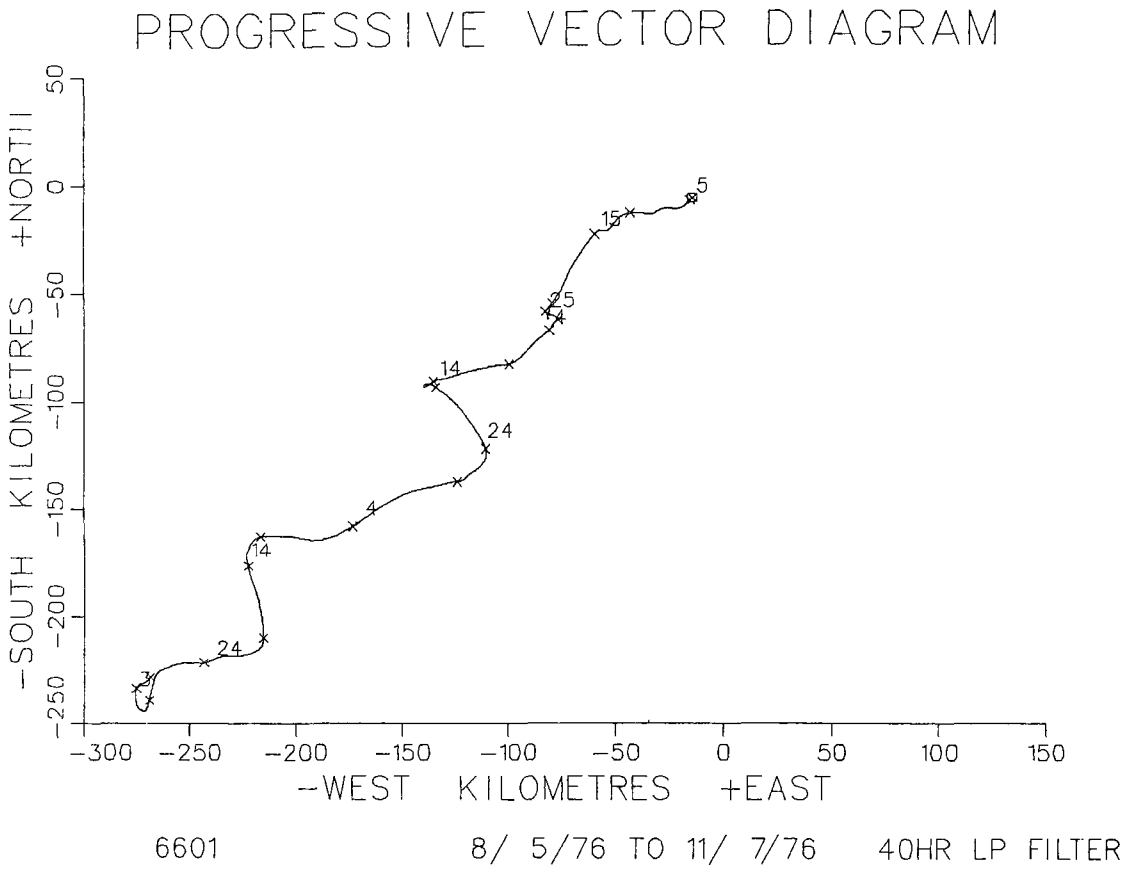

Figure 4.20. Progressive Vector Diagram for 06601. Low passed filtered data. The date is indicated every 10 days.

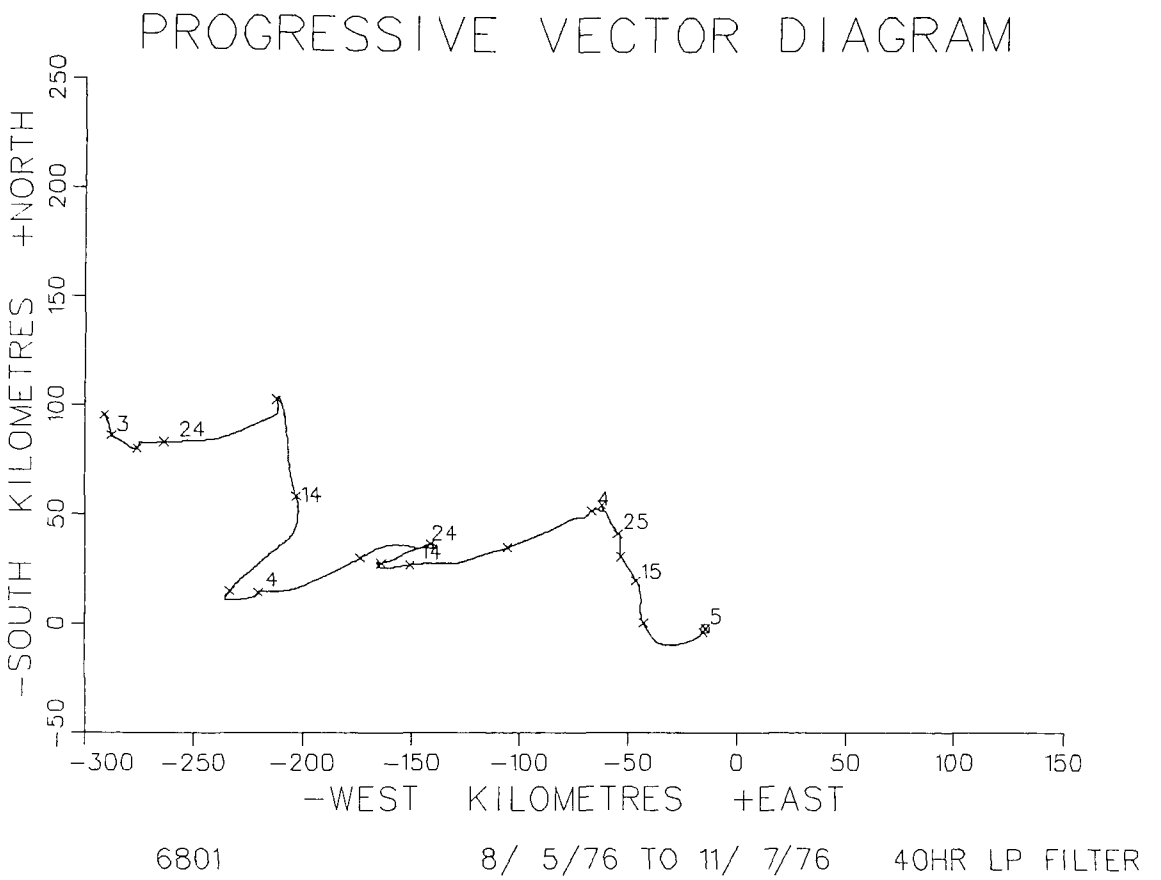

Figure 4.22. Progressive Vector Diagram for 06801. Low passed filtered data. The date is indicated every 10 days.

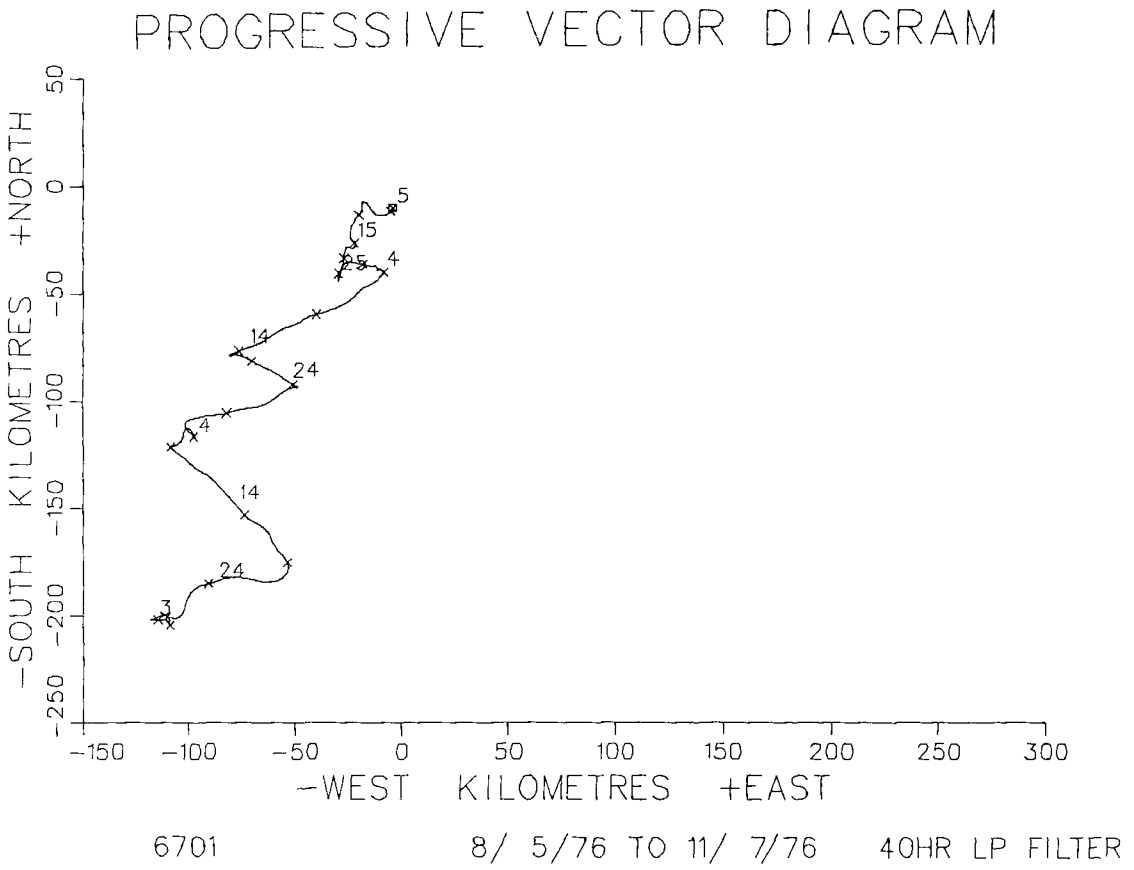

Figure 4.21. Progressive Vector Diagram for 06701. Low passed filtered data. The date is indicated every 10 days.

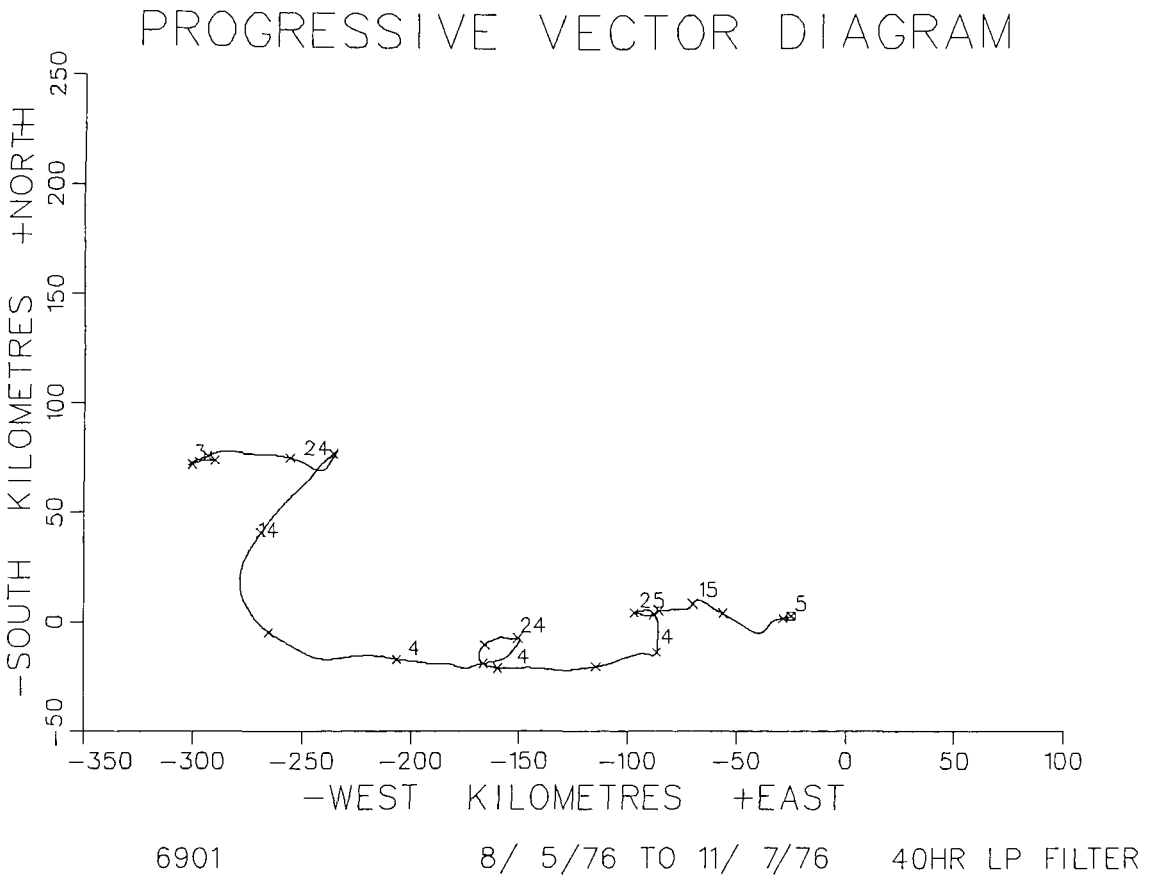

Figure 4.23. Progressive Vector Diagram for 06901. Low passed filtered data. The date is indicated every 10 days.

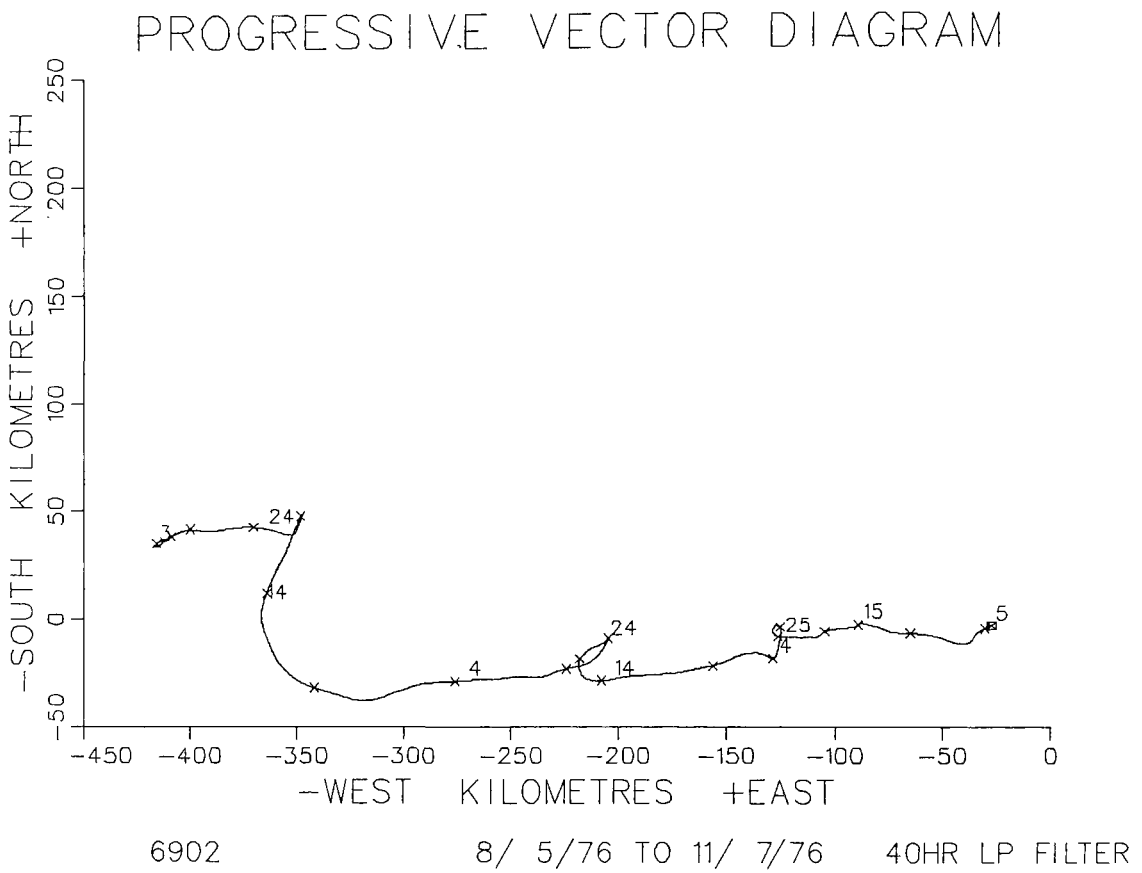

Figure 4.24. Progressive Vector Diagram for 06902. Low passed filtered data. The date is indicated every 10 days.

To show an estimate of Lagrangian motion, the progressive vector diagrams of the five current meters are shown in Figure 4.20-4.24. These diagrams are not to be interpreted as the path that a particular particle of radioactivity would follow in this time period, as the true Lagrangian path is influenced by the local topography. Rather, they should be viewed as estimates of the distances and directions such a particle may follow in a three month period. Evidently, even though the current meters are only 17-20 km apart, the directions are quite different, reflecting the influence of the local topography on the mean currents. The effects of very steep topographic features, such as canyons, on the mean flow over the Continental Rise is not understood at this time. The progressive vector diagrams also illustrate the excursions from the mean path of a water particle caused by the low frequency wave motions. The largest apparent excursion occurs between 4-29 of October 1976 (e.g. Figure 4.22) which indicates deviations of ± 40-50 km from the mean path. An excursion of this magnitude would bring a water particle to the region of the slope-rise junction, thus possibly being influenced by the more complex dynamics (Ou and Beardsley, 1980). The effect of the low frequency wave motions may be to disperse radionuclides over much of the Continental Rise to the southwest of the dumpsite. If the total distance traveled along the 2800 m isobath is taken to be approximately 300 km from the progressive vector diagram over the period of the measurements, then the particle will be just north of Cape Hatteras. From Cape Hatteras, we may speculate that the water particle may be transported by the Western Boundary Undercurrent under the Gulf Stream and enter the South Atlantic Bight. Such a particle may also become part of the deep Gulf Stream system and be dispersed into the northwestern Atlantic as indicated by the quasi-lagrangian float tracks shown in Figure 2.2 as discussed in Section 2.

It is of also interest to use the temperature fluxes to estimate horizontal eddy diffusivities due to low frequency wave motions, i.e.

$$\langle U'T' \rangle = -K_x \, \partial T/\partial x, \quad \langle V'T' \rangle = -K_y \, \partial T/\partial y$$

where K_x, K_y are eddy diffusion coefficients and the horizontal gradients are given by $\partial T/\partial x$ and $\partial T/\partial y$ (rotated frame of reference). Using the results from Table 4.1, if $\langle U'T' \rangle$ and $\langle V'T' \rangle$ for the four lower meters are averaged, and

estimating $\partial T/\partial x$, $\partial T/\partial y$ across the corners of the array, then the values calculated for K_x and K_y are 7×10^6 cm^2/s and 7.3×10^6 cm^2/s, respectively. These diffusion coefficients are reasonable values for the deep ocean and indicate a reasonable amount of dispersion is occurring from the low frequency fluctuating currents. Note that due to the depths of the four lower current meters, the cross slope and long slope gradients and diffusion coefficients are calculated parallel to the bottom rather than in the horizontal plane in which eddy fluxes are normally defined.

This section may be summarized by asking the question, "how do the relatively well understood dynamics of these energetic low frequency motions contribute to the dispersion of radioactivity leaking slowly from a source on the bottom?" The problem is essentially that of motions of water and sediment in the bottom boundary layer. Dispersion of dissolved constituents is discussed above, and the horizontal eddy diffusion coefficients estimated. Sediment transport is also important because radionuclides attach readily to sediment particles. The current measurements at 5.1 m off the bottom show evidence of Ekman veering and are similar in magnitude to currents measured at 96 m from the bottom, and for reasons cited above, can be considered to be within the boundary layer but probably near the top of the boundary layer (see Section 4.4). A typical example of the statistics of these boundary layer currents is given in the form of a bivariate frequency distribution in Table 4.4 (for data from 06902), which includes high frequency inertial and tidal motions. The currents exceed 10 cm/s 30% of the time, and exceed 15 cm/s about 6% of the time. The most persistent current direction is approximately southwards (27% of the time), which also shows the highest speeds. Only the highest speeds above 18 cm/s, which occur less than 1% of the time, would be capable of suspending fine grain sediment. Sediment suspension by currents depends upon the detailed shear structure in the boundary layer which is influenced by stratification and small scale topographic variations (Weatherly and Martin, 1978). This detailed vertical structure is not given by this data, thus deductions made on the transport of sediments sediments are not precise. It appears that transport of very fine grain sediments from the dumpsite by the currents is not an important process in the dispersal of radionuclides in the bottom boundary layer. This conclusion ignores possible catastrophic events such as turbidity currents flowing down from the Slope

FREQUENCY DISTRIBUTION
1.00 HOURLY DATA STATION: 06902 3HRLP SPANNING 8/ 3/76 TO 11/11/76

DIRECTION DEGREES								PERCENT	MEAN SPEED	MIN SPEED	MAX SPEED	STD. DEV.
0- 30	.8	1.7	1.0	.7	1.2	.5	.1	6.0	8.33	1.42	19.82	4.90
30- 60	.8	3.0	1.7	1.0	.4	.0	.0	7.0	6.17	.26	14.35	3.29
60- 90	1.2	3.0	1.6	.5	.0	.0	.0	6.3	5.28	1.13	11.64	2.48
90-120	.9	1.9	1.3	.2	.0	.0	.0	4.3	4.97	1.06	14.46	2.86
120-150	.6	1.3	.8	.3	.2	.1	.0	3.3	5.91	.80	16.97	3.66
150-180	.5	1.1	.9	.5	.0	.1	.0	3.1	6.41	.74	17.63	3.36
180-210	.3	1.5	1.7	.9	.1	.1	.0	4.7	7.13	1.42	16.56	2.94
210-240	.8	1.8	2.9	2.1	.8	.3	.0	8.7	7.84	.41	16.29	3.63
240-270	.7	2.5	4.8	6.7	6.6	2.7	.6	24.5	10.76	1.46	20.55	3.96
270-300	.4	2.7	4.6	5.0	4.2	1.9	.9	19.6	10.45	1.24	20.47	4.21
300-330	.5	2.2	1.5	1.4	.8	.3	.0	6.7	7.80	2.02	16.18	3.84
330-360	.7	1.9	1.1	.9	.8	.2	.2	5.8	7.93	.52	20.14	4.65

SPEED CM/S	0 - 3	3 - 6	6 - 9	9 - 12	12 - 15	15 - 18	18 - 21	
PERCENT	8.3	24.4	24.0	20.3	15.1	6.1	1.8	100.00
MEAN DIR	160	179	209	236	243	247	269	
STD DEV	106	107	92	79	82	69	65	

SUMMARY STATISTICS

MEAN SPEED = 8.56 CM/S MAXIMUM = 20.55 CM/S MINIMUM = .26 CM/S RANGE = 20.30 CM/S

STANDARD DEVIATION = 4.25 CM/S SKEWNESS = .39

IN A COORDINATE SYSTEM WHOSE Y AXIS IS POSITIONED .00 DEGREES CLOCKWISE FROM TRUE NORTH

MEAN X COMPONENT = -4.48 CM/S STANDARD DEVIATION = 6.82 CM/S SKEWNESS = .02

MEAN Y COMPONENT = .41 CM/S STANDARD DEVIATION = 4.95 CM/S SKEWNESS = .44

Table 4.4. Bivariate Frequency Distribution for speed and direction for meter 06902 (east and north frame of reference).

FREQUENCY DISTRIBUTION
1.00 HOURLY DATA STATION: 06601 3HRLP SPANNING 8/ 3/76 TO 11/10/76

DIRECTION DEGREES								PERCENT	MEAN SPEED	MIN SPEED	MAX SPEED	STD. DEV.
0- 30	.5	1.6	.7	.1	.0	.0	.0	3.0	4.92	1.79	10.23	2.30
30- 60	.4	1.0	.8	.2	.0	.0	.0	2.3	5.48	1.65	10.48	2.72
60- 90	.9	1.1	.6	.2	.0	.0	.0	2.8	4.59	1.48	9.75	2.51
90-120	1.0	1.7	.8	.3	.2	.0	.0	4.0	5.37	1.08	13.98	2.95
120-150	.8	1.9	1.6	2.0	.3	.0	.0	6.6	7.16	1.67	14.12	3.17
150-180	.7	2.0	3.8	2.1	.6	.0	.0	9.2	7.45	1.14	13.97	3.14
180-210	1.8	4.0	3.5	3.0	1.1	.1	.0	13.5	7.01	1.28	16.00	3.55
210-240	1.3	5.5	5.2	2.9	1.2	.7	.1	16.9	7.39	.75	18.32	3.86
240-270	1.5	4.6	6.4	6.2	3.1	1.5	.1	23.4	8.72	.77	19.04	3.96
270-300	.9	3.4	3.0	2.3	.9	.3	.2	11.0	7.62	1.20	19.88	3.84
300-330	.8	1.7	1.0	.4	.1	.0	.0	4.1	5.58	.20	16.84	2.98
330-360	.9	1.3	.6	.3	.0	.0	.0	3.1	4.85	1.58	11.42	2.45

SPEED CM/S	0 ! 3	3 ! 6	6 ! 9	9 ! 12	12 ! 15	15 ! 18	18 ! 21	
PERCENT	11.6	29.8	28.2	19.9	7.5	2.6	.4	100.00
MEAN DIR	197	204	210	218	230	249	258	
STD DEV	92	84	71	60	42	32	31	

SUMMARY STATISTICS

MEAN SPEED = 7.23 CM/S MAXIMUM = 19.88 CM/S MINIMUM = .20 CM/S RANGE = 19.68 CM/S

STANDARD DEVIATION = 3.58 CM/S SKEWNESS = .59

IN A COORDINATE SYSTEM WHOSE Y AXIS IS POSITIONED .00 DEGREES CLOCKWISE FROM TRUE NORTH

MEAN X COMPONENT = -3.17 CM/S STANDARD DEVIATION = 5.41 CM/S SKEWNESS = -.09

MEAN Y COMPONENT = -2.68 CM/S STANDARD DEVIATION = 4.32 CM/S SKEWNESS = .02

Table 4.5. Bivariate Frequency Distribution for speed and direction for meter 06601 (east and north frame of reference).

FREQUENCY DISTRIBUTION
1.00 HOURLY DATA STATION: 06701 3HRLP SPANNING 8/ 3/76 TO 11/ 9/76

DIRECTION DEGREES															PERCENT	MEAN SPEED	MIN SPEED	MAX SPEED	STD. DEV.
0- 30	.6	1.1	.8	.1	.0	.0	.0	.0	.0	.0	.0	.0	.0	.0	2.6	4.95	1.06	9.86	2.33
30- 60	.8	1.3	1.5	.2	.0	.0	.0	.0	.0	.0	.0	.0	.0	.0	3.7	5.37	.94	11.66	2.50
60- 90	1.1	2.1	1.8	.4	.1	.0	.0	.0	.0	.0	.0	.0	.0	.0	5.5	5.65	1.09	38.43	4.20
90-120	1.4	4.4	2.5	.6	.3	.0	.2	.1	.0	.2	.1	.0	.0	.1	9.8	7.22	.94	40.04	6.44
120-150	1.5	3.9	3.6	1.5	.5	.2	.3	.1	.1	.0	.0	.0	.0	.0	11.5	7.07	.83	28.96	4.48
150-180	1.7	3.3	3.0	1.5	.2	.1	.1	.1	.0	.0	.0	.0	.0	.0	10.0	6.58	.67	27.26	4.38
180-210	1.2	4.3	3.7	1.4	.2	.2	.0	.0	.0	.0	.0	.0	.0	.0	11.1	6.47	.42	31.32	3.74
210-240	1.4	4.5	3.9	2.8	1.6	.5	.2	.0	.0	.0	.0	.0	.0	.0	15.0	7.75	.45	39.30	4.54
240-270	.9	3.4	4.2	4.1	2.8	.6	.1	.0	.0	.0	.0	.0	.0	.0	16.2	8.74	.94	21.01	4.06
270-300	.9	1.5	1.7	1.8	.8	.3	.1	.0	.0	.0	.0	.0	.0	.0	7.1	7.99	.26	18.33	4.25
300-330	.9	1.9	1.3	.3	.0	.0	.0	.0	.0	.0	.0	.0	.0	.0	4.4	5.17	.47	13.37	2.82
330-360	.6	1.5	.5	.3	.0	.0	.0	.0	.0	.0	.0	.0	.0	.0	3.0	4.93	1.15	10.84	2.56
SPEED	0	3	6	9	12	15	18	21	24	27	30	33	36	39					
CM/S	3	6	9	12	15	18	21	24	27	30	33	36	39	42					
PERCENT	13.1	33.1	28.5	14.8	6.4	1.9	.9	.4	.2	.3	.1	.0	.0	.1	100.00				
MEAN DIR	177	182	183	214	229	231	183	150	154	122	138	96	79	142					
STD DEV	90	83	79	66	52	32	62	57	47	22	36	0	0	77					

SUMMARY STATISTICS

MEAN SPEED = 7.06 CM/S MAXIMUM = 40.04 CM/S MINIMUM = .26 CM/S RANGE = 39.77 CM/S

STANDARD DEVIATION = 4.32 CM/S SKEWNESS = 2.11

IN A COORDINATE SYSTEM WHOSE Y AXIS IS POSITIONED .00 DEGREES CLOCKWISE FROM TRUE NORTH

MEAN X COMPONENT = -1.24 CM/S STANDARD DEVIATION = 6.40 CM/S SKEWNESS = .52

MEAN Y COMPONENT = -2.50 CM/S STANDARD DEVIATION = 4.45 CM/S SKEWNESS = -.54

Table 4.6. Bivariate Frequency Distribution for speed and direction for meter 06701 (east and north frame of reference).

FREQUENCY DISTRIBUTION
1.00 HOURLY DATA STATION: 06801 3HRLP SPANNING 8/ 3/76 TO 11/10/76

DIRECTION DEGREES										PERCENT	MEAN SPEED	MIN SPEED	MAX SPEED	STD. DEV.
0- 30	1.7	3.0	1.7	.8	.7	.3	.0	.0	.0	8.1	6.28	.42	18.44	3.96
30- 60	1.0	2.5	1.3	1.0	.8	.9	.3	.0	.0	7.9	8.17	.56	19.90	5.23
60- 90	1.1	1.2	1.0	.8	.1	.1	.0	.0	.0	4.3	5.94	.64	15.55	3.74
90-120	1.0	1.0	.5	.1	.0	.0	.0	.0	.0	2.7	4.28	1.08	9.38	2.54
120-150	1.4	1.7	.5	.0	.0	.0	.0	.0	.0	3.7	4.13	.87	9.29	1.67
150-180	.6	1.1	1.0	.1	.0	.0	.0	.0	.0	2.8	5.10	.87	12.47	2.87
180-210	.9	1.9	1.1	.3	.0	.0	.0	.0	.0	4.1	5.11	.39	10.90	2.38
210-240	1.2	2.4	1.6	.8	.5	.7	.4	.1	.0	7.8	8.06	.96	23.90	5.49
240-270	.7	3.1	4.5	4.3	3.1	2.5	2.3	.6	.1	21.4	11.26	1.55	26.00	5.26
270-300	1.0	4.5	4.4	1.6	1.0	.7	.3	.1	.0	13.6	7.63	.08	23.39	4.18
300-330	1.5	4.5	4.1	1.3	.0	.0	.0	.0	.0	11.4	5.85	.47	12.73	2.65
330-360	1.3	4.2	2.2	1.4	1.7	1.4	.0	.0	.0	12.2	8.01	.98	17.96	4.69

SPEED CM/S	0 ! 3	3 ! 6	6 ! 9	9 ! 12	12 ! 15	15 ! 18	18 ! 21	21 ! 24	24 ! 27	
PERCENT	13.6	31.2	24.0	12.4	8.1	6.5	3.3	.8	.1	100.00
MEAN DIR	178	212	229	227	233	234	231	251	249	
STD DEV	112	112	100	99	104	98	70	38	76	

SUMMARY STATISTICS

MEAN SPEED = 7.75 CM/S MAXIMUM = 26.00 CM/S MINIMUM = .08 CM/S RANGE = 25.92 CM/S

STANDARD DEVIATION = 4.82 CM/S SKEWNESS = .96

IN A COORDINATE SYSTEM WHOSE Y AXIS IS POSITIONED .00 DEGREES CLOCKWISE FROM TRUE NORTH

MEAN X COMPONENT = -3.45 CM/S STANDARD DEVIATION = 6.53 CM/S SKEWNESS = -.29

MEAN Y COMPONENT = 1.12 CM/S STANDARD DEVIATION = 5.25 CM/S SKEWNESS = .42

Table 4.7. Bivariate Frequency Distribution for speed and direction for meter 06801 (east and north frame of reference).

FREQUENCY DISTRIBUTION
1.00 HOURLY DATA STATION: 06901 3HRLP SPANNING 8/ 3/76 TO 11/11/76

DIRECTION DEGREES									PERCENT	MEAN SPEED	MIN SPEED	MAX SPEED	STD. DEV.
0- 30	.4	1.2	1.5	.6	1.1	.5	.1	.1	5.5	9.26	2.05	22.17	4.82
30- 60	1.0	1.7	.9	.9	.9	1.0	.3	.0	6.8	9.10	.99	21.08	5.52
60- 90	1.0	2.8	1.8	.7	.5	.2	.0	.0	7.0	6.42	1.85	16.95	3.54
90-120	1.1	3.4	1.0	.7	.0	.0	.0	.0	6.3	5.25	1.64	13.86	2.49
120-150	1.5	1.4	1.3	.6	.3	.0	.0	.0	5.0	5.67	.76	14.60	3.33
150-180	.9	1.4	1.5	.6	.2	.1	.0	.0	4.6	6.21	.93	17.03	3.43
180-210	.8	1.3	1.4	.6	.4	.0	.0	.0	4.5	6.56	1.69	18.48	3.67
210-240	.8	2.2	3.6	2.0	.7	.2	.0	.0	9.5	7.49	.92	17.13	3.49
240-270	.7	2.6	4.8	5.0	2.7	1.0	.5	.0	17.2	9.44	.65	19.64	4.01
270-300	.5	2.8	4.0	5.6	4.0	1.6	.9	.0	19.5	10.34	.78	20.77	4.10
300-330	.4	1.9	2.6	2.3	1.7	.4	.2	.0	9.5	9.09	1.14	21.16	4.18
330-360	.4	1.3	2.0	.5	.4	.1	.0	.0	4.7	7.30	1.84	17.96	3.20
SPEED	0	3	6	9	12	15	18	21					
CM/S	! 3	! 6	! 9	! 12	! 15	! 18	! 21	! 24					
PERCENT	9.5	24.0	26.5	19.9	12.8	5.1	2.0	.2	100.00				
MEAN DIR	160	180	215	234	225	195	228	100					
STD DEV	89	100	95	83	101	116	102	144					

SUMMARY STATISTICS

MEAN SPEED = 8.33 CM/S MAXIMUM = 22.17 CM/S MINIMUM = .65 CM/S RANGE = 21.52 CM/S

STANDARD DEVIATION = 4.21 CM/S SKEWNESS = .52

IN A COORDINATE SYSTEM WHOSE Y AXIS IS POSITIONED .00 DEGREES CLOCKWISE FROM TRUE NORTH

MEAN X COMPONENT = -3.27 CM/S STANDARD DEVIATION = 6.92 CM/S SKEWNESS = .11

MEAN Y COMPONENT = .77 CM/S STANDARD DEVIATION = 5.28 CM/S SKEWNESS = .32

Table 4.8. Bivariate Frequency Distribution for speed and direction for meter 06901 (east and north frame of reference).

region and is based on only three months of data. Statistics of the data from the other bottom current meters are shown in Tables 4.5-4.8. The maximum speeds measured vary considerably for the five meters with the highest speed of 40 cm/s measured at meter 06701. However, distribution of speeds below 18 cm/s is similar for all five current meters and speeds above 18 cm/s generally occur less than 3% of the total length of each record.

In this section on dispersion by low frequency currents, a few parameters such as eddy diffusivities, correlation times, and particle excursions have been estimated from the data, which will be of use for any dispersion calculations made at this site. A qualitative discussion of sediment transport at the 2800 m dumpsite indicates that suspension of sediments due to high currents will occur less than 1% of the time and thus transport of contaminated sediments away from the site is likely to be minimal.

V. INERTIAL CURRENTS

The next most energetic part of the spectrum after the low frequency topographic wave motions is the inertial motions. Inertial currents are internal wave motions which occur with periods near $2\Pi/f$, where f is the Coriolis parameter. The inertial period is closely related to a half pendulum day and is a natural resonance period of the ocean which varies with latitude. The inertial wave motions are caused by rapid changes in wind forcing and possibly also by the interaction of low frequency currents with rough bottom topography. Inertial currents can be characterized as a nearly horizontal current vector rotating clockwise at frequency, ω, which is close to the inertial frequency, f. The energy of the inertial oscillations propagates downwards from the generation zone at the surface, thus any instant the velocity vector turns 360° over the depth of the vertical wave length of the inertial oscillation. This turning of the velocity vector is equivalent to a vertical phase difference, and this phase change with depth results in instantaneous vertical shears due to the inertial wave. These shears, along with vertical mixing, are a very effective mechanism for the horizontal dispersion of radionuclides in deep water by analogy with the horizontal dispersion of pollutants by oscillating tidal currents (Bowden, 1965).

Apart from horizontal dispersion, inertial currents also contribute to the turbulent fluxes in the bottom boundary layer. The downward inertial energy flux into the boundary layer for an inertial current magnitude of 10 cm/s is of the same order of magnitude as the rate of turbulence production n the bottom boundary layer by a steady current of 10 cm/s just above the boundary layer (Kundu, 1976). Since 10 cm/s is a representative magnitude for the low frequency currents and maximum inertial currents at the 2800 dumpsite then inertial events originating from the surface layer can significantly stir the boundary layer.

Inertial oscillations can be summarized as clockwise rotating currents (V leads U by 90°) generated by storms in the surface layer. The vector speed is almost constant with the rotation over one inertial period, but the oscillations are highly intermittent. Figure 5.1 shows inertial currents

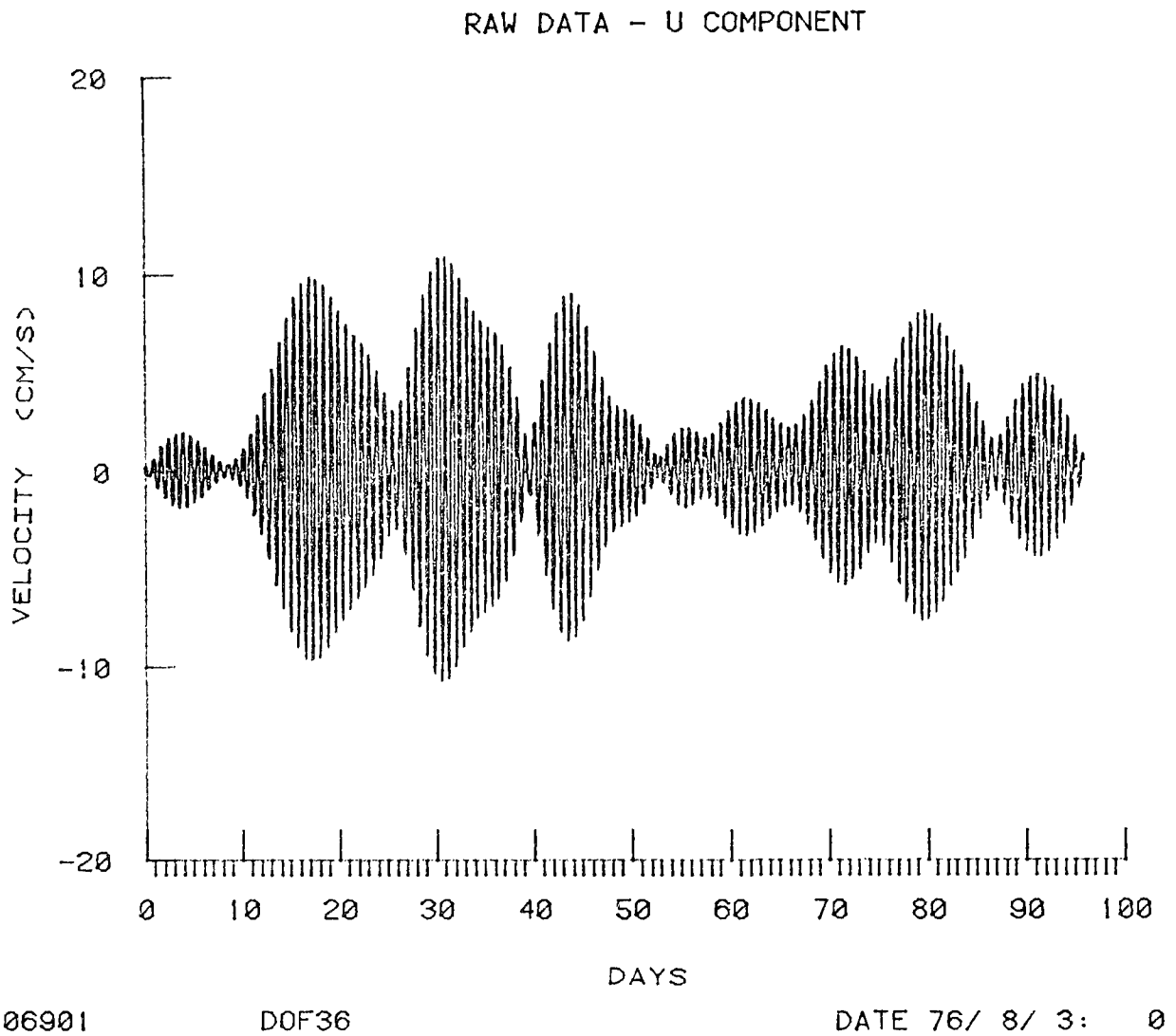

Figure 5.1. Band passed (frequency = 1.2428 cpd, band width 0.1875 cpd) inertial currents for meter 06901.

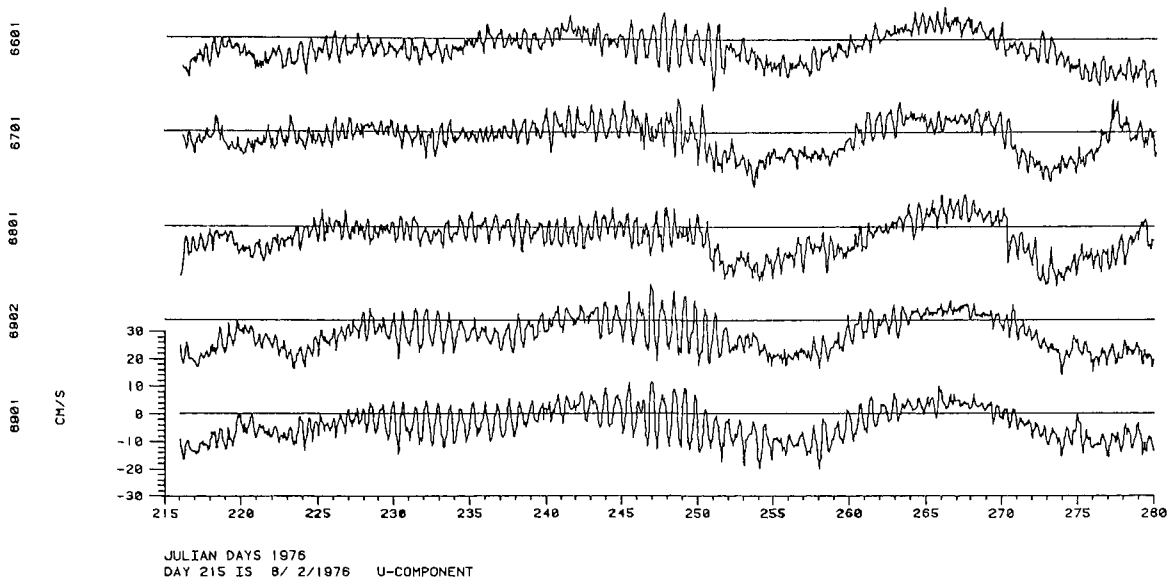

Figure 5.2. U component time series plots for 3 hour low passed data.

generated by bandpass filtering about the inertial period. The currents achieve maximum magnitudes of about 10 cm/s. The intermittent growth and decay of the envelope is a striking feature of these oscillations, which have also been observed in other studies of inertial currents (Kundu, 1976; Perkins, 1976). The first 60 days of the U component of all five currents meters are presented in Figure 5.2 to show the inertial and tidal oscillations superimposed on the low-frequency currents. The maximum inertial currents occur at approximately 17 and 31 days from the beginning of the record (Figure 5.1) (Julian days 233 and 247, respectively, Figure 5.2). These peaks in inertial energy are possibly related to the passage of Hurricane Belle (see Figure 1.1). The spacing of the current meter array at the 2800 m dumpsite makes possible some estimates of the horizontal and vertical wavelengths and vertical phase and group velocities for deep inertial wave motions. This analysis follows Kundu (1976), who studied inertial motion in shallow water using current meter records from the Oregon Continental Shelf.

Previous studies of inertial currents in the Mid-Atlantic Bight include Wunsch and Hendry (1972), who used a small triangular array with approximately 1 km horizontal spacing placed on the Continental Slope (39°50'N, 70°56'W) south of Cape Cod at a depth of about 1000 m. The experiment was designed to study bottom intensification of internal waves due to reflection from the bottom slope. Tidal and inertial currents were examined, but emphasis was placed on the former. Perkins (1976) studied inertial currents from the site D observations and correlated shifts in the observed inertial frequency from $2\Pi/f$ with the relative vorticity of the low frequency currents. Mayer et al. (1981) studied inertial oscillations generated on the Continental Shelf by the passage of Hurricane Belle (Figure 1.1).

Measurements of inertial oscillations usually show upward propagation of phase and hence downward propagation of energy. The observed frequency is also between 5-10% above f; the local inertial frequency, and the spectral peaks (see Figures 4.6-4.10) are broad and not sharply defined. This is partly due to the intermittent nature of the oscillations.

The relevant formulae are the dispersion relation (Kundu, 1976)

$$m^2 = (k^2 + \ell^2) \quad \frac{(N^2 - \omega^2)}{\omega^2 - f^2} \qquad (5.1)$$

where m is the local vertical wave number; k and ℓ the horizontal wave numbers, N the Brunt Väisälä frequency, f the Coriolis parameter and also the local inertial frequency, and ω the observed frequency. The vertical components of the phase and group velocities, c and c_g, respectively, are related by

$$c_g = \frac{\partial\omega}{\partial m} \cong c((f/\omega)^2 - 1) \qquad (5.2)$$

where $c = \omega/m$.

Figure 5.3 shows an EOF analysis for U and V components of the five current meters for a frequency band of width of 0.188 cpd centered on the inertial frequency 1.245 cpd (corresponding to 38°30'N). The computations are made using 36 degrees of freedom and 95% significance level for coherence squared is 0.162. The first EOF mode accounts for 73.3% of the total variance in this frequency band, and the coherence squared of the individual records with the mode is high for all the meters except 06701. Thus, excluding 06701, the horizontal and vertical wave numbers can be estimated from the remaining four meters using the phase differences similar to the method employed for the topographic Rossby wave numbers. The three bottom meters, 06902, 06801, and 06601 were used to estimate horizontal wave numbers, using a least square fit to the phase differences. The results were displayed in Table 5.1, where the inertial frequency has been estimated from a detailed plot of the spectral peak (Figures 5.4-5.8). The vertical wave number, m, is calculated directly from the phase differences between the measurements at 06901 and 06902 and through the dispersion relation (5.1) where N is assumed to be $1.33 \times 10^{-3} s^{-1}$ and $\omega = 1.3362$ cpd. It can be seen that they agree fairly well, which gives confidence in the vertical phase and group speed estimates. The phase and group speeds are higher by an order of magnitude than Kundu's estimate for the shelf, and their vertical wavelength is on the order of half the water depth as against 110 m estimated by Kundu for a water depth of 100 m. The results depend upon the local value of the Brunt-Väisälä frequency, N, which is a

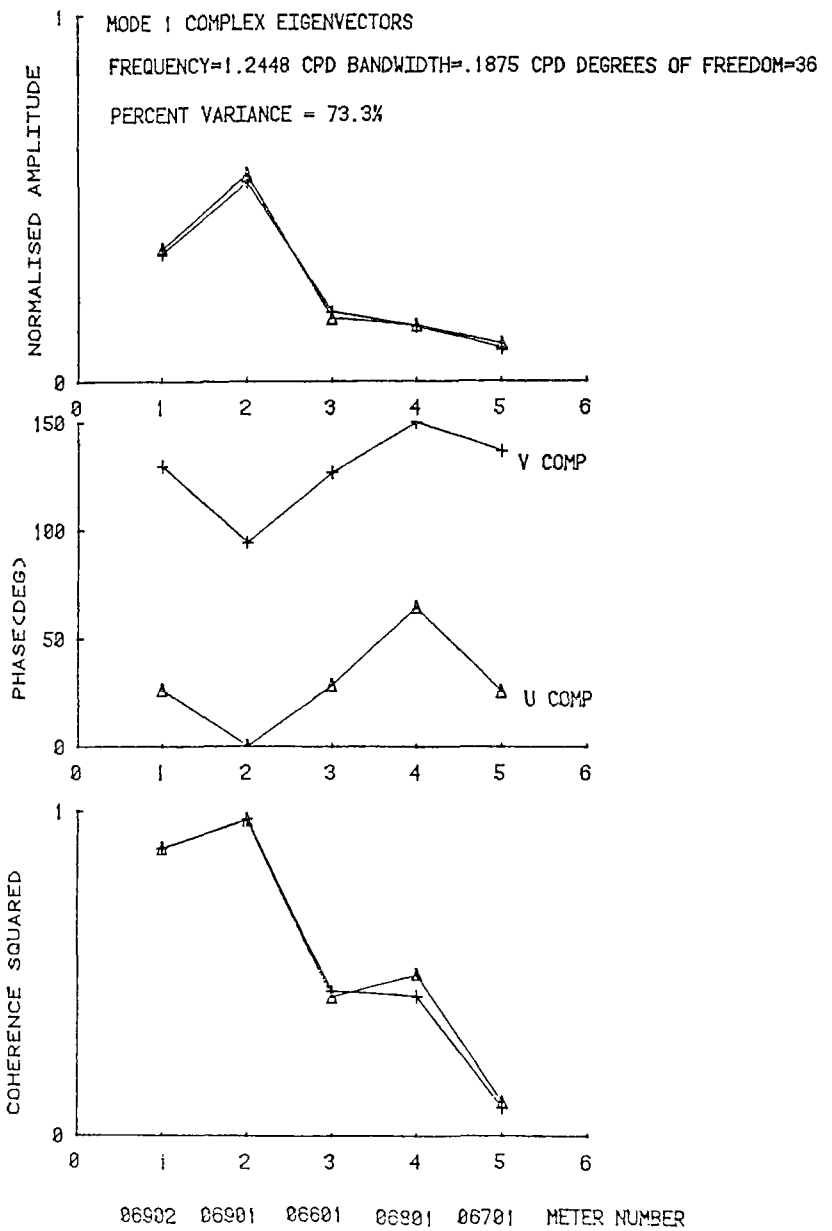

Figure 5.3. Amplitude, phase and coherence squared of the record with the mode for the first mode EOF for the inertial frequency band.

EPA CURRENT METER DATA

VERTICAL WAVENUMBER

Meter	Wavenumber m (cycles/m)	Wavelength (m)	Inertial Frequency ω (cpd)	Phase speed c (cm/s)	Group Velocity c_g (cm/s)
6901	9.405×10^{-4}	1063	1.3103	1.61	- 0.16
6902	$\pm 1.35 \times 10^{-4}$	± 743	1.3362	1.64	- 0.22

HORIZONTAL WAVENUMBER

Variable	Wavenumbers (cycles/km) k	ℓ	$K = (k^2+\ell^2)^{1/2}$	Wavelength (km)	Angle from North (Degrees)	Calculated Vertical wavenumber (cycles/m)
U	.000215	-.00517	.00517	193	178°	12.539×10^{-4}
V	.000745	-.00276	.00286	350	164°	6.936×10^{-4}
U,V	.000480	-.00397	.00400	250	173°	9.701×10^{-4}

Table 5.1. Inertial Oscillation Parameters.

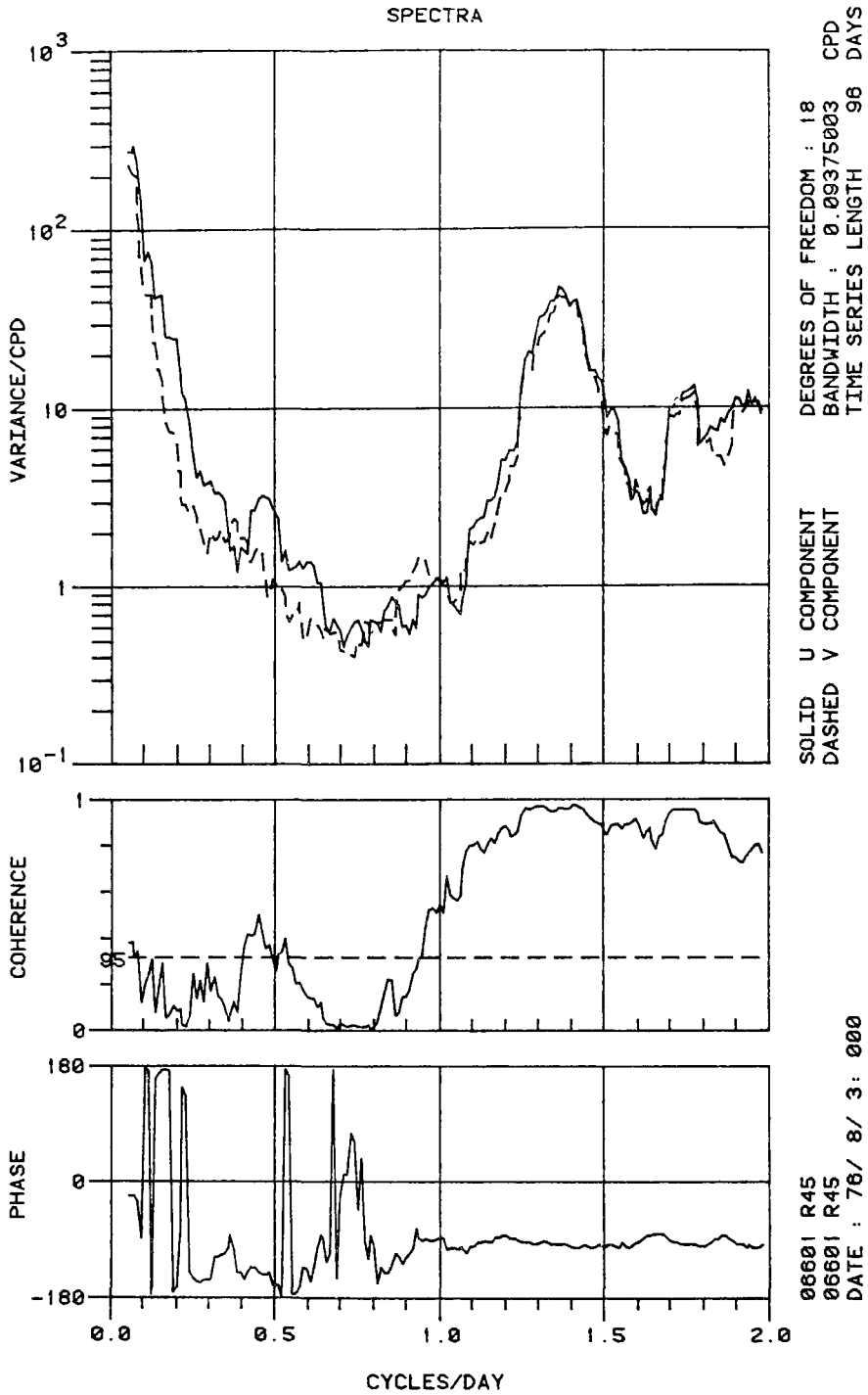

Figure 5.4. Power spectra plots for U and V components for meter 06601.

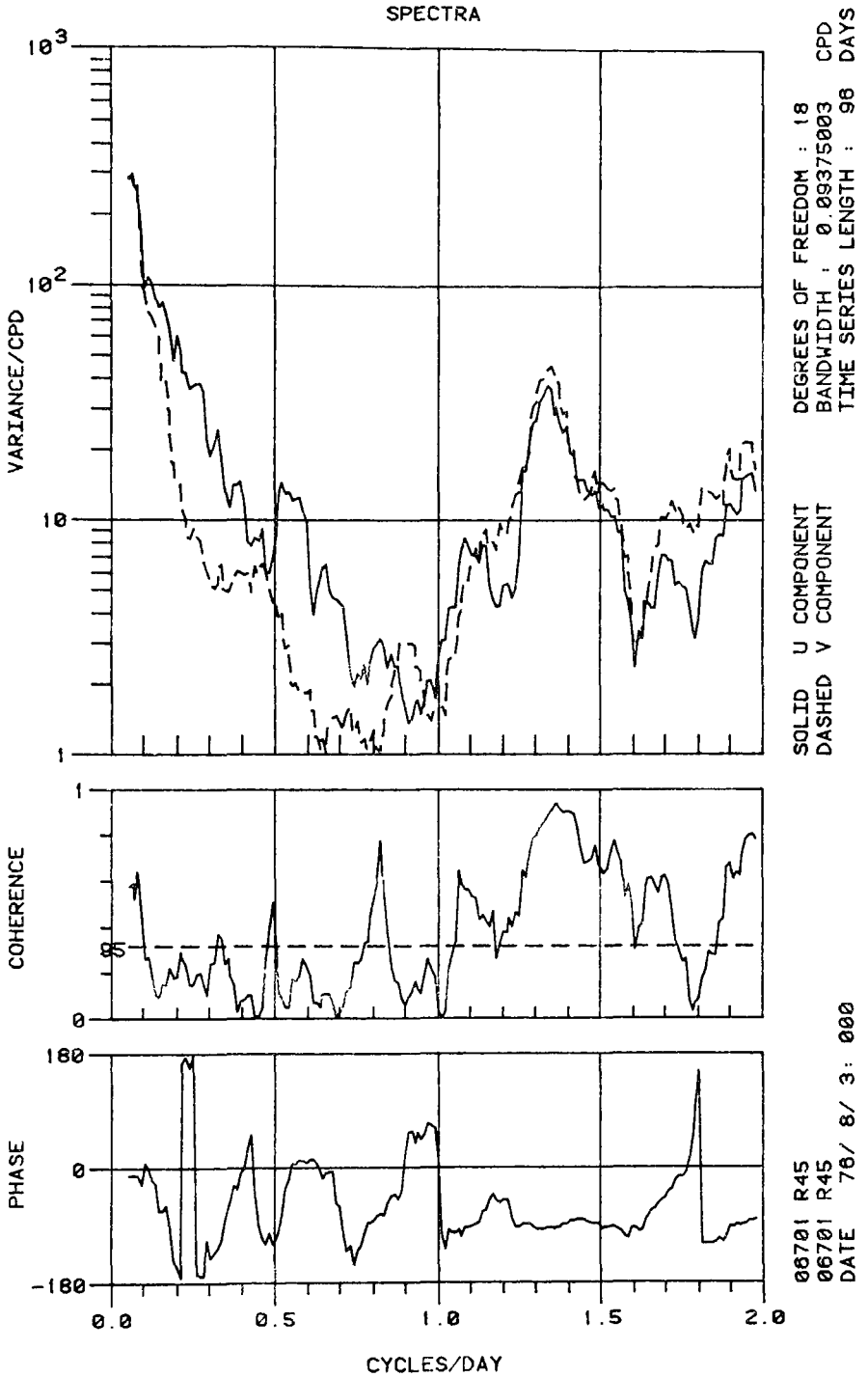

Figure 5.5. Power spectra plots for U and V components for meter 06701.

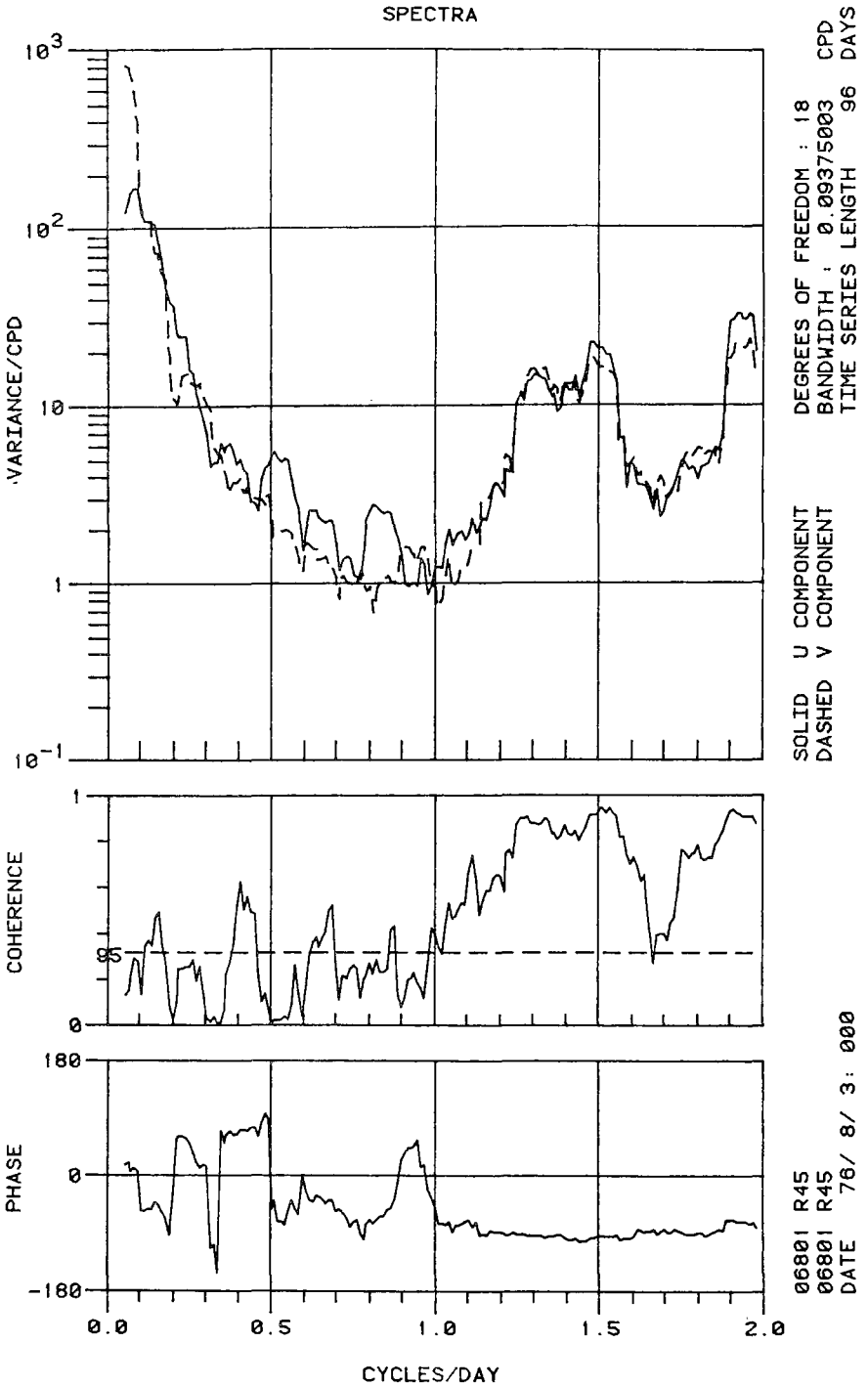

Figure 5.6. Power spectra plots for U and V components for meter 06801.

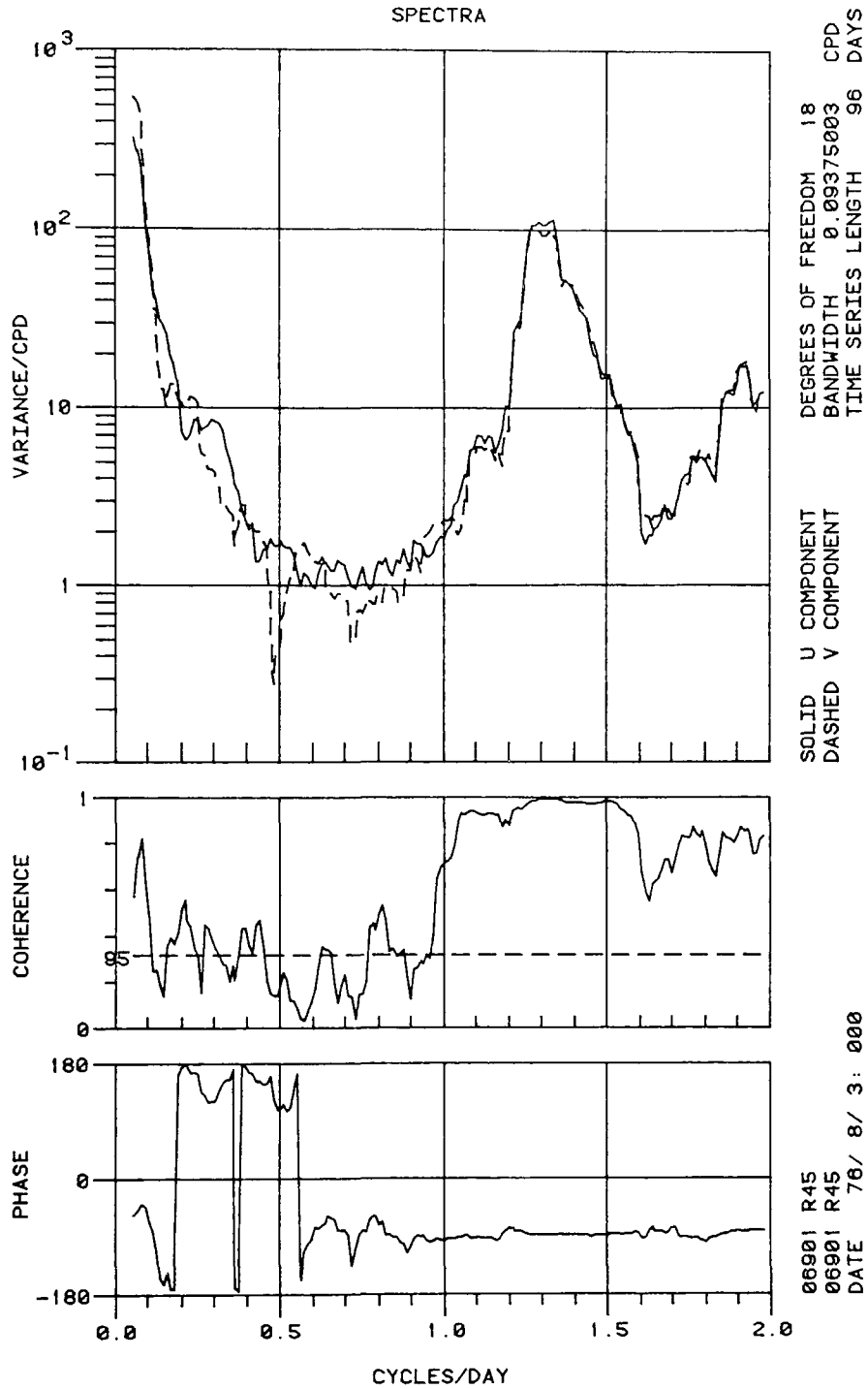

Figure 5.7. Power spectra plots for U and V components for meter 06901.

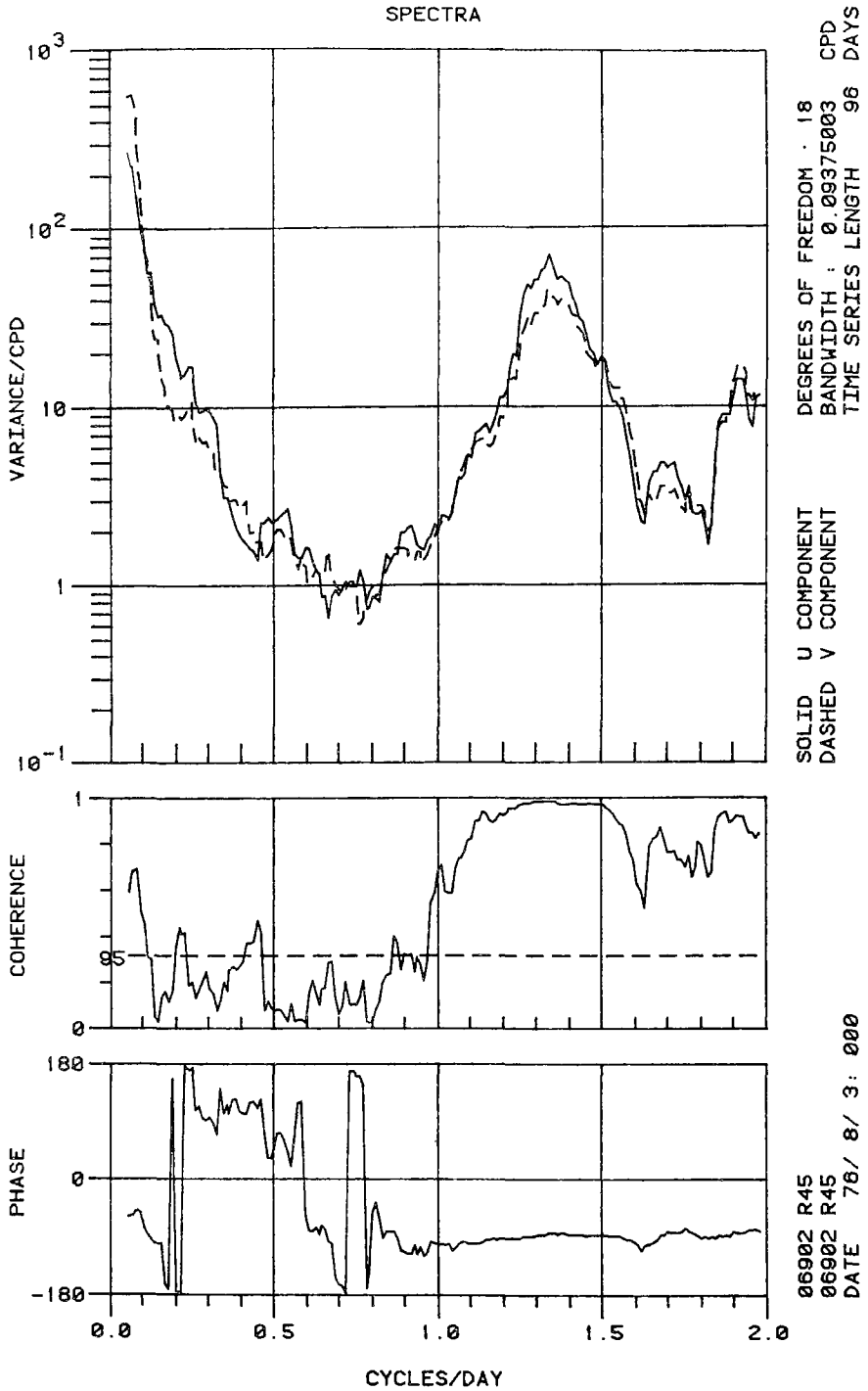

Figure 5.8. Power spectra plots for U and V components for meter 06902.

factor 10 smaller at the 2800 m dumpsite than off the Oregon coast, and so these estimates of wave number, vertical phase, and group speeds are reasonable when compared with Kundu's estimates. The results of the analysis are also consistent with the inertial wave dispersion relation, in that the rotation is clockwise (V leads U by approximately 90°) at all meters, and the U and V amplitudes are almost equal for the first EOF mode (Figure 5.3), with the phase velocity being upwards and the vertical component of the group velocity downwards. The latter represents the vertical propagation speed of the inertial energy down from the surface. The group velocity estimates represent a travel time for inertial energy between 15 and 20 days for 2800 m of water. These travel times for inertial energy to reach the bottom are under estimates because the group velocities will be much smaller in the upper half of the water column due to higher stratification. It is noted that there is a decrease in amplitude between 96 m and 5.1 m off the bottom at the SW mooring 069 of about 35%. This indicates that the inertial oscillations are being damped within the boundary layer. Mooring 069 also has the highest inertial energy of the four moorings. There is also a possibility that inertial energy is being reflected from the bottom, as well as being frictionally dissipated. In a reflected inertial wave, the velocity vector rotates anticlockwise. The energy in the anticlockwise component is two orders of magnitude smaller than the clockwise component at both 06901 and 06902 (Figures 4.9-4.10). There is, however, a small increase in the height of the anticlockwise inertial peak at 06902 compared with 06901, indicating there may be a very small amount of reflected inertial energy which decays with height above the bottom.

The horizontal wave number estimates in Table 5.1 indicate that horizontal phase propagation is towards the south, which indicates that the energy source, in the surface layers, is situated to the north of the site. The horizontal wavelength ($\sim$ 250 km) is similar to that of topographic Rossby waves and the wave vector direction is also similar for both types of waves. A possible speculation is that there is resonance between the two types of waves, which would imply a non-linear transfer of energy between inertial and topographic Rossby waves.

The inclination of the group velocity vector with the horizontal is given by $\tan^{-1}$ (K/m) $\cong$ 0.24, which is very similar to the slope of the bottom $\cong 0.3°$. According to Wunsch and Hendry (1972), when K/m > α (the bottom slope) the waves are refracted so that the waves are turned parallel to the slope, rather than being reflected, which may account for the lack of a reflected wave in the records.

The estimates of the travel time for inertial energy to reach the bottom from the generation zone at the surface, given above, are relevant to the passage of Hurricane Belle. If we assume that maximum wind stress on the surface layers above 2800 m dumpsite occurred on the August 9-10, 1976, then the minimum time that a peak in the inertial energy would occur at the bottom is 15-20 days after this date, but may be as long as 30-40 days. The maximum inertial currents (Figures 5.1 and 5.2) measured at meter 06902 occurred 24 days after August 10, though another maximum only slightly less intense occurred 10 days after August 10. Therefore, either of these peaks could have been caused by Hurricane Belle, but given that the travel times estimated are minimum estimates, that peak on Julian day 247, 24 days after August 10 is more likely to be the direct result of Hurricane Belle winds.

The final part of this section on inertial oscillations draws attention to the spectra plots (Figures 5.4-5.8), where the frequency axis is linear so that details of the inertial and tidal motions between 1 and 2 cpd may be examined. The power spectra exhibit prominent peaks between the inertial ($\sim$1.3 cpd) and M2 tidal peaks ($\sim$1.99 cpd) which are difficult to explain. Particularly note the prominent peak at $\sim$1.5 cpd, just above the inertial peak at $\sim$1.3 cpd on record 06801, which also may be present for 06701 (Figures 5.5, 5.6). A little less prominent are the peaks at $\sim$1.75 cpd, seen in the spectra of 06601 and 06701 (Figures 5.4, 5.5). A common feature is the high coherence between U and V, and the 90° phase lag between U and V, which indicates that the velocity vector is rotating in a clockwise sense. The origin of these motions is uncertain, but could be due to dispersive effects of internal waves and/or the interaction of the inertial wave with the complex bottom topography.

VI. TIDAL CURRENTS

Tidal Currents in deep water over the Continental Rise are primarily the result of the interaction of the barotropic deep sea tide, which is generated by astronomical tidal forces and produces a tidal current which does not vary with the depth coordinate, and the steep topography of the Continental Slope. This interaction generates internal waves at tidal frequencies which are larger than the inertial frequency. These internal waves propagate along characteristic ray paths from the generation zones on the Continental Slope towards the deeper water of the Continental Rise. These internal wave rays intersect the bottom where they are reflected or dissipate in the bottom boundary layer. Thus there may be regions of the Continental Rise boundary layer where enhanced mixing occurs due to the reflection and dissipation of the internal tidal energy. One of the major features of internal tides in deep water is the localization of tidal energy in the water column, which may only be 20-50 m thick and positioned according to the path of the characteristics. The kinematics of the internal tidal waves can be described by the dispersion relation (5.1), and the path of the characteristics refract due to changing horizontal and vertical density gradients. Present information indicates that baroclinic tidal energy may not be present more than 50-100 km seaward of the generation zones on the Continental Slope, which would include the dumpsite in the region where internal tides may be expected to influence the high frequency currents. Theories of the generation and propagation of baroclinic tides have been developed by Rattray et al. (1969) and Baines (1974), among others. Baines (1974) applied this theory to the New England Continental shelf and slope and Torgrimson and Hickey (1979) have investigated the internal tide from current meter data for the Oregon shelf.

The only energtic tidal motions observed in the current meter data are the semi-diurnal or M2 tides with a period of 12.42 hours. The astronomical M2 tide is generated by the gravitational force of the moon as it orbits the earth. A classical harmonic tidal analysis was performed on the current meter records, where the observations are least square fitted to a time series generated from astronomical considerations. The method used follows the treatise of Godin (1972) as implemented by Foreman (1979). The rotary spectra

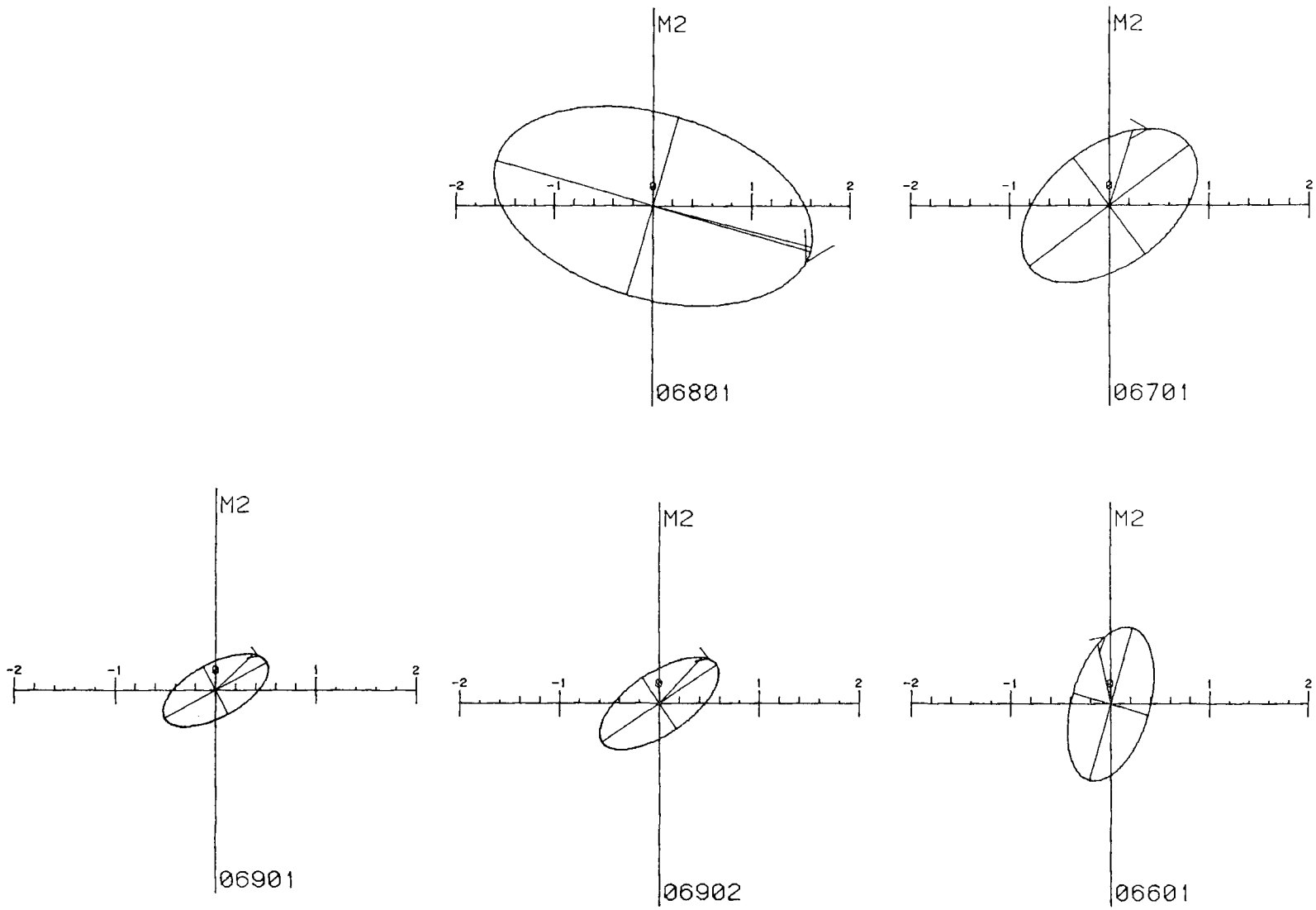

Figure 6.1. Hodographs of M2 tidal motion at all five meters. Axis units : cm/s.

(Figures 4.6-4.10) show relatively broad peaks compared with the sharp tidal lines seen in shallow water current spectra, and are thus some indications of the dispersive internal wave nature of the tidal signal. The results from the tidal harmonic analysis are shown in the form of current ellipses in Figure 6.1. Note the small amplitudes of the currents (0.5-1.6 cm/s), the uneven distribution of energy, and the variability in the direction of the axes of the elipses. Tidal currents are stronger at the two northern than at the two southern moorings, with most energy at the shallowest NW mooring closest to the Continental Slope (068). The two current meters on the SW mooring 069 have similar energy at the M2 frequency, with bottom tidal currents being slightly more energetic. However, unlike the other three moorings, the tidal currents at 069 are also energetic at another semi-diurnal frequency; the N2 with a period of 12.66 hours. The N2 tidal elipses have similar amplitudes and phases to the M2 elipses for mooring 069. The ratio of current energy at the N2 and M2 frequencies is 3.42 for 06901, and 1.50 for 06902. The reason for the dominance of the N2 tide over the closely related M2 tide at 069, which is unlike the results from the other three current measurements, is difficult to determine with the present data.

An EOF analysis centered at the M2 tidal frequency, 1.93227 cpd, with 36 degrees of freedom for all five current meters was performed. The relatively wide bandwidth covers all semi-diurnal motions, including the N2 tidal frequency. The first mode accounts for 54% of the total variance and all records are significantly coherent with the mode. Figure 6.2 shows the results for the first mode. The vertical phase differences indicate slight upward propagation of phase, but the 5.2° and 3.5° phase difference between 06902 and 06901 U and V components, respectively, are not significant at the 95% level. The slope of the characteristics, K/m, has the value 0.1, which is equivalent to a bottom slope of 6.9°, is much greater than the local bottom slope and implies reflection off the bottom rather than dissipation in the bottom boundary layer. Horizontal wave number estimates are given in Table 6.1, and the vertical wave number, m, was estimated using the mean of the phase differences for the U and V components, given above, assuming 91 m separation between 06901 and 06902. Again, clockwise rotary motion dominates and has characteristic horizontal scales of about 62 km. The direction of the horizontal phase propagation is clearly offshore and away from the generation

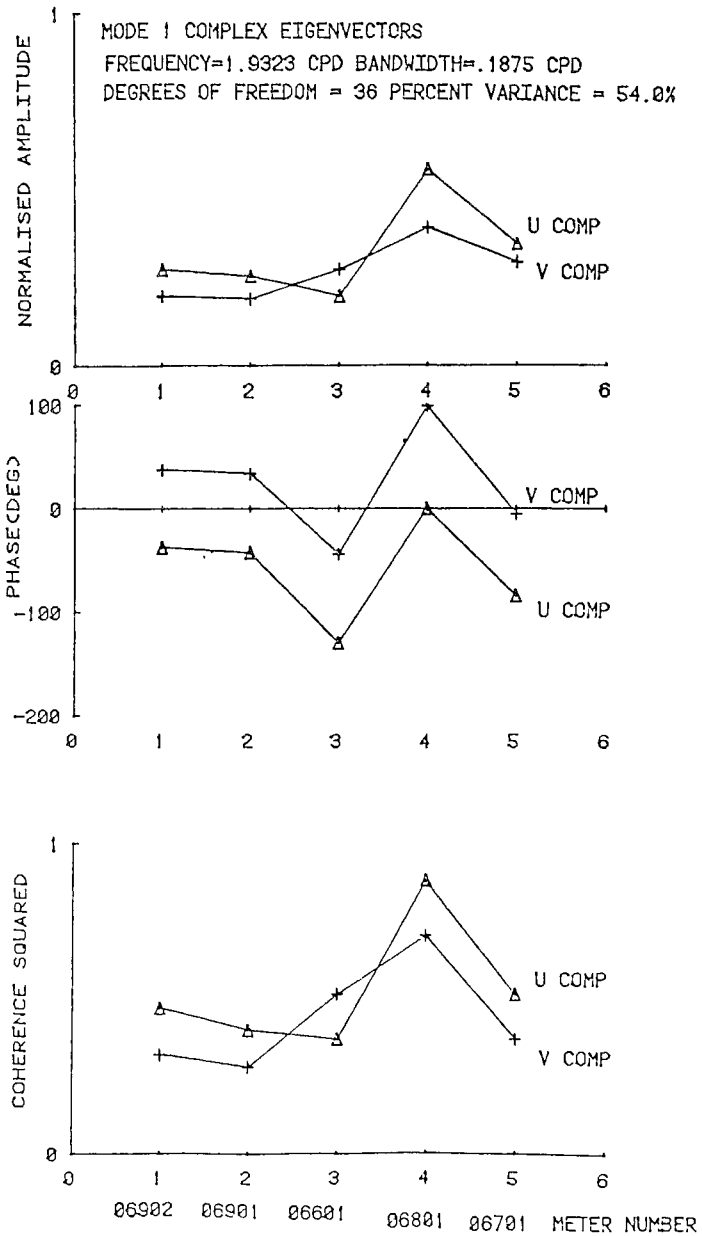

Figure 6.2. Amplitude, phase and coherence squared of the record with the mode for the first mode EOF for the M2 tide.

EPA CURRENT METER DATA

Variable	Wavenumbers k	ℓ	(cycles/km) $K = (k^2+\ell^2)^{\frac{1}{2}}$	Wavelength km	Angle from North (Degree)
U	0.01429	-.00584	.01543	65	112°
V	0.01512	-.00723	.01676	60	116°
U,V	0.01470	-.00653	.01609	62	114°

Table 6.1. M2 Tide: Horizontal Wavenumber Estimates.

zones on the Continental Slope. This fact along with short horizontal wavelengths, confirms the hypothesis that measurements are of the baroclinic tide rather than the long wavelength (several 1000 km) barotropic tide. Evidently, where the tidal beams reflect off the bottom, additional energy will be input into the bottom boundary layer with possible increases in mixing and turbulent levels over ambient.

VII. HIGH FREQUENCY INTERNAL WAVES

Between the M2 tide and the Brunt Väisälä frequency, the energy seen in the spectra is due to internal wave motions. Examination of the temperature spectra at these frequencies for the four moorings (Figures 4.11-4.13) shows that the energy levels increase towards the slope and decrease towards the bottom. The records are not coherent for the horizontal and vertical spacing of this dumpsite array as given in Table 2.1. The increase in high frequency energy towards major topographic features, such as the slope and canyons, has been commented upon by Wunsch and Webb (1979) and is probably related to the reflection of energy by the steep slopes of these features (Wunsch and Hendry, 1972) and consequently increases in mixing in the boundary layers. The velocity spectra (Figures 4.6-4.10) show isotropy at the highest frequencies, but increasing anisotropy with the clockwise component dominating, as the frequency decreases towards the M2 tide. This may be due to focusing effects of the internal waves by the steep bottom of the Continental Slope (Wunsch and Webb, 1979).

VIII. THE NORTHWEST ATLANTIC 3800 m RADIOACTIVE WASTE DUMPSITE

The deeper radioactive waste dumpsite centered at 37°50'N and 70°35'W is situated close to the deepest part of the lower Hudson Canyon. The data analyzed in the present report is not directly relevant to this site. However, this data and the Rise Array Data (Thompson, 1977; Luyten, 1977; Hogg, 1981; c.f. Section 2.2) allow some inferences to be made on the general statistics of the motion which might be expected at this site. Only motions above the bottom boundary layer in the lower part of the water column are considered. No current measurements have been made exactly within this 3800 m dumpsite.

The closest moorings to this dumpsite are WHOI moorings 530 and 533, with meters at nominally 1000 m and 200 m (533 only) off the bottom. One thing that is immediately apparent is the higher energy levels at these WHOI mooring sites compared with the upper Continental Rise and the 2800 m dumpsite measurements (Luyten, 1977), with total low-frequency variance being from 2-5 times the energy levels on the upper Continental Rise (e.g., Site D). The analyses by Thompson (1977) and Hogg (1981) also show that Rossby wave dynamics dominate at periods longer than eight days. However, rather than being short wavelength, bottom trapped topographic Rossby Waves, the low-frequency wave motions are barotropic, long Rossby Waves, with horizontal wavelengths of order 300 km (Hogg 1981). Currents have been known to exceed 60 cm/s in deepwater of 4000 m depth.

How the topography of the deep Hudson Canyon interacts and modifies these energetic low-frequency motions is not known at the present time, though some clues as to the variability over short distances when rough topography is present can be found in Hogg and Schmitz (1980). The surface waters of the dumpsite are likely to be frequently under the direct influence of the Gulf Stream, which may explain the high energy levels found below 1000 m in this vicinity.

There is again a gap in the spectra between one and eight days, and since the bottom slope is less in this region than on the upper continental rise,

the cut-off frequency shifts to a lower frequency. Hogg (1981) shows that in the southern part of the Rise Array the peak in the low frequency energy occurs in the 22-108 day period rather than the 12-20 day period of the shallower northern measurements. Hogg (1981) shows that the deep currents over the whole of the Continental Rise can be considered as part of the same system of Rossby waves. This system of deep wave motions is modified by the bottom slope as the waves propagate towards the Continental Slope.

The inertial and tidal motions of the Rise Array measurements have been investigated by Perkins (1976) and Baines (1974), and it is concluded that in the deeper water and at greater distance from the slope, the baroclinic M2 tide is expected to be much less prominent at the 3800 m site, though inertial motions could still be important at these depths and may be expected to again dominate the high frequency part of the spectrum.

IX SUMMARY

The current and temperature measurements from the 2800 m dumpsite have been analyzed with a view to identifying the dominant space and time scales in the records and identify, where possible, the dynamics responsible for the motions and how these dynamics relate to potential transfer of materials from the dumpsite.

The records can be divided into three energetic frequency bands: low frequencies, with periods greater than about 8-days; the inertial frequency band; and the M2 tidal band.

Mean currents over the 3-month period from August to November 1976 were substantial (3-4 cm/s), directed westwards or southwestwards, and influenced by the relatively variable topography of the site.

Low-frequency energy dominates the measurements and agrees fairly well with short wavelength, topographic bottom trapped Rossby wave theory (Rhines, 1970). The 10-20 day period motions dominate the spectra, with the peak at about 16-days. The low-frequency variability exceeds the mean flows. Analysis of the length scales, using phase differences estimated from the first mode of an empirical orthogonal function (EOF) analysis, showed phase propagation towards the south and wavelengths estimated to be about 200 km. The phase relations between U, V, and T generally agreed with the theory, even though the near bottom current meters are within the bottom boundary layer. Comparing currents at 96 m and 5 m off the bottom at the SW mooring (069) showed evidence of a minor amount of Ekman turning and frictional dissipation in the boundary layer. Otherwise, the results generally agree with measurements taken on the upper Rise at Site D (Thompson, 1977) and along 70°W (Luyten, 1977; Hogg, 1981).

The analysis of the low frequency currents indicates that the long term transport of radionuclides is dominated by the mean currents with the transport being approximately pa rallel to the isobaths and directed towards the southwest. In the boundary layer, Ekman turning of this mean current will

produce a small component of the mean current normal to the isobaths and directed shorewards. The low frequency wave motions serve to disperse the radionuclides by causing excursions of water parcels from a particular isobaths. Horizontal diffusion coefficants of approximately $7x10^6$ cm^2/s were calculated from the fluctuating components of temperature and current. The estimated displacement over three months of a water particle at the site is of the order of 300-400 km and is comparable with the displacements of Lagrangian float measurements made by Schmitz et al. (1981) over the Mid-Atlantic Bight Continental Rise (Figures 2.1, and 4.20-4.24). Thus the major processes responsible for transport and dispersion of radionuclides at the 2800 m dumpsite are the mean currents and the low frequency Rossby waves, which can be considered as continuous processes. There is no evidence of near bottom jets or periods of exceptionally strong currents which might be mechanisms for accelerated transport of material. The 3800 m dumpsite, however, is situated in the Hudson Canyon, and it is unknown whether flows within the canyon would enhance the transport. Above the lip of the canyon, low frequency currents would be expected to be similar in nature to those at the 2800 m dumpsite, but 2-5 times more energetic.

At periods less than one day, the spectra are dominated by a broad inertial peak at frequencies about 5-10% above the local inertial frequency, f, (about 19.3 hours). Clockwise rotary currents dominate, with nearly vertically upwards propagation of phase. The group velocity vector has a small downwards component and a horizontal component directed towards the south. The horizontal and vertical wavelengths are 250 km and 1 km, respectively, and the wave parameter relationships agree fairly well with the linear internal wave dispersion relation. The passage of Hurricane Belle close to the dumpsite on August 10, 1976, seems to increase the inertial currents at the bottom about 24 days later. The large amplitude inertial events input about as much energy into the boundary layer as do the maximum low frequency currents, and thus may be responsible for enhanced vertical mixing and resuspension of fine sediment particles. Sediment particles would be transported by the low frequency currents while suspended in the boundary layer until they sink to the bottom by the action of gravity. Thus transport of radionuclides attached to fine sediment particles would be very intermittent, but generally in the direction of the mean currents.

The next important process is the baroclinic M2 tide, which is generated in regions of steep bathymetry (∿6°) on the Continental Slope. Amplitudes are about 1-2 cm/s, and again clockwise rotary currents predominate. Horizontal wavelengths of about 60 km with offshore horizontal phase propagation were calculated from phase difference analysis, using the first EOF mode.

There is also energy between the M2 tide and the inertial frequency, which, at least at one mooring (068), exceeds the inertial peak. The origin of these motions, which are again predominantly clockwise rotating currents, is not known, as the frequencies (1.5 and 1.75 cpd for example) do not correspond to any known dynamics or forcings as far as is known to the author. They would thus appear to be non-linear phenomena.

Therefore, apart from these latter currents occurring at frequencies between the inertial and the M2 tide, the origin and dynamics of the energetic parts of the spectra can be accounted for by similar general observations at corresponding depths in the surrounding area.

The data described in this report could be used as the basis for a model of the dynamics of the benthic boundary layer over sloping topography forced by a mean current and linear topographic Rossby waves. This type of model would be similar to that of Weatherly and Martin (1978), except for the inclusion of Rossby wave motions. A quantitative simulation or hindcast of the boundary layer currents at the 2800 m dumpsite, using a fully three dimensional boundary layer model, is not possible because the data does not adequately define the boundary conditions in terms of currents and density on the open boundaries. Information on the detailed structure of the density field is lacking, so that initialization of such a simulation model could only be achieved by making some assumption on the distribution of salinity and temperature.

X. RECOMMENDATIONS

The low-frequency motions between 100 m and 1000 m off the bottom are fairly well understood. The basis for this knowledge are the WHOI measurements from Site D and the Rise Array, and the theories of topographic Rossby waves (Rhines, 1970). The bottom current measurements made by EPA at the 2800 m dumpsite are within the boundary layer; however only one mooring had measurements outside the boundary layer at 96 m from the bottom. Therefore, detailed analysis of the space and phase relationships of boundary layer currents to the currents above 100 m from the bottom over variable topography is unavailable from this data. It was pointed out in Section 4.5 that boundary layer shears and mixing processes are vital to the understanding of dispersion from the bottom. Detailed shear measurements are not available from the limited number of current meters used in this dumpsite survey. Since the large scale dispersion may be regarded as a stochastic or random walk process, the details of how the waste is dispersed within the bottom boundary layer should be the focus of further experiments. The complex topography of both dumpsites might be expected to impose small space scale variability on the boundary layer flows, which will need to be investigated because of impact on local dispersion. Therefore, future studies should concentrate on boundary layer measurements, including investigations of the mixing processes and the time and space dependence of the depth of the boundary layer over the site. However, the flow above the boundary layer should also be measured so that the forcing for the boundary layer is well defined.

Since topographic waves and internal wave dynamics are functions of the stratification and the bottom topography, both these parameters should be carefully measured in future studies. A detailed bottom topography map of the 3800 m site is crucial, because the only generally available topographic maps of this region are from Uchupi (1965) which lack the fine detail required in a deep canyon.

The 3800 m dumpsite in the lower Hudson Canyon needs measurements both within and upstream and downstream of the canyon in order to determine the effects of the canyon the large scale mean flow and wave motions. At the

present time, the effects of canyons on deep abyssal flows on the lower Continental Rise is unknown.

The final point to be made is that future measurements should be made for a period of at least 9-12 months so as to resolve the dominant low-frequency motions; also to give more stable estimates of the substantial mean flows on the Continental Rise.

A detailed simulation model of the time and space dependant flows in a boundary layer over a dumpsite requires a large measurement program to adequately define the boundary conditions of the horizontal and vertical boundaries delineating the dumpsite. However the data requirement for models is determined by the type of model employed and the purpose to which the model is being put. Thus a model of large scale transport and dispersion may require the modeling of the whole ocean basin in all four dimensions, whereas a model of mixing processes within the abyssal boundary layer may use a quasi-theoretical model of boundary layer dynamics which is compared with data in only a general qualitative sense, so that some determination of whether this type model includes all the most important dynamical processes can be made. Thus assessing the data needs for models cannot be performed until the types of models to be employed to investigate the fate of radionuclides have been chosen. The recommendations above, therefore, concentrate on a measurement program which will improve knowledge of boundary layer flows and dispersion, particularly for the unexplored flows in the lower Hudson Canyon, which in turn may give a better basis on which modeling of the fates of radionuclides may be made in the future.

ACKNOWLEDGEMENTS

Thanks are due to Nelson Hogg, Robert Beardsley and G. T. Csanady for useful contribution on this work during a visit to Woods Hole Oceanographic Institution in January 1981.

REFERENCES

Baines, P. G., 1974. The generation of internal tides over steep continental slopes. Phil. Trans. Roy. Soc. London, A277, pp 27-58.

Bisagni, J. J., 1981. Physical oceanographic studies at 106-mile site, July 1977. In Assessment report on the effects of waste dumping in 106-mile Ocean Waste Disposal Site. NOAA Dumpsite Evaluation Report 81-1, Rockville, MD, pp 233-242.

Bisagni, J. J., 1980. Circulation study at 106 mile dumpsite uses satellite to track drogued buoys. Coastal oceanography and Climatology News, 3(1): 6-7.

Bowden, K. F., 1965. Horizontal mixing in the sea due to a shearing current. J. Fluid Mech. 21:83-95.

Csanady, G. T., 1973. Turbulent diffusion in the environment. Reidel, 248 pp.

Devine, M., E. R. Meyer, and T. O'Connor, 1981. Assessment Report on the Effects of Waste dumping in 106-Mile Ocean Waste Disposal Site. Part I: NOS Assessment. NOAA Dumpsite Evaluation Report 81-1, Rockville, MD, pp 3-30.

Dyer, R. S., 1976. Environmental surveys of two deep-sea radioactive waste disposal sites using submersibles. International Symposium on the Management of Radioactive Wastes from the Nuclear Fuel Cycle, International Atomic Energy Agency, Vienna, 22-26 March 1976, IAEA-SM-207/65.

Foreman, M. G. G., 1979. Manual for tidal currents analysis and prediction. Institute of Ocean Sciences, Patricia Bay, Victoria, B.C. Pacific Marine Science Report 78-6.

Godin, G., 1972. The Analysis of Tides. University of Toronto Press, Toronto, 264 pp.

Hasselmann, K., 1976. Stochastic climate models. Part I. Theory. Tellus 28:473-485.

Hogg, N. G., 1981. Topographic waves along 70°W on the continental rise. J. Mar. Res. 39:627-649.

Hogg, N. G. and W. J. Schmitz, Jr., 1980. A dynamical interpretation of low frequency motions near very rough topography - the Charlie Gibbs Fracture Zone. J. Mar. Res., 38:215-248.

Ingham, M. C., J. J. Bisagni and D. Mizenko, 1977. The general physical oceanography of deepwater dumpsite 106 In Baseline Report of Environmental Conditions in Deepwater Dumpsite 106 (Volume 1), NOAA Dumpsite Evaluation Report 77-1, Rockville, MD, pp 29-86.

Kundu, P. J., 1976. An analysis of inertial oscillations observed near the Oregon coast. J. Phys. Oceanogr. 6:879-893.

Luedecke, A. R., 1959. Disposal of radioactive wastes into the Atlantic Ocean and the Gulf of Mexico. Industrial Radioactive Waste Disposal Hearings Before the Joint Committee on Atomic Energy 5 Washington, D. C.

Luyten, J. R., 1977. Scales of motion in the deep Gulf Stream and across the Continental Rise. J. Mar. Res., 35:49-74.

Mayer, D. A., H. O. Mofjeld and K. D. Leaman, 1981. Near-inertial waves observed on the outer shelf in the Middle Atlantic Bight in the wake of Hurricane Belle. J. Phys. Oceanogr., 11, 87-106.

Mizenko, D. and J. L. Chamberlin, 1981. Gulf Stream anticyclonic eddies and shelf water at 106-mile site during 1977. In Assessment report on the effects of waste sumping in 106-mile Ocean Waste Disposal Site. NOAA Dumpsite Evaluation Report 81-1, Rockville, MD, pp 207-232.

Ou, H. W. and R. C. Beardsley, 1980. On the propogation of free topographic Rossby waves near continental margins. Part II: Numerical model. J. Phys. Oceanogr. 10:1323-1339.

Ou, H. W., J. A. Vermersch, W. S. Brown and R. C. Beardsley, 1980. New England Shelf/Slope Experiment (February-August, 1976). Data Report: The moored array WHOI. Tech. Rep. 59pp.

Perkins, H., 1976. Observed effect of an eddy on inertial oscillations. Deep-Sea Res., 23, 1037-1042.

Rattray, Jr., M., J. G. Dworski and P. E. Kovala, 1969. Generation of long internal waves at the continental slope. Deep-Sea Res. 16 (Supplement), pp 179-196.

Rhines, P. B., 1970. Edge-, bottom-, and Rossby waves in a rotating stratified fluid. Geophysical Fluid Dynamics. 1:273-302.

Richardson, P. L., 1981. Gulf Stream trajectories measured with free-drifting buoys. J. Phys. Oceanogr., 11, 999-1010.

Schmitz, Jr., W. J., J. F. Price, P. L. Richardson, W. B. Owens, D. C. Webb, R.E. Cheney and H. T. Rossby, 1981. A preliminary exploration of the Gulf Stream system with SOFAR floats. J. Phys. Oceanogr. 11, 1194-1204.

Schmitz, Jr., W. J., 1980, Weakly depth-dependent segments of the North Atlantic circulation. J. Mar. Res. 38, 111-113.

Schmitz, Jr., W. J., 1974. Observations of low-frequency current fluctuations on the continental slope and rise near Site D. J. Mar. Res. 32:233-251.

Thompson, R.O.R.Y., 1971. Topographic Rossby waves at a site north of the Gulf Stream. Deep-Sea Res. 18:1-19.

Thompson, R.O.R.Y., 1977. Observations of Rossby waves near site D. Prog. Oceanogr. 7:135-162.

Torgrimson, G. M. and B. M. Hickey, 1979. Barotropic and baroclinic tides over the continental slope and shelf off Oregon. J. Phys. Oceanogr. 9:945-961.

Uchupi, E., 1965. Map showing relations of land and submarine topography, Nova Scotia to Florida. U. S. Geological Survey, Washington, D. C. G65040.

Volkmann, G., 1962. Deep current observations in the western north Atlantic. Deep-Sea Res. 9:493.

Wallace, J. M., and R. F. Dickinson, 1972. Empirical orthogonal representation of time series in the frequency domain, Part I: Theoretical Considerations. J. Appl. Meteor., 11:887-892.

Warsh. C. E., 1975. Physical oceanographic observations at deepwater dumpsite 106 - May 1974. NOAA dumpsite evaluation report 75-1, Rockville, MD., pp 141-188.

Weatherly, G. L. and P. J. Martin, 1978. On the structure and dynamics of the oceanic bottom boundary layer. J. Phys. Oceanogr. 8:557-570.

Wunsch, C. and R. Hendry, 1972. Array measurements of the bottom boundary layer and the internal wave field on the continental slope. Geophysical Fluid Dynamics. 4:101-145.

Wunsch, C. and S. Webb, 1979. The climatology of deep ocean internal waves. J. Phys. Oceanogr. 9:235-243.

Zimmerman, H. B., 1971. Bottom currents on the New England continental rise. J. Geophys. Res. 76:5865-5876.

☆ U.S. GOVERNMENT PRINTING OFFICE: 1982 0 — 361-085/4467

TECHNICAL REPORT DATA
(Please read Instructions on the reverse before completing)

1. REPORT NO. EPA 520/1-82-002	2.	3. RECIPIENT'S ACCESSION NO.
4. TITLE AND SUBTITLE Analysis of Current Meter Records at the Northwest Atlantic 2800 Metre Radioactive Waste Dumpsite		5. REPORT DATE June, 1982 Date of Preparation
		6. PERFORMING ORGANIZATION CODE
7. AUTHOR(S) Peter Hamilton		8. PERFORMING ORGANIZATION REPORT NO.
9. PERFORMING ORGANIZATION NAME AND ADDRESS Science Applications, Inc. 4900 Water's Edge Drive, Suite 255 Raleigh, North Carolina 27606		10. PROGRAM ELEMENT NO.
		11. CONTRACT/GRANT NO. 68-01-6235
12. SPONSORING AGENCY NAME AND ADDRESS Office of Radiation Programs U.S. Environmental Protection Agency 401 M Street, S.W. Washington, D.C. 20460		13. TYPE OF REPORT AND PERIOD COVERED Final
		14. SPONSORING AGENCY CODE ANR-461

15. SUPPLEMENTARY NOTES

16. ABSTRACT

In August, 1976, four current meter arrays were deployed for a period of three months at the Atlantic 2800 meter radioactive waste disposal site as part of a scientific survey by the U.S. Environmental Protection Agency to assess the environmental conditions at this formerly used site. The disposal site is located on the Continental Rise and is centered at 38°30'N, 72°06'W. The four arrays were placed in a rectangle near the periphery of the site, each with a current meter 5.1 meters off the bottom, with an additional meter located 96 meters from the bottom at the southwest mooring. The principal findings included a 3-4 cm/s southwesterly mean current observed near the bottom. The low frequency part of the spectrum is explained as bottom trapped topographic Rossby waves. The high frequency motions are dominated by inertial oscillations with a maximum amplitude of about 10 cm/s. The potential for sediment transport during the measurement period is considered very small based on the observed current speeds.

17. KEY WORDS AND DOCUMENT ANALYSIS

a. DESCRIPTORS	b. IDENTIFIERS/OPEN ENDED TERMS	c. COSATI Field/Group
Ocean Dumping/Sea Disposal Radioactive Waste Disposal/Nuclear Waste Disposal Deepsea Currents Ocean Currents		

18. DISTRIBUTION STATEMENT Unlimited Release	19. SECURITY CLASS *(This Report)* Unclassified	21. NO. OF PAGES 101
	20. SECURITY CLASS *(This page)* Unclassified	22. PRICE

EPA Form 2220-1 (Rev. 4-77) PREVIOUS EDITION IS OBSOLETE